

2020

## Experimental Assessment of the Current Load Rating Procedures for a Corroded Steel Ridge Girder in Massachusetts

Brendan T. Knickle  
*University of Massachusetts Amherst*

Follow this and additional works at: [https://scholarworks.umass.edu/cee\\_structural](https://scholarworks.umass.edu/cee_structural)



Part of the [Structural Engineering Commons](#)

---

Knickle, Brendan T., "Experimental Assessment of the Current Load Rating Procedures for a Corroded Steel Ridge Girder in Massachusetts" (2020). *Structural Engineering Masters Projects*. 3.  
Retrieved from [https://scholarworks.umass.edu/cee\\_structural/3](https://scholarworks.umass.edu/cee_structural/3)

This Article is brought to you for free and open access by the Civil and Environmental Engineering at ScholarWorks@UMass Amherst. It has been accepted for inclusion in Structural Engineering Masters Projects by an authorized administrator of ScholarWorks@UMass Amherst. For more information, please contact [scholarworks@library.umass.edu](mailto:scholarworks@library.umass.edu).

**EXPERIMENTAL ASSESSMENT OF THE CURRENT LOAD RATING  
PROCEDURES FOR A CORRODED STEEL BRIDGE GIRDER IN  
MASSACHUSETTS**

A Masters Project Presented

by

BRENDAN T. KNICKLE

Submitted to the Graduate School of the  
University of Massachusetts Amherst in partial fulfillment  
of the requirements for the degree of

MASTER OF SCIENCE IN CIVIL ENGINEERING

February 2020

Civil Engineering



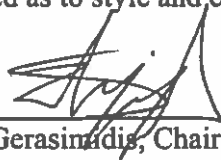
**EXPERIMENTAL ASSESSMENT OF THE CURRENT LOAD RATING  
PROCEDURES FOR A CORRODED STEEL BRIDGE GIRDER IN  
MASSACHUSETTS**

A Masters Project Presented

by

**BRENDAN T. KNICKLE**

Approved as to style and content by:



---

Simos Gerasimidis, Chairperson



---

Sergio Breña, Member



---

Caitlyn Butler  
Civil and Environmental Engineering Department

**ABSTRACT**

**EXPERIMENTAL ASSESSMENT OF THE CURRENT LOAD RATING  
PROCEDURES FOR A CORRODED STEEL BRIDGE GIRDER IN  
MASSACHUSETTS**

February 2019

BRENDAN T. KNICKLE, B.S., UNIVERSITY OF MASSACHUSETTS AMHERST  
M.S., UNIVERSITY OF MASSACHUSETTS AMHERST

Directed by: Professor Simos Gerasimidis

The work conducted for this project involves an experimental assessment of the Massachusetts Department of Transportation's (MassDOT) existing procedure for determining the resistance of a corroded steel girder end when load rating a bridge. Three steel girders with significant corrosion developed over a 79-year service life were obtained from a recently rehabilitated bridge and loaded to determine the girders corroded resistance. A testing rig was designed in the UMass Amherst Brack Structural Testing Laboratory to both apply a shear dominated load to the corroded girder and withstand the developed lateral loads throughout the analysis. Reaction force data obtained from the load testing was compared against the corroded web factored resistance determined from the MassDOT LRFD Bridge Design Manual. Resistances were under predicted by 75% for specimen 1, 37% for specimen 2 and the manual predicted no resistance for specimen 3. Lastly influences for the discrepancies between manual resistance and experimental resistance are determined.

## TABLE OF CONTENTS

	Page
ABSTRACT.....	iii
LIST OF TABLES.....	vi
LIST OF FIGURES.....	viii
CHAPTER	
1. INTRODUCTION.....	1
1.1 Published Research.....	3
1.1.1 Research on Remaining Capacity of Corroded Steel Girder Ends....	3
1.1.2 Research on Rehabilitation of Corroded Steel Girder Ends.....	6
1.2 Objective.....	7
2. COLRAIN, MASSACHUSETTS CANDIDATE BRIDGE	
2.1 Structural Layout.....	9
2.2 North Approach Span Superstructure.....	9
2.3 Summary.....	11
3. EXPERIMENTAL TEST SETUP.....	14
3.1 Design of Testing Rig .....	14
3.1.1 Loading Configuration.....	15
3.1.2 Lateral Bracing .....	19
3.1.3 Vertical Support.....	21
3.2 Specimen Geometry.....	22
3.2.1 Specimen 1.....	22
3.2.2 Specimen 2.....	26
3.2.3 Specimen 3.....	28
3.3 Instrumentation.....	29
3.3.1 Load Cells.....	30
3.3.2 Linear Potentiometers.....	31
3.3.3 Strain Rosettes.....	31
3.4 Summary.....	31
4. CORRODED STEEL GIRDER TEST RESULTS.....	33
4.1 Introduction.....	33
4.2 Testing Procedure.....	33

4.3 Specimen 1 Final Setup.....	34
4.3.1 Experiment 1 Results.....	36
4.4 Specimen 2 Final Setup.....	41
4.4.1 Experiment 2 Results.....	43
4.5 Specimen 3 Final Setup.....	48
4.5.1 Experiment 3 Results.....	50
4.6 Comparison of Experimental Results to Code Predicted Resistances.....	55
5. MASSDOT LOAD RATING PROCEDURE.....	57
5.1 Introduction.....	57
5.2 Description of Typical Load Rating Methodology for Candidate Bridge.....	57
5.2.1 Dead Loads of Candidate Bridge.....	61
5.2.2 Live Loads of Candidate Bridge.....	63
5.3 Description of Special Provisions for Corrosion in Web.....	66
5.4 Load Rating Results of Specimens using the Current MassDOT Procedure....	68
5.4.1 Corroded Web Factored Resistance.....	69
5.4.2 Rating Table.....	71
5.5 Load Rating Results of Specimens using Experiment Values.....	72
5.5.1 Resistances from Experiments.....	72
5.5.2 Rating Table.....	74
5.6 Comparison of Results.....	75
6. CONCLUSIONS.....	76
BIBLIOGRAPHY.....	79
APPENDIX A: Experimental Test Rig Design Sheets.....	83
APPENDIX B: Raw Data Test Results.....	111
APPENDIX C: Load Rating Procedure.....	123

## LIST OF TABLES

Table	Page
Table 3.1: Maximum Loading Position Away from Centerline of Bearing of Tested End.....	18
Table 3.2: Geometric Properties of a 33WF128 Rolled Steel Beam.....	22
Table 3.3: Geometric Properties of a 33WF132 Rolled Steel Beam.....	26
Table 4.1: Relative Location of Strain Rosettes for Specimen 1.....	35
Table 4.2: Relative Location of Strain Rosettes for Specimen 2.....	42
Table 4.3: Relative Location of Strain Rosettes for Specimen 3.....	49
Table 4.4: Comparison of Code Predicted Resistances against Experimental Results.....	55
Table 5.1: Factored Dead Load Shear for Girder 1 (Specimen 2).....	62
Table 5.2: Factored Dead Load Shear for Girder 3 (Specimen 3).....	63
Table 5.3: Factored Dead Load Shear for Girder 4 (Specimen 1).....	63
Table 5.4: Unfactored Shear from Live Loads and Appropriate Load Factors.....	64
Table 5.5: Inventory and Operating Live Load Shears.....	64
Table 5.6: Corrected Shear Distribution Factors for Interior and Exterior Girder.....	65
Table 5.7 Inventory and Operating Level Live Load Shears for Interior and Exterior Girder.....	65
Table 5.8: Corroded Web Factored Resistance (CWFR) of Tested Specimens.....	69
Table 5.9: Design and Legal Load Rating Factors using the Current MassDOT Procedure.....	71
Table 5.10: Reaction Force of Corroded End at Peak Load.....	72

Table 5.11 Design and Legal Load Rating Factors using Reaction Force from Experiments.....	74
--	----

## LIST OF FIGURES

Figure	Page
Figure 2.1: Bridge ID C18028-0KQ-DOT-NBI, Colrain, Massachusetts; Span 5 beginning from the right.....	9
Figure 2.2: Span 5 Structural Layout.....	10
Figure 2.3: Bearing Details.....	12
Figure 2.4: Cross Section View at Bearing.....	12
Figure 2.5: Cross Section View at Midspan.....	13
Figure 3.1: Typical Experimental Set-Up.....	14
Figure 3.2: Loading Configuration for Experimental Set-Up.....	16
Figure 3.3: Lateral Support at Beam End.....	21
Figure 3.4: Test Specimen 1 a) before deconstruction in the field, b) before testing in the lab.....	23
Figure 3.5: (Top) 2"x3" hole under end diaphragm; (Bottom) 5"x2" hole next to crippled section at web-flange connection.....	25
Figure 3.6: Test Specimen 2 a) before deconstruction in the field, b) before testing in the lab.....	27
Figure 3.7: 45° Deteriorated Region in Web.....	27
Figure 3.8: Test Specimen 3 a) before deconstruction in the field, b) before testing in the lab.....	28
Figure 3.9: (Top) 4"x2" hole under end diaphragm; (Bottom) Initial Out-of-Alignment and Web-Flange Discontinuity.....	29
Figure 3.10: Typical Instrumentation Set-Up.....	30

Figure 4.1: Specimen 1 Instrumentation Placement.....	34
Figure 4.2: (Left) Strain Rosettes (Right) Linear Potentiometers.....	35
Figure 4.3: (Left) Applied Load – Vertical Displacement Curve (Right) Measured Force Applied by Hydraulic Cylinder on Each Side of Crossbeam.....	36
Figure 4.4: (Left) Recorded Reaction Force at Intact End (Right) Calculated Reaction Force at Corroded End.....	37
Figure 4.5: Force Distribution to Intact End for Specimen 1.....	38
Figure 4.6: Lateral Deformation of Corroded End.....	38
Figure 4.7: (Left) Principal Strain in Web for Specimen 1 (Right) Principal Strain Direction in Web for Specimen 1.....	39
Figure 4.8: Principal Strain Directions Specimen 1.....	40
Figure 4.9: Residual Deformation of Corroded Web End.....	40
Figure 4.10: Specimen 2 Instrumentation Placement.....	41
Figure 4.11: (Left) Strain Rosettes (Right) Linear Potentiometers.....	42
Figure 4.12: (Left) Applied Load – Vertical Displacement Curve (Right) Measured Force Applied by Hydraulic Cylinder on Each Side of Crossbeam.....	43
Figure 4.13: (Left) Recorded Reaction Force at Intact End (Right) Calculated Reaction Force at Corroded End.....	43
Figure 4.14: Force Distribution to Intact End for Specimen 2.....	44
Figure 4.15: Lateral Deformation of Corroded End.....	45
Figure 4.16: (Left) Principal Strain in Web for Specimen 2 (Right) Principal Strain Direction in Web for Specimen 2.....	46
Figure 4.17: Principal Strain Directions Specimen 2.....	47



Figure 4.18: Residual Deformation of Corroded Web End.....	47
Figure 4.19: Specimen 3 Instrumentation Placement.....	48
Figure 4.20: (Left) Strain Rosettes (Right) Linear Potentiometers.....	49
Figure 4.21: (Left) Applied Load – Vertical Displacement Curve (Right) Measured Force Applied by Hydraulic Cylinder on Each Side of Crossbeam.....	50
Figure 4.22: (Left) Recorded Reaction Force at Intact End (Right) Calculated Reaction Force at Corroded End.....	51
Figure 4.23: Force Distribution to Intact End for Specimen 3.....	52
Figure 4.24: Lateral Deformation of Corroded End.....	52
Figure 4.25: (Left) Principal Strain in Web for Specimen 3 (Right) Principal Strain Direction in Web for Specimen 3.....	53
Figure 4.26: Principal Strain Directions Specimen 3.....	54
Figure 4.27: Residual Deformation of Corroded Web End.....	54

# CHAPTER 1

## INTRODUCTION

Infrastructure resilience has been a topic of increasing attention in the last decades from the research community. There has been significant research efforts to study different building structural systems under extreme events (Pantidis et al 2018, Gerasimidis et al 2017, Sideri et al 2017, Pantidis et al 2017, Gerasimidis 2016a, 2016, Gerasimidis et al 2015, Gerasimidis et al 2014, Gerasimidis et al 2013, Gerasimidis et al 2012a, , Gerasimidis et al 2012b, Gerasimidis et al 2011a, Gerasimidis et al 2011b, Gerasimidis et al 2011c, Gerasimidis et al 2009). However, the concept of resilience usually is applied under the assumption that the structural system has remained intact up until the appearance of the extreme event. In reality, every structural system ages in time and its operational capacity deteriorates. A significant part of infrastructure which has been undergoing deterioration is bridges and in particular steel bridges experiencing deterioration. This thesis is focused on addressing this problem.

According to the 2017 Federal Highway Administration's (FHWA) National Bridge Inventory (NBI) 47,619 of the United States 614,919 bridges (7.7%) are considered structurally deficient (FHWA 2017). A bridge is classified as structurally deficient by receiving a condition of 4 (poor) or lower for one of the components: deck, superstructure, substructure, or culvert during a load rating. Frequently resulting in time costly weight postings or rehabilitation, agencies have also documented occurrences where a bridge had to be closed for rebuild. The American Society of Civil Engineers (ASCE) approximates 188 million trips are made over structurally deficient bridges daily in the United States, with an estimated \$123 billion dollars in funds necessary to rehabilitate the entire bridge

program (ASCE 2017). This prominent and expensive issue has sparked a variety of research into the existing condition of the nation's bridges.

Primarily in the Northern region of the country, various state Department of Transportation (DOTs) have investigated corrosion as a critical reason for structurally deficient ratings in steel girder bridges. Due to the typical weather of these regions, deicing measures are used on bridge roadway surfaces to ensure safety for motor vehicles. State inspectors have documented water runoff from the deicing agents leaking through bridge joints, causing buildup on the girder ends. Leading to severe thickness loss in the web, flange and bearing of the girder, with extreme cases seeing deep pitting or complete material loss. The continuing deterioration has led to the interest of Massachusetts Department of Transportation (MassDOT) officials.

The state of Massachusetts maintains 5,189 bridges, with the NBI report stating 473 being rated as structurally deficient (FHWA 17). Due to seeing the common deterioration of girder ends in the structurally deficient bridges, MassDOT has updated the impact of corrosion to steel girders in the Mass LRFD Bridge Manual. The procedure determines the remaining capacity of the corroded girder end by taking the minimum of the web local yielding ( $R_{n,yield}$ ) and factored web local crippling capacity ( $\phi R_{n,crip}$ ), with the demands being shear forces from permanent loads and a HS20 live load (MassDOT 2018). As previous DOTs have done, research into the reality of the capacity values used in the procedure must be done in the interest of future decisions with rehabilitating the states bridges.

## **1.1 Published Research – Literature review**

Since the early 2000's, a combined effort to experimentally investigate the true behavior of corroded steel girders has been made by state agencies and research universities. PennsylvaniaDOT, MichiganDOT, VirginiaDOT, ConnecticutDOT, have all been a part of research regarding corroded bridges in their state. Until now, the common experimental practice was introducing artificial corrosion to new steel girders. Artificial corrosion allows for the researching engineer to design for a predicted failure mode. It also ignores the corrosion that had been naturally developed along the length of the specimen, which although typically not as aggressive some inspection reports have shown significant section loss away from the bearing. There have also been several groups who researched rehabilitation into corroded girder ends. Though not a focus in the scope of this thesis, rehabilitation will still be examined along with previous research on the resultant capacity of corroded girder ends.

### **1.1.1 Research on Remaining Capacity of Corroded Steel Girder Ends**

Significant research of this topic picked up in the late 20<sup>th</sup> century behind the work of Kulicki et al. (Kulicki 1990). The group proposed guidelines to the PennDOT in respect to evaluating corrosion from an inspection standpoint. The work left the agency with a new method of recording corrosion in the field with various instruments, while also supplying engineers in the office how to interpret the field inspections (Kulicki 1990). The work done by Kulicki on the importance of properly inspecting corrosion in steel bridges, led to several other agencies progressing these methods to determine the strength impact of corrosion. Fifteen years later guidelines for deteriorated steel girder ends were conducted

by van de Lindt (van de Lindt 2005) on behalf of MichiganDOT (MDOT). The research involved a crushing analysis of several fabricated, three-foot-long, 50 ksi steel girders with artificial corrosion. The MDOT had previously used methods from AISC to determine the minimum capacity of girder ends assuming an average thickness loss over the entire depth. The research resulted in a series of design charts with deterioration factors based on corrosion dimensions, which were to be used in conjunction with the AISC methods (van de Lindt 2005).

Similarly to the United States, corrosion of steel structures has also been a documented problem internationally. Japan has had notable bridge collapses over the last two decades, with some failures being attributed to severe corrosive conditions (Kim 2013). Inspections from Japan reports show that typical methods in steel girder bridge design involve the use of bearing stiffeners. The inclusion of stiffeners significantly changes the structural response of the girder end by creating a column design over the bearing. The failure mode of the web panel is also significantly affected when a stiffener is present, due to the unbraced depth of the web being reduced to zero, while also resulting in the development of a diagonal tension field in the web panel between stiffeners. Korean researchers Kim et al., investigated the effect of pitting and through-hole corrosion that protruded into the diagonal tension field critical area, using multiple fabricated steel girders with artificial corrosion (Kim 2013). The diagonal tension field theory states when a thin plate is loaded beyond the critical buckling load the tensile stresses will significantly out factor the compressive stresses, resulting in the buckling mode lining up along the tension field angle (Kuhn 1952). According to Kuhn, the tension field angle of a typical steel panel averages around  $40^\circ$ . To better illustrate the response of a web panel of a full girder, the

research group fabricated ten-foot-long specimens, with equal spaced stiffeners centered over each bearing location and at midspan of the girder under the point of loading. Aligning with the fabrication method taken by van de Lindt (van de Lindt 2005), various artificial corrosion patterns were implemented to the girders in lower critical regions of the central web panels. Analysis concluded if the deterioration in the web protrudes into the original diagonal tension field then the tension field angle deviated from the expected average (Kim 2013). The same research group also investigated the strength impact of significant deterioration damage to web panels of girders in the forms of deep pitting and through-hole section loss (Ahn 2015). Aside from the corrosion pattern, the test specimens and procedure followed the work previously presented by Kim et al. It was determined that through-hole corrosion distorts the angle of the tension field and reduces shear buckling capacity of the web panel, while pitting did not deviate the strength much from intact (Ahn 2015).

The research into deteriorated web and stiffener effect on the bearing capacity of steel girder ends was conducted by Khurram et al. (Khurram 2014). Experimental analysis was done on four-foot-long specimens which had corrosion artificially applied both to the bearing stiffener only, then additionally to a combination of stiffener and web. The study concluded if there is a combination of local web corrosion along with a significant section loss to the bearing stiffener, the failure mode changes from buckling to crippling within the deteriorated region (Khurram 2014).

### **1.1.2 Research on Rehabilitation of Corroded Steel Girder Ends**

Maintenance procedures on corrosion of steel bridges has gradually been improving in the United States. In 2002, Koch et al. determined 15% of the nation's bridges are structurally deficient due to corrosion, with the government spending \$8.3 billion dollars of annual direct cost from corrosion of highway bridges (Koch 2002). It was also approximated that weight postings, traffic delays and other indirect costs, exceeded the maintenance costs by 10 times (Koch 2002). The financial impact of rehabilitating deteriorated bridges has led to research into the most efficient method to recover strength of corroded steel girders.

There are typically one of two approaches taken in repairing corroded steel girders in the field. The first includes bolting a series of new steel plates, angles, etc., to the deteriorated region. The second, and more researched method, is adhering various forms of reinforced sheets to the girder end. Ogami et al. researched the strength recovery and failure mode of a repaired specimen by attaching rebar to the corroded area and encasing it in resin (Ogami 2015). The study fabricated experiments on non-repaired and repaired girder ends, both with artificial corrosion. Results showed that when rebar and resin was applied as a repair method, the specimen regained strength and the buckling mode was shifted above the deteriorated zone (Ogami 2015).

The use of carbon fiber reinforced polymer (CFRP) sheets in steel bridge rehabilitation was first researched by Miller et al., during a study conducted on tension flange CFRP cover plates (Miller 2001). Until recently, the application of CFRP sheets to deteriorated girder ends was not significantly examined. Researchers in Japan studied and put into practice the repair method of fiber reinforced polymers (FRP) in reinforced

concrete (RC) bridges. This led to the motivation of Okuyama et al. (Okuyama 2012), studying the mechanical behaviors of steel plates bonded with FRP. The study concluded when low-elasticity FRP sheets are bonded to both sides of a steel plate the elastic buckling load is increased (Okuyama 2012). Also found, if a polyurea putty is used as a primer, the FRP sheets were able to stay bonded during large buckling deflections (Okuyama 2012). These conclusions were later validated for application to steel bridge girders in Japan by the work of Miyashita et al. (Miyashita 2015), who tested through-hole deteriorated girders repaired with putty bonded CRFP sheets. Results showed even with severe deterioration in the web, shear strength can fully be recovered with appropriately bonded CFRP sheets (Miyashita 2015).

Research conducted by Zmetra et al. (Zmetra 2017), investigated the strength recovered by a corroded specimen through welding shear studs to the deteriorated web and encasing the region in ultrahigh-performance concrete (UHPC). Experimental studies were conducted on fabricated, 14-foot-long specimens with artificial corrosion applied to the lower web at the bearing. Additionally, tests were conducted on identical specimens repaired by the proposed UHPC method. Results showed with proper arrangement of shear studs to allow composite action the shear capacity of the girder end increased past that of intact, while shifting the failure mode to flexural yielding at the point of loading (Zmetra 2017).

## **1.2 Objective**

Literature shows most of the research into resultant capacity of a deteriorated steel girder has been focused around the presence of a stiffener. Researches such as Kayser et



al. (Kayser 1989) have challenged if these practices can be accurately applied to unstiffened webs. The first objective of this thesis is to experimentally investigate the resultant capacity of three naturally corroded, unstiffened steel girders. Unlike previous research, the test specimens were not fabricated and instead were removed from an existing bridge in Western Massachusetts that was undergoing replacement. The second objective is to compare experimental results with the current MassDOT procedure for determining the resultant capacity of unstiffened, corroded steel girder ends. A load rating of the three bridge members using both methods will be presented to gain insight into the reliability of the current procedure. Part of this research has been presented in international conferences (Tzortzinis 2019).

## CHAPTER 2

### COLRAIN, MASSACHUSETTS CANDIDATE BRIDGE

#### 2.1 Structural Layout

The test specimens for this project were obtained from a two lane, five span, steel bridge in Colrain, Massachusetts (Bridge ID: C18028-0KQ-DOT-NBI). The structure carries State 112 (Jacksonville Road) over the North River, at a 40° skew. Originally constructed in 1933 as a three-span continuous steel riveted girder, however, in the late 1930's large storm floods occurred in the North River causing scour issues for the previous



Figure 2.1: Bridge ID C18028-0KQ-DOT-NBI, Colrain, Massachusetts; approach span pictured on the right.

abutments. Due to this the state decided on the addition of one approach span on each end of the bridge, see Figure 2.1.

In 2017 the bridge received a condition rating of 3 (poor), with a documented average daily traffic (ADT) of 1,440 vehicles (NBI 2017). Around the time of this study, MassDOT decided to undergo replacement of the approach spans (1 & 5). Both of which were carried by a superstructure of seven simply supported, unstiffened, rolled steel girders, where a significant amount of deterioration had developed at the girder ends. The system of girders relied on a series of concrete end and intermediate diaphragms. For a plan view of the framing for span 5, see figure 2.2.

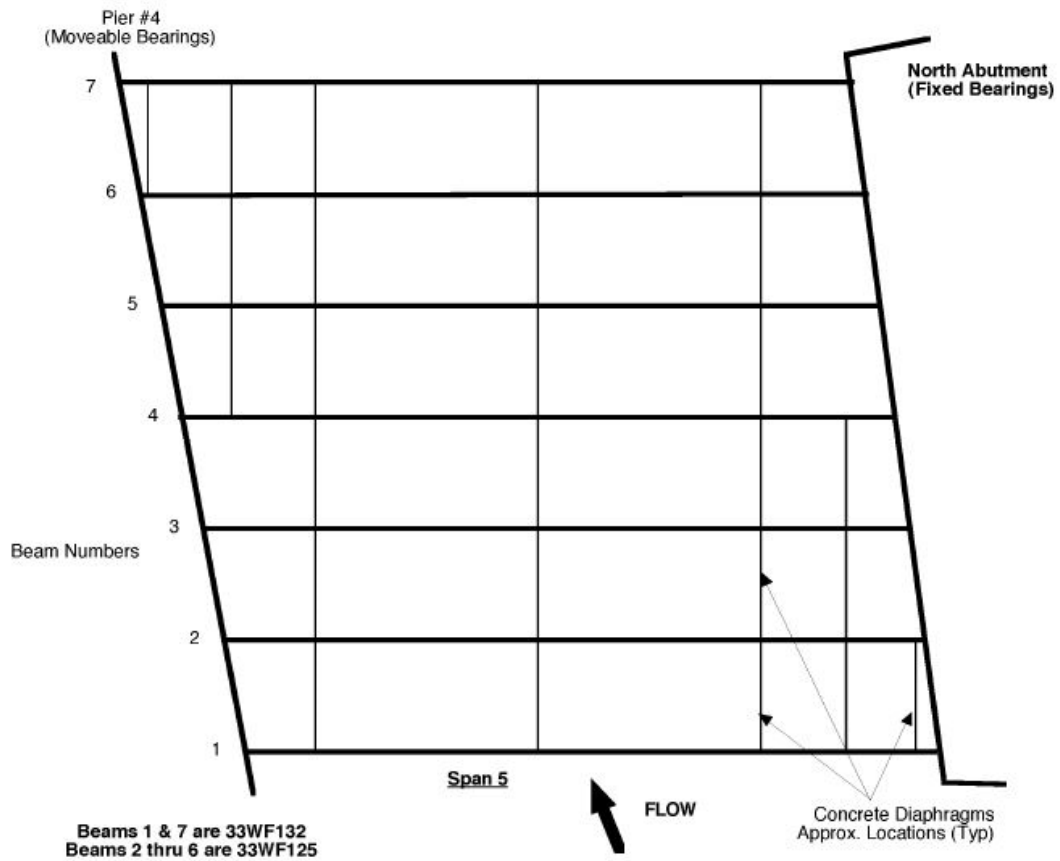


Figure 2.2: Span 5 Structural Layout

Girder ends one through four from span five were selected as the best test subjects due to more severe corrosion noted in the inspection report. This is most likely evident due

to the fact the elevation view shows a high-point elevation change of two feet from span 1 to span 5, so excess rain water or melting ice with chemicals have a greater chance of pooling up on span 5. Additionally, the inspection report notes several locations where scupper drain pipes were either missing or not efficiently working, allowing for water to come out of the drains and directly onto the girders. The ½” Asphaltic bridge joint above the girder ends on Pier #4 was also said to have been compromised. The girders were carefully deconstructed from the bridge, cut at midspan and shipped to UMass Amherst’s Brack Structural Testing Laboratory. Selection of delivered specimens for testing was done based on the amount of damage done to the girders during removal. All intact dimensions and sectional properties were determined through the work of AISC (AISC 1953).

## **2.2 North Approach Span Superstructure**

The north approach span superstructure is consisted of a 6½” thick reinforced concrete deck, supported by (7)-rolled steel girders. Exterior girders 1 & 7 are 51-foot-long 33WF132, while interior girders 2-6 are 50-foot-long 33WF128. The system of girders is braced laterally by intermediate concrete diaphragms that are 31” deep (full web depth) by 8” wide. The intermediate diaphragms spacing can be seen in Figure 2.1. Additionally, along skewed supports, beams are braced by end concrete diaphragms that are 16” deep by 12” wide, which are composite with the concrete deck and attached to the top portion of the web end through two bolted steel shelf L’s. The single span girders are supported by fixed bearings at the North Abutment, with an expansion bearing located on Pier #4. Both bearings are comprised of (2) - welded 12”x16”x¾” sole plates atop concrete pedestals, with the expansion bearing having 2-inch slotted holes to allow movement due to thermal

forces. The bearings go to the end of the girder, allowing no beam overhang past the bearing, refer to Figure 2.3 for a detail of the bearing condition. The span supports two

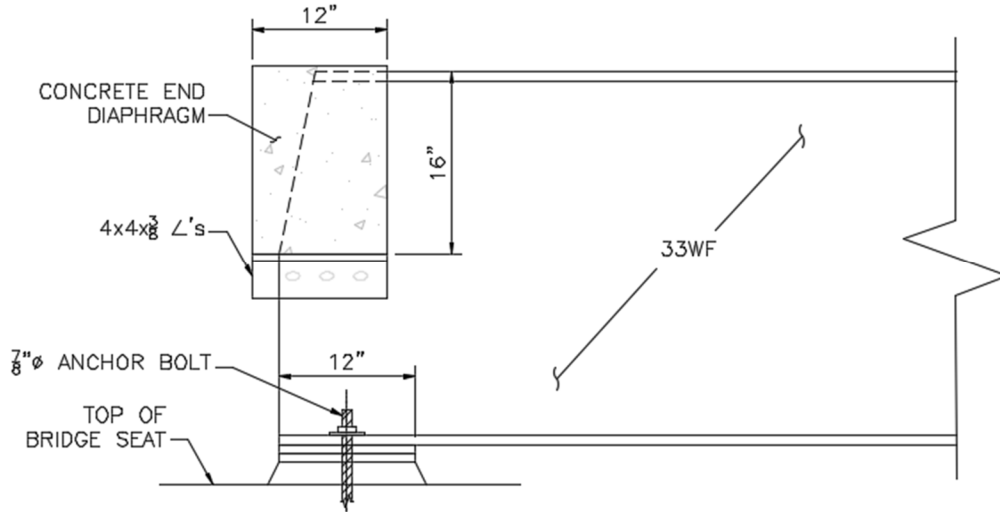


Figure 2.3: Bearing Details

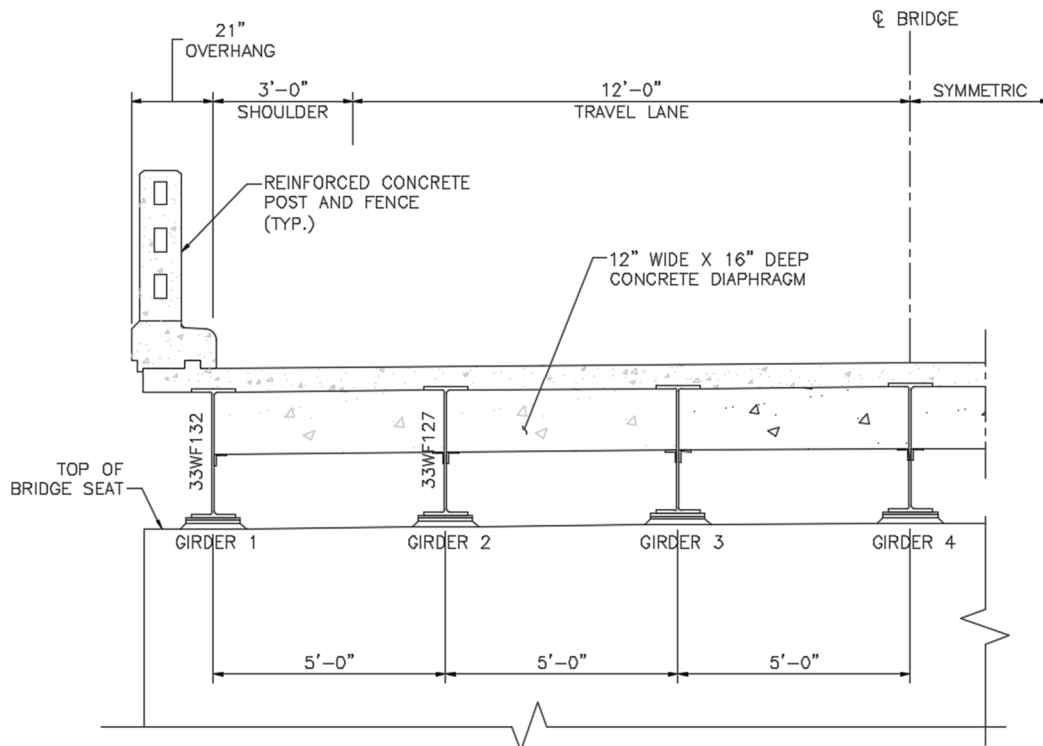


Figure 2.4: Cross Section View at Bearing

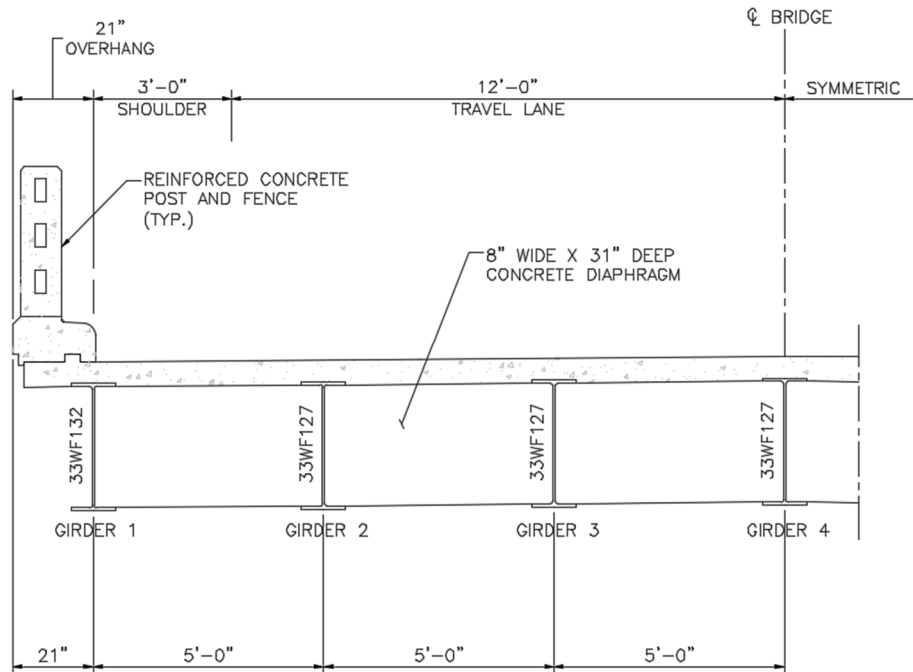


Figure 2.5: Cross Section View at Midspan

lanes of traffic with a reinforced concrete post and fence barrier on a mountable safety curb along each edge. The face of curb is directly above the centerline of exterior girder. Refer to Figure 2.4 for a cross section view at support locations and Figure 2.5 for a cross section view at midspan.

### 2.3 Summary

The test specimens for this research project were obtained from the North Approach Span of a five span bridge in Colrain, MA. The span was supported by (7) steel rolled girders that have developed significant end deterioration. At the time of this research project MassDOT was undergoing replacement of all seven girders, which were cut in half and shipped to UMass Amherst's Brack Structural Testing Lab.

## CHAPTER 3

### EXPERIMENTAL TEST SETUP

#### 3.1 Design of Testing Rig

The experiments for this thesis were carried out in the University of Massachusetts Amherst's (UMass Amherst) Brack Structural Testing Laboratory. The lab was set up with an 80' x 30' strong floor, with tie down spots centered every five feet. With a maximum tensile capacity of 200 kips, the tie down spots could distribute this force over four, 1-1/8"-8 anchor bolt holes equally spaced at eight inches. Due to length restriction in the structural lab, it was determined to field cut the original 50-foot-long bridge specimens roughly in half longitudinally. Reducing the length keeps the full-scale aspect of the girder end, while not affected the natural corrosion developed along the complete end. The design of the braces for the testing rig followed the procedures in the AISC Steel Construction Manual (SCM) (AISC 2016) based off the work of Joseph Yura done on beam bracing (Yura 2001). The vertical supports were supplied from previous research projects done at UMass Amherst, which were sufficient to resist the maximum expected load throughout the

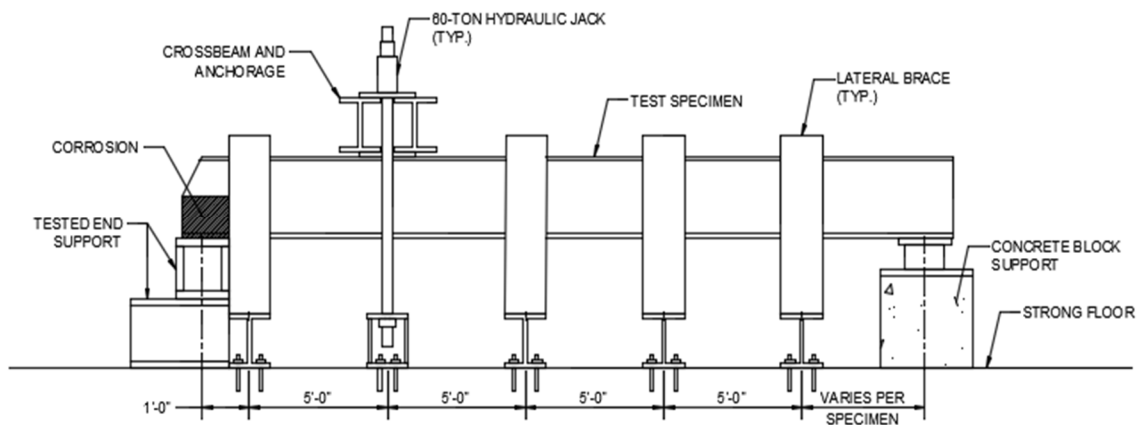


Figure 3.1: Typical Experimental Set-Up

experiments. See Figure 3.1 for a typical elevation view of the experimental test set-up. Reference Appendix A for design and calculation sheets of each structural member.

### **3.1.1 Loading Configuration**

The loading configuration was a combination of two hydraulic cylinders and a cross beam anchored to the strong floor through threaded rods to an anchor block. The SPX Power Team 60-ton hydraulic cylinders (No. RH606 B) were applied and loaded to the anchor rods on each end of the cross beam, as per Figure 3.1. The cross beam was made up of two, six foot, A992 Grade-50 W12x58 beams. This shape was selected to withstand the reaction force developed at midspan of the cross beam during testing. According to the strong floor restrictions a maximum load of 400 kips can be applied to the midpoint of the cross beam, resulting in a 200-kip tensile force in each anchor spot. With the length between rods being 60 inches (5-foot tie down spacing), the maximum expected moment is 6,000 kip-in. The selection process for a W-shape assumed the max moment will not surpass yield of the rig components. Additional to the beams, an amount of the steel cover plates will contribute to the overall section modulus of the composite girder. The shear strength was determined according to Chapter G in the SCM. The nominal shear strength for one W12x58 beam was determined to be 131.76 kips, with the ultimate shear from structural analysis being 200 kips. Once welded together the composite section will have enough capacity to resist direct shear failures, however, for potential future use the cross beam will have 4" x ¼" stiffeners designed in the three locations where load is applied. With no requirement for stiffeners, the spacing and size were conceptually designed then checked to make sure the maximum spacing met the required stiffener inertia. Welds for



cross-beam stiffeners were all around 3/16" fillet welds with 70 ksi filler metal. Refer to Appendix A for a physical representation of the cross-beam design.

The individual beams were combined into one composite section through six, 12"x18"x1-1/2", A36 cover plates, which were connected by all around 1/4" fillet welds to the top and bottom flanges of each beam. The weld strength was determined by the procedure in section J2.2.4 of the SCM. The filler metal classification strength, which for all design cases in this thesis is 70 ksi. The rupture strength was determined to be 567 kips, and where the ultimate shear can never be higher than the maximum possible applied load of 400 kips, the welds are considered sufficient.

A three-inch space was left between the beams, along with a 2" Ø hole in the two end cover plates to allow passage of a ten-foot-long, 1-3/4" Ø anchor rod. The maximum stress to be developed in the rod is 83.15 ksi, thus, 150 ksi all threaded anchor rods were selected. The rods were restricted by high strength hex nuts above the hydraulic cylinders and on the inside on anchor blocks in the strong floor. The anchor blocks were comprised

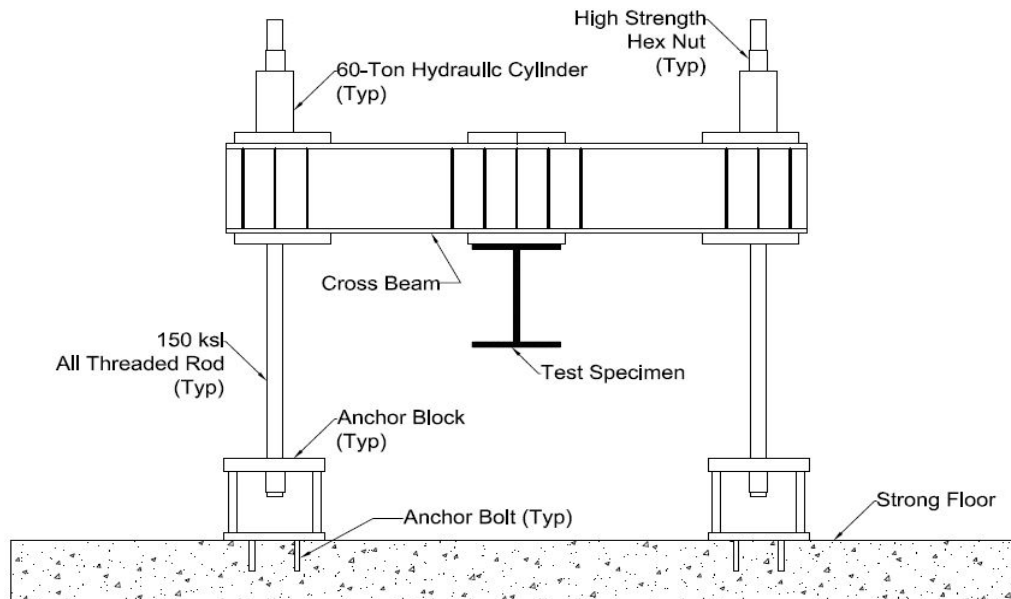


Figure 3.2: Loading Configuration for Experimental Set-Up

of four A36 plates welded together in a rectangular box, with the top plate having a 2" Ø hole for the anchor rod. The welds were all around 5/16" fillets using, 70 ksi filler material. It was determined the rupture strength of one single 12" x 5/16" weld on the anchor block is 157.5 kips. The maximum ultimate shear on the top plate is 100 kips, thus each individual weld is sufficient. Additionally, the top plate had to be checked in bending, with the maximum allowable force to be applied to the top plate is determined by analyzing it as a simply supported beam. The anchor blocks can withstand a maximum tensile force of 150 kips. During the experimental procedure the maximum possible load applied from one of the 60-ton hydraulic cylinders is 120 kips, thus the design is sufficient for the test purposes.

Due to restrictions in the strong floor, the anchor bolts had to be 1-1/8"-8 anchor bolts. No design check was done on these bolts due to each tie down spot having a pre-determined resistance of 200 kips in tension. Refer to Figure 3.2 for a physical representation of the loading configuration.

The loading beam had limitations to its placement longitudinally along the test specimen due to both the strong floor and the desire to laterally brace the tested end of the specimen. For this the point of loading was place 6 feet away from the centerline of bearing. According to the MassDOT Bridge Manual, the desired force is to be shear when determining the load rating of a deteriorated girder. To ensure the specimen would be undergoing a shear-dominated failure the following two equations for a simply supported beam with a point load not at midspan were inspected:

$$M_u = \frac{P_u * a * b}{L} \quad (\text{Eq. 3.1})$$

$$V_u = \frac{P_u * b}{L} \quad (\text{Eq. 3.2})$$

where:

a = Distance from centerline of bearing of tested end to centerline of loading (ft)

b = Distance from centerline of loading to centerline of bearing of untested end (ft)

L = length between supports (ft)

Using a system of equations of Eq. 3.1 and 3.2 to solve for the distance away from the tested end the loading position can be to ensure a shear dominated range. When the value “a” is determined, any loading to cause failure within that limit will be considered a shear dominated failure. The system of equations results in the following ratio:

$$a = \frac{M_u}{V_u} \quad (\text{Eq. 3.3})$$

The ultimate moment and shear for this ratio will be considered as the nominal capacities of the test specimens. However, due to the presence of heavy deterioration in the web, it will be included in the calculation rather than using intact dimensions of a new beam. Including the corroded web area will significantly reduce the nominal shear of the specimen compared to the flexural resistance, resulting in Eq. 3.3 increasing from that of intact values. Table 3.1 lists the calculated values of “a” due to different corrosion conditions.

Table 3.1: Maximum Loading Position Away from Centerline of Bearing of Tested End

$F_y$ (ksi)	$t_w$ (in)	$V_n = 0.6 \cdot F_y \cdot t_w \cdot D$ (kips)	$Z_x$ (in <sup>3</sup> )	$M_n = F_y \cdot Z_x$ (kip*in)	a (ft)
33	0.58	380.69	461.15	15217.80	3.33
33	0.562	368.88	456.70	15071.01	3.40
33	0.544	357.07	452.25	14924.22	3.48
33	0.526	345.25	447.80	14777.43	3.57
33	0.508	333.44	443.35	14630.64	3.66
33	0.49	321.62	438.90	14483.86	3.75
33	0.472	309.81	434.46	14337.07	3.86

$F_y$ (ksi)	$t_w$ (in)	$V_n = 0.6 * F_y * t_w * D$ (kips)	$Z_x$ (in <sup>3</sup> )	$M_n = F_y * Z_x$ (kip*in)	$a$ (ft)
33	0.454	297.99	430.01	14190.28	3.97
33	0.436	286.18	425.56	14043.49	4.09
33	0.418	274.36	421.11	13896.70	4.22
33	0.4	262.55	416.66	13749.91	4.36
33	0.382	250.73	412.22	13603.13	4.52
33	0.364	238.92	407.77	13456.34	4.69
33	0.346	227.10	403.32	13309.55	4.88
33	0.328	215.29	398.87	13162.76	5.09
33	0.31	203.47	394.42	13015.97	5.33
33	0.292	191.66	389.98	12869.18	5.60
33	0.274	179.85	385.53	12722.40	5.90
33	0.256	168.03	381.08	12575.61	6.24
33	0.238	156.22	376.63	12428.82	6.63
33	0.22	144.40	372.18	12282.03	7.09
33	0.202	132.59	367.73	12135.24	7.63
33	0.184	120.77	363.29	11988.45	8.27

According to the Manual for Bridge Evaluation 3<sup>rd</sup> Edition, bridges constructed with steel girders from 1936 to 1963 should be assumed to have a yield strength of 33 ksi. According to the latest inspection report for the candidate bridge, the beam ends all had deterioration with minimum remaining thickness between 0.13 in to 0.24 in, along with the presence of holes and large general section reduction. With this information going into Table 3.1, the loading position can be over 6 feet and a shear dominated failure can still be expected. It is observed that by including the corrosion in this calculation a shear dominated failure will occur. This will be validated by post processing of the strain rosettes if a 45° Principal strain direction is observed.

### 3.1.2 Lateral Supports

The lateral supports were comprised of two 5-foot-long cantilevered W12x40 steel I-beams with bolted MC8x8.5 C-Channel arms to resist the lateral movement of the test

specimen. The cantilevers are welded to a base plate then bolted to a 6-foot-long W12x72 floorbeam that was bolted into the strong floor. The braces are spaced every five feet along the test specimen due to the strong floor restrictions. The specimen was positioned so that the first of four braces was as close as possible to the beam end to prevent the specimen from sliding off the bearing, with the remaining three braces spaced equally at 5-foot intervals along the length of the specimen. The cantilever I-beams were design according to Appendix 6 in the SCM as discrete braces to ensure the entire system does not sway when lateral movement of the test specimen begins. The design required the beams to meant two limits: strength and stiffness. The required strength was determined by the comparing the max moment the loading configuration can put into the system without failing the strong floor and the plastic moment of the test specimen. It was determined that the plastic moment was the minimum of these two forces and the resulting lateral force transferred to the cantilever is 10.49 kips. For the 5-foot-long cantilevers this resulted in a maximum moment of 52.45 kip\*ft, where the nominal moment capacity of a cantilevered W12x40 was calculated to be 232.8 kip\*ft, thus the design is sufficient. The stiffness of the brace was required to be 7.28 kip/in, where a cantilevered W12x40 has a bending stiffness of 124.8 kip/in.

The MC8x8.5 channel arms were designed to withstand the 10.49 kip lateral load from the plastic moment of the test specimen. The moment developed in the c-channel was assumed to act as a simply supported beam with a concentrated load applied to the weak axis of the web between welded threaded rods. Additionally, the c-channels had ¼” thick sheets of Ultra High Molecular Weight Polyethylene (UHMW) a strong and durable plastic, to ensure a frictionless surface was along the sharp edges of the specimen’s top

flange. The channels were bolted to the cantilevered beam flange to transfer the force to the brace.

Refer to Figure 3.3 for a front view of the lateral torsional buckling brace at the tested end bearing location.

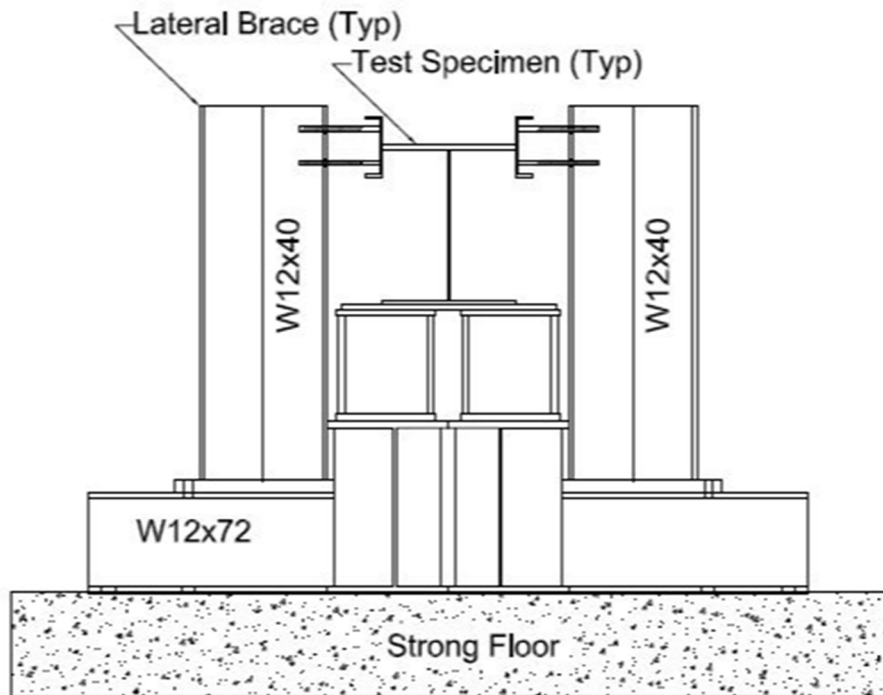


Figure 3.3: Lateral Support at Beam End

### 3.1.3 Vertical Supports

The test specimen rested upon a 2 inch thick steel bearing plate on both the tested and untested end. For the tested end, bearing was supported by (2)-rolled I beams with bolted steel open box sections on the top flange. Additionally, to account for the warped bottom flange high-strength grout was placed beneath the test specimen on top of the bearing plate. This ensured a flat and uniform surface for bearing to distribute over. For the untested end, bearing was supported by a 2'x2'x3' concrete block. Both supports were previously designed members of experiments conducted at UMass and were

sufficient in strength to resist the expected reaction forces. Refer to Figure 3.1 and Figure 3.3 for a representation of the supports.

### 3.2 Description of Specimens

Specimens were selected out of the removed steel girders from the North Approach Span of the candidate bridge. The northbound lane was under deconstruction at the start of this project which was supported by girders 1-4. The girders were cut at midspan and shipped to UMass Amherst for selection. Inspection shows that the girder ends supported by the abutment did not have any significant section loss. The girder ends supported by Pier #4 were heavily deteriorated with general section loss, pitting and holes in various locations along the web and bottom flange.

#### 3.2.1 Description of Specimen 1

The first test specimen was girder 4 from the north approach span. The specimen was a 27'-8" long, interior 33WF125 (33" x 11.5") steel girder. The intact dimensions for this specific beam are listed in Table 3.2.

Table 3.2: Geometric Properties of a 33WF128 Rolled Steel Beam

Beam Type	33WF128
Weight per foot (lb/ft)	128.0
Area, $A_{125}$ (in <sup>2</sup> )	36.78
Flange Thickness, $t_{f,125}$ (in)	0.805
Flange Width, $b_{f,125}$ (in)	11.50
Web Thickness, $t_{w,125}$ (in)	0.57
Total Depth, $D_{125}$ (in)	33.0
Web Depth, $H_{125}$ (in)	31.39
Moment of Inertia, $I_{x,125}$ (in <sup>4</sup> )	6354.7
Section Modulus, $S_{x,125}$ (in <sup>3</sup> )	385.1
Radius of Gyration, $r_{y,125}$ (in)	2.26

The girder end had significant corrosion damage, with a combination of severe thickness loss and multiples holes in the web, see Figure 3.4 for a side view of the girder end. The

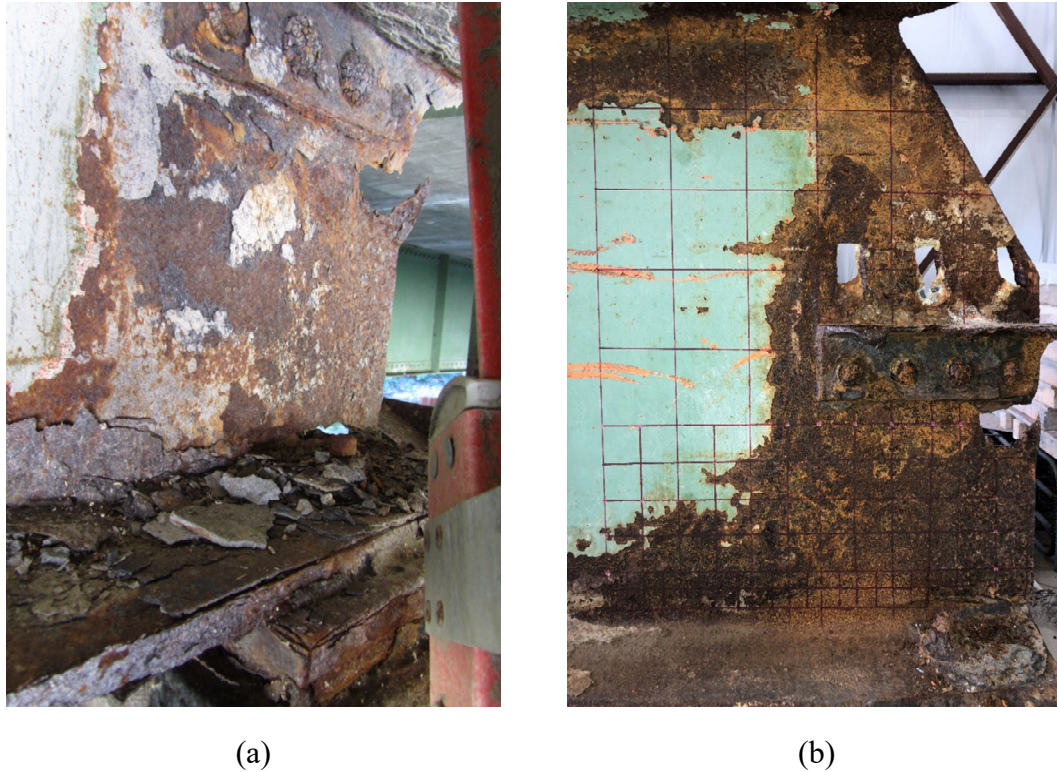


Figure 3.4: Test Specimen 1 a) before deconstruction in the field, b) before testing in the lab.

first hole located below the bolted angles, had dimensions 3" x 2" (length x width). In several cases during reviewing inspection reports, a hole of these dimensions was found in this location under a concrete diaphragm. The second hole is located at the girder end where the web and flange connect, with dimensions 5" x 2". Refer to Figure 3.5 for hole details. In order to accurately be able to capture the full effects of corrosion, a PocketMIKE was used to measure the remaining thickness of the girder ends. A series of measurements were taken along the intersection points of the grid pictured in Figure 2.2b. For the following experiments this same procedure was taken for each deteriorated end. The complete thickness results were used for future FEA analysis and will not be presented. For the



purpose of this thesis when investigating the remaining capacity of the girder ends, to appropriately judge the current code the thickness reported from the last state inspection report will be used. Specimen 1 had an average remaining thickness in the bottom 4 inches of web above bearing of 0.33 inches with hole area neglected from the average thickness.

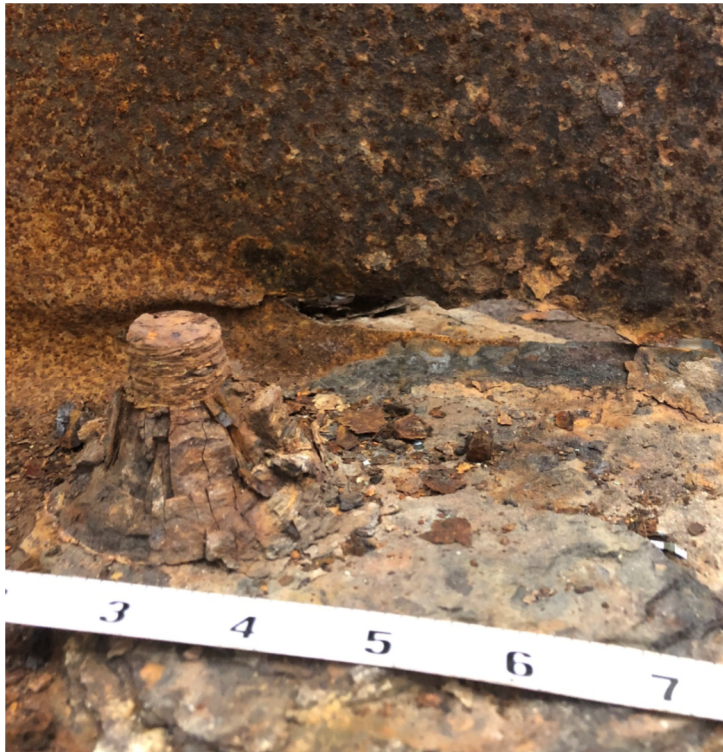


Figure 3.5: (Top) 2"x3" hole under end diaphragm; (Bottom) 5"x2" hole next to crippled section at web-flange connection.

### 3.2.2 Description of Specimen 2

The second specimen was girder 1 in span 5. The beam type was an exterior 33WF132 (33" x 11.51") steel girder, measuring 23'-4" long. The intact dimensions can be found in Table 2.2. The critical aspects of this specimen included sever deterioration of the bottom flange and initial displacement of the web, see Figure 3.6.

Table 2.2: Geometric Properties of a 33WF132 Rolled Steel Beam

Beam Type	33WF132
Weight per foot (lb/ft)	132.0
Area, $A_{132}$ (in <sup>2</sup> )	38.84
Flange Thickness, $t_{f,132}$ (in)	0.880
Flange Width, $b_{f,132}$ (in)	11.51
Web Thickness, $t_{w,132}$ (in)	0.58
Total Depth, $D_{132}$ (in)	33.15
Web Depth, $H_{w,132}$ (in)	31.39
Moment of Inertia, $I_{x,132}$ (in <sup>4</sup> )	6856.8
Section Modulus, $S_{x,132}$ (in <sup>3</sup> )	413.7
Radius of Gyration, $r_{y,132}$ (in)	2.31

As seen, the flange at the bearing plate has been completely corroded, leaving a 5" x 3" hole at the connection. The web was corroded more aggressively along the bottom portion; however, a 45° angle of deteriorated web can be seen going across the length of the bearing plate, refer to Figure 3.7. It will be assumed this will be the expected failure region for this specimen. In conjunction with this deteriorated region, the web also had an initial out of plane displacement of 1.5" from its original  $\bar{C}$ . Previous inspection reports stated initial signs of out of alignment for the web, which ensures this imperfection was not caused due to deconstruction. Specimen 2 had an average remaining thickness in the bottom 4 inches of web along the bearing of 0.32 inches. This specimen differs because there is no hole along the web-flange connection at the girder end.



(a)



(b)

Figure 3.6: Test Specimen 2 a) before deconstruction in the field, b) before testing in the lab.

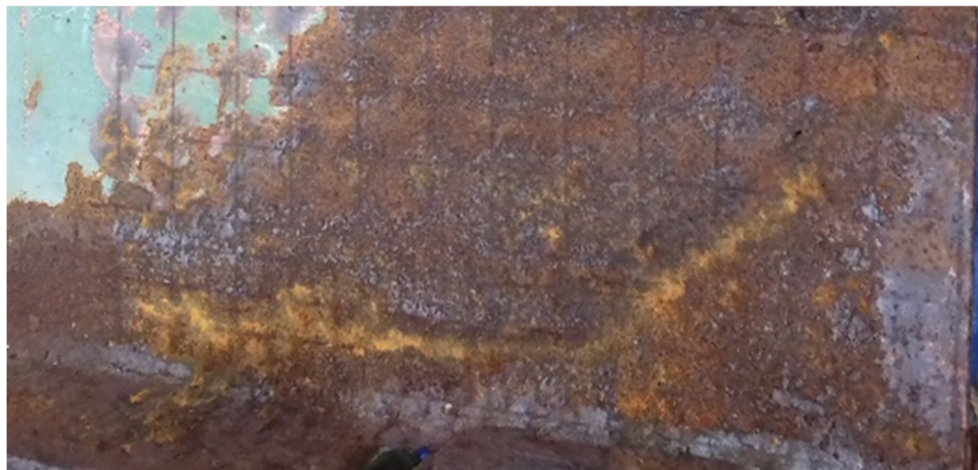


Figure 3.7: 45° Deteriorated Region in Web



### 3.2.3 Description of Specimen 3

The final specimen was girder 3 in span 5, see Figure 3.8. The beam type for this specimen was a 33WF125, the geometric and section properties follow that listed in Table 2.1. The critical conditions of the girder included severe deterioration of the web and multiple holes. Similar to specimen 1, this girder had a whole in the web under the location of the concrete diaphragm, which measured 4" x 2". Observed along the bottom 18" of the web-flange connection is a slit that creates a discontinuity between the two, see Figure 3.9. Unlike the previous specimen with a large hole at the web-flange connection, very little vertical displacement needs to occur before the web is back in contact with the flange. Specimen 3 had an average remaining thickness in the bottom 4 inches of web above bearing of 0.29 inches, neglecting hole area.



(a)



(b)

Figure 3.8: Test Specimen 3 a) before deconstruction in the field, b) before testing in the lab.



Figure 3.9: (Top) 4"x2" hole under end diaphragm; (Bottom) Initial Out-of-Alignment and Web-Flange Discontinuity.

### 3.3 Instrumentation

The instruments used during the experiments included linear potentiometers, displacement transducer, strain rosettes, pressure transducer and load cells. Figure 3.10

represents a typical view of the instrumentation layout. For details on the relative location of linear potentiometers and strain rosettes see Chapter 4 of this paper.

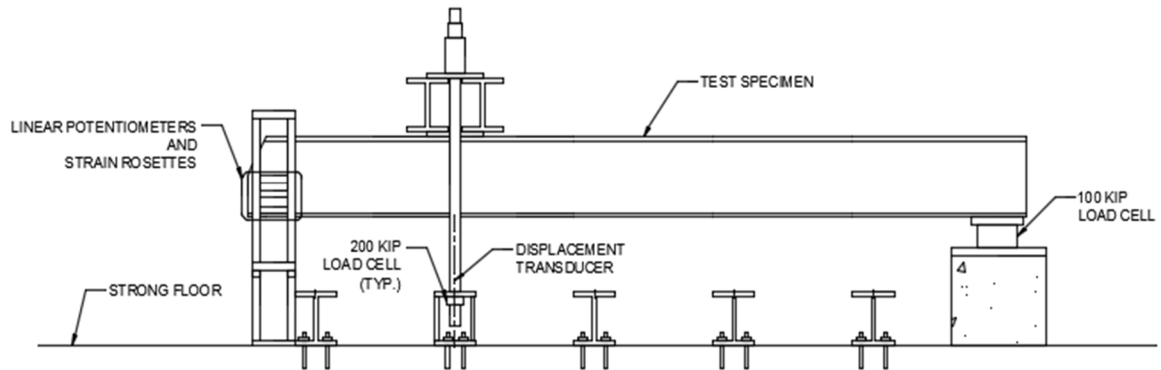


Figure 3.10: Typical Instrumentation Set-Up  
Note: Lateral Bracing and Tested End Support Not Shown for Clarity

### 3.3.1 Load Cells

Various types of load cells were used in order to capture and track the forces on the specimen throughout the experiments. In order to track the force being applied into the system, 200kip through-hole load cells were placed around both threaded anchor rods and positioned inside the anchor block. This captured the force being applied through the hydraulic cylinders into the anchor rod, which was verified with the use of a pressure transducer on the pump applying the pressure. The hydraulic cylinders were able to apply a 60-ton (120 kip) force each at 10,000 psi pressure. The conversion of pressure into force from the transducer should equal the summation of load being tracked by the through-hole load cells at all times during the experiment. In order to prevent instability of the tested end, a third 100 kip load cell was placed at the undamaged and untested end of the girder. Using static equilibrium, the reaction force of the tested end can be solved for.

### **3.3.2 Linear Potentiometers**

Linear potentiometers were bolted to a stud and track frame that was placed next to the tested end to capture the out-of-plane displacement during the experiments. Two vertical rows of four linear potentiometers were used to capture the failure mode at the free end of the girder web and the web within bearing. The potentiometers were spaced vertically at different intervals based on the obstruction and deterioration of the girder end. Additional to the potentiometer, a displacement transducer was attached to the specimen bottom flange and placed under the center of the cross beam in order to record vertical displacement throughout the applied loading.

### **3.3.3 Strain Rosettes**

For each experiment, six strain rosettes were placed within the damaged portion of the tested girder end. The focus was to capture the change in Principal strain direction throughout the duration of loading in the bottom 4" of web. Locations were decided based on the corrosion profile of each girder to capture areas where significant damage was expected to occur.

### **3.4 Summary**

The test rig was designed to withstand the maximum force the strong floor within the UMass Amherst Brack Structural Testing Lab could resist. Additionally, the lateral bracing was designed to withstand any lateral force and displacement through the plastic moment of the test specimens. The three test specimens selected were each from span 5, and the tested end was over pier #4. Similarities in the severity of deterioration to the web,



local to the girder end, was observed in the specimens. Each girder end had extreme deterioration resulting in complete loss of section. Test specimen 1 had holes located under the diaphragm and at the web-flange connection. Test Specimen 2 showed a deteriorated region following a 45° angle within the web along the length bearing, combined with significant initial out-of-plane displacement. Lastly, test specimen 3 had a slit along the last 12” of web-flange connection, allowing full separation between the two. Forces, displacements and strains were all recorded during the experiments using load cells, linear potentiometers, and strain rosettes, respectively.

## CHAPTER 4

### CORRODED STEEL GIRDER TEST RESULTS

#### 4.1 Introduction

This chapter will describe the testing process along with the results from each respective experiment. The specimens were loaded via the hydraulic jack and crossbeam assembly until the failure. Due to the lack of previous research on corroded steel girders from an in-service condition, failure criteria was defined when the force in the system was no longer gaining resistance and only vertical displacement was occurring. While the specimens were being loaded during the experiment, instruments placed within the system measured forces, displacements and strains through and past failure.

#### 4.2 Testing Procedure

The specimens were manual loaded using a SPX Power Team pump and hydraulic cylinder by slowly applying pressure into the system based on the response of the girders. As the specimens were loaded vertical displacement was recorded under the point of loading and forces were recorded by the preciously defined load cells. The hydraulic cylinders were restricted by high-strength hex nuts around the threaded anchor rods, which transferred the force through the crossbeam into the test specimen. The crossbeam was placed so the central connector plate was along the length of the top flange, to prevent a fine point from crushing the web at the location of loading. In most experiments, as the web began to buckle the crossbeam would begin to rotate along with it. This was corrected by the use of valves to control if pressure was being supplied to both or one jack respectively. During the experiment of specimen 3, the shelf-angles began rotating onto

the linear potentiometers leading to the removal of the instruments before peak load. Loading was applied until an increase in reaction force was no longer being seen and the response of the girder to more load resulted only in an excess vertical displacement. Upon termination of the experiments data was collected and analyzed to investigate the force-displacement, failure mode and Principal strain directions of the corroded web end.

### 4.3 Specimen 1 Final Set-Up

Specimen 1 was denoted as a 33WF125 and was interior girder 4 from the north approach span of the candidate bridge. The specimen measured a total length of 27 feet – 8 inches and had an initial effective span length of 24 feet between supports. The specimen was instrumented with eight linear potentiometers and six strain rosettes in the corroded

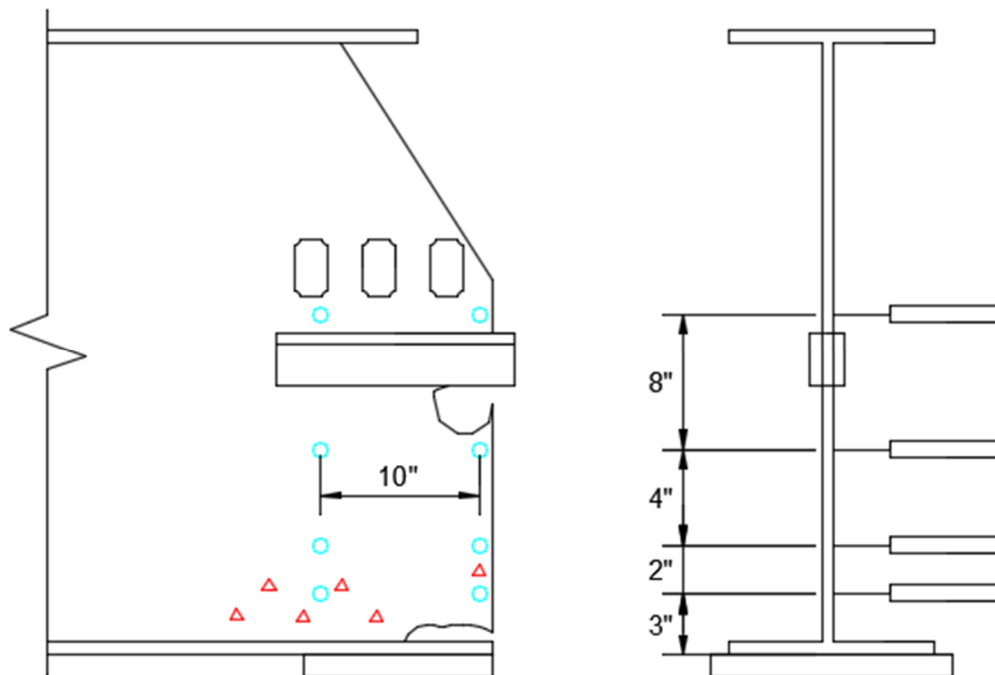


Figure 4.1: Specimen 1 Instrumentation Placement  
 Note: Circles represent location of linear potentiometers and triangles represent location of strain rosettes.

area of the tested end. Figure 4.1 is a detail representation the geometric locations of the

instruments where Figure 4.2 is a photo of instruments on the specimen before loading, Table 4.1 lists the coordinates of the strain rosettes.



Figure 4.2: (Left) Strain Rosettes (Right) Linear Potentiometers

Table 4.1 Relative Location of Strain Rosettes for Specimen 1

Strain Rosette	Relative Coordinates	
	x (in)	y (in)
1	16	2.4
2	14	3.8
3	12	2.4
4	10	3.8
5	8	2.4
6	1	3.8

The relative displacement of the rosettes was measured from the bottom of the girder web at the end web-flange connection. The placement was focused within the bottom 4-inches of web along the critical bearing length according to the MassDOT Bridge Manual.

### 4.3.1 Experiment 1 Results

Specimen 1 was loaded to a maximum applied force of 134.08 kips with a corresponding vertical displacement of 0.48-inches. The specimen stayed stable throughout the experiment and did not experience a large variation in applied load on each side of the crossbeam, see Figure 4.3 for the load-displacement curve.

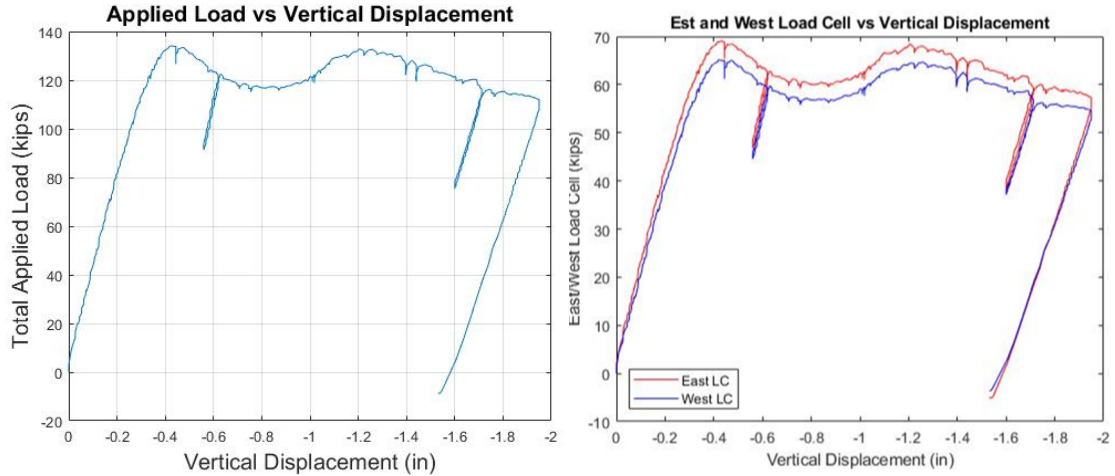


Figure 4.3: (Left) Applied Load – Vertical Displacement Curve (Right) Measured Force Applied by Hydraulic Cylinder on Each Side of Crossbeam.

After the peak load was reached the applied force began to decrease while the specimen saw an increase in vertical displacement, this occurred until a displacement of 0.81-inches, in which the laterally displaced web began bearing on the protruded anchor bolt on the top face of the bottom flange. This allowed the web to enter a new equilibrium and regain back to peak loading. This will not be accounted for in the resistance due to the large vertical displacement it occurred at which would be detrimental to the service condition of the bridge. At the untested and intact end of the specimen was a load cell recording the load being transferred throughout the beam, which using static equilibrium can be used to

calculate the reaction force at the corroded end. Figure 4.4 represents both the intact end and corroded end reaction force from the applied loading.

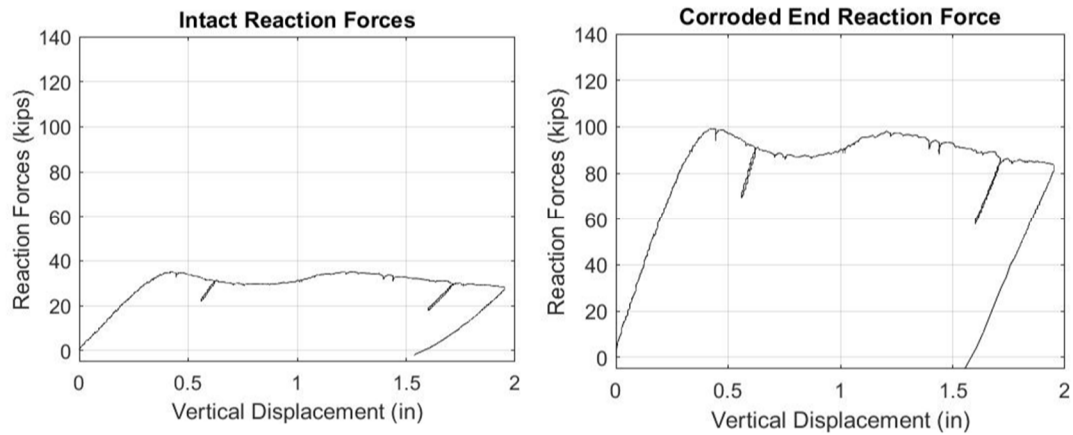


Figure 4.4: (Left) Recorded Reaction Force at Intact End  
(Right) Calculated Reaction Force at Corroded End

The corroded end reached a max reaction force of 99 kips at a displacement of 0.48-inches. According to the geometric layout of the tested span the loading is at 6-feet from the center line of bearing on the tested end, leaving 18-feet from loading to intact. Statics says the load distribution from the applied loading to the intact end should equal 25%. Figure 4.5 shows the distribution of load throughout the experiment to the intact end. Two other effective span lengths were also investigated: outer edge to outer edge of bearing resulting in an effective span length of 25-feet and inside edge to inside edge of bearing resulting in an effective span length of 23-feet. The results show that throughout the duration of loading the effective span length stays around the centerline of bearing, however, after the web began bearing on the anchor bolt the bearing force focused on the outside edge of the corroded end but stayed on the inside edge of the intact end, keeping the same effective span length but allowing closer to 27% of the load to be distributed to the intact end.

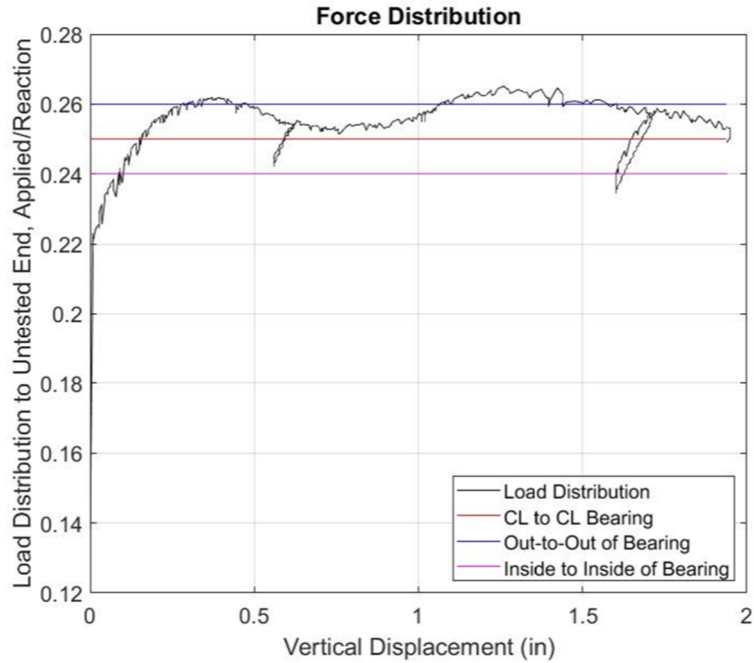


Figure 4.5: Force Distribution to Intact End for Specimen 1

The linear potentiometers were used to capture the failure mode of the corroded end and were placed in two vertical columns of four potentiometers spaced 10-inches apart (see Figure 4.1). The outside column, capturing the lateral displacement right at the girder end

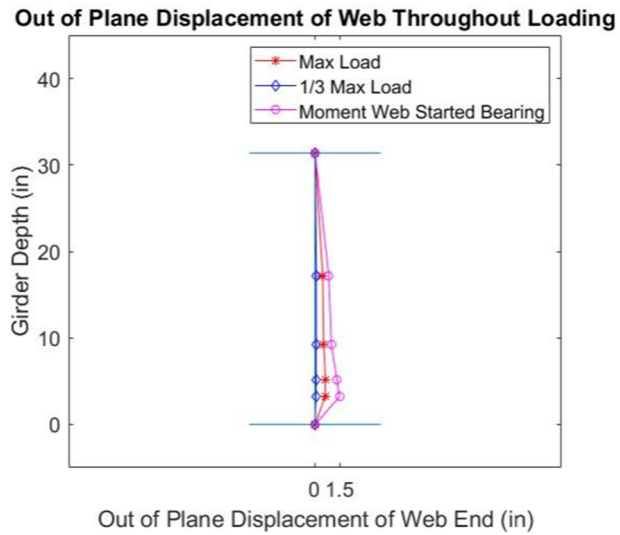


Figure 4.6: Lateral Deformation of Corroded End

is reported in Figure 4.6 for three different positions throughout loading: first at 33% of the peak load, at the peak load and when the web began bearing on the protruded anchor bolt.

In order to validate a shear dominated loading and how the strains within the web vary throughout loading, the strain rosettes were analyzed to determine the Principal strain and direction. Figure 4.7 presents the Principal strain and directions for each of the six rosettes installed on the web of specimen 1.

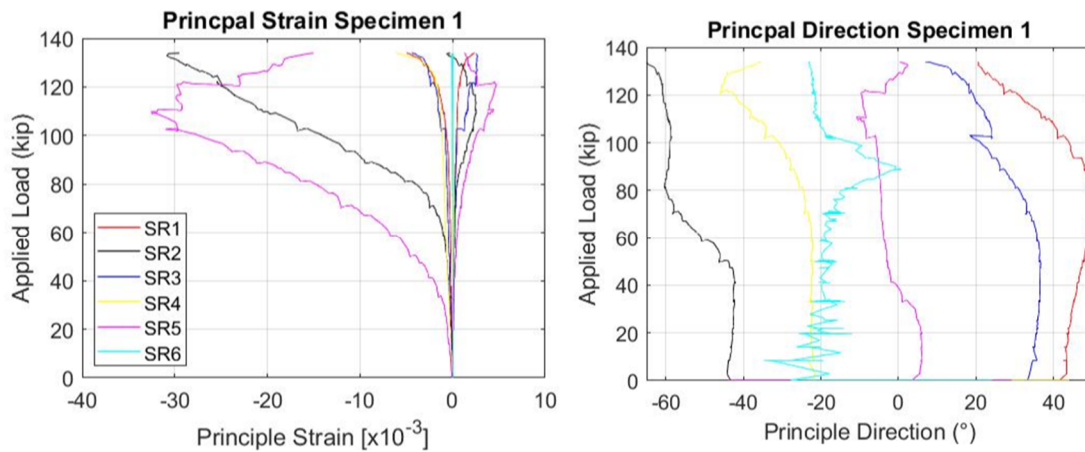


Figure 4.7: (Left) Principal Strain in Web for Specimen 1  
(Right) Principal Strain Direction in Web for Specimen 1

The legend in the Principal strain figure also applies to the corresponding Principal strain direction figure. Strain rosette 5 recorded larger compressive (negative) strains due to its position directly over bearing, whereas strain rosette 2 recorded more compressive strains as the experiment progressed due to it become the location where the web began folding onto itself. The remaining rosettes recording compressive and tensile (positive) strains which means shear strains were present in the web. Using the data presented in Figure 4.7 a visual representation of the changing Principal direction and magnitude is presented in Figure 4.8, where half peak load strains are represented in red and peak load strains in blue.



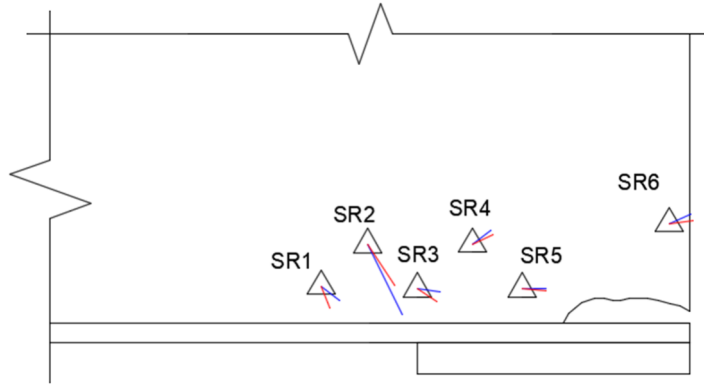


Figure 4.8: Principal Strain Directions Specimen 1

Figure 4.9 shows the failed bottom of web at the end of loading for specimen 1. The web resting on the anchor bolt can be seen and the sliding of the web end occurred due to the hole above bearing.



Figure 4.9: Residual Deformation of Corroded Web End

#### 4.4 Specimen 2 Final Set-Up

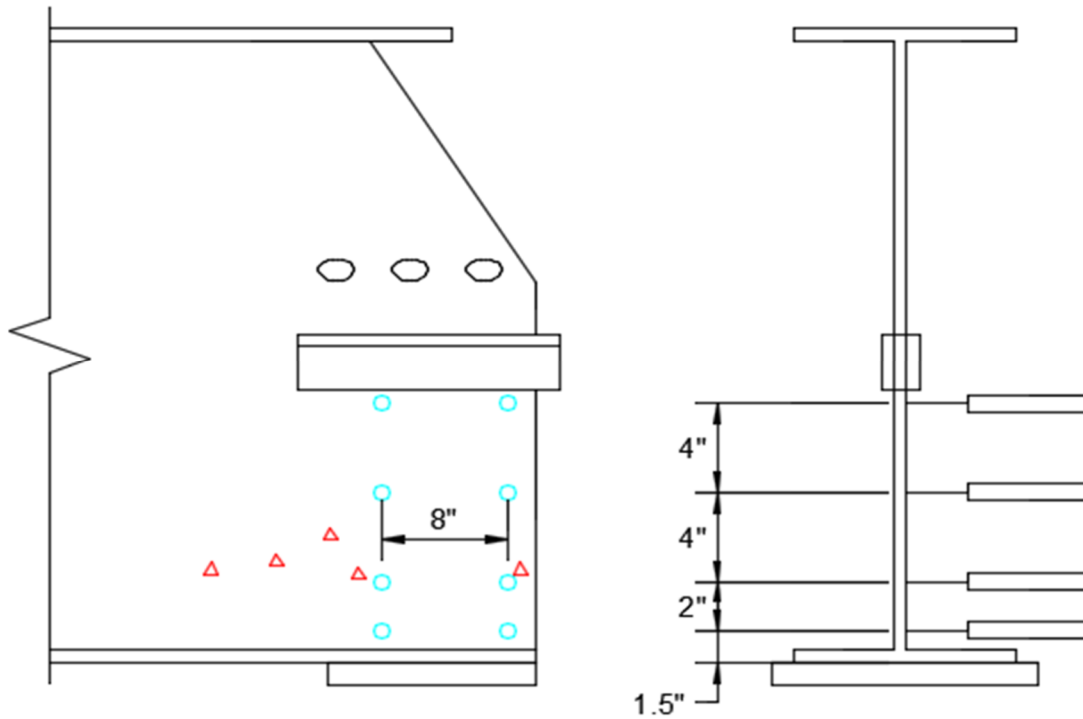


Figure 4.10: Specimen 2 Instrumentation Placement  
Note: Circles represent location of linear potentiometers and triangles represent location of strain rosettes.

Specimen 2 was denoted as a 33WF132 and was exterior girder 1 from the north approach span of the candidate bridge. The specimen measured a total length of 23 feet – 11 inches and had an initial effective span length of 22 feet – 9 inches between supports. The specimen was instrumented with eight linear potentiometers and six strain rosettes in the corroded area of the tested end. Figure 4.10 is a detail representation the geometric locations of the instruments where Figure 4.11 is a photo of instruments on the specimen before loading, in which the initial out-of-plane displacement of the web can be seen. Table 4.2 lists the coordinates of the strain rosettes. Strain rosette 1 was placed on the flange to gain data for future possible work and will not be represented in this paper.

Table 4.2 Relative Location of Strain Rosettes for Specimen 2

Strain Rosette	Relative Coordinates	
	x (in)	y (in)
2	18	4
3	14.5	4.5
4	10	4
5	12	6.5
6	1	4.5



Figure 4.11: (Left) Strain Rosettes (Right) Linear Potentiometers

The relative displacement of the rosettes was measured from the bottom of the girder web at the end web-flange connection. The placement was focused within the bottom 4-inches of web along the critical bearing length according to the MassDOT Bridge Manual.

#### 4.4.1 Experiment 2 Results

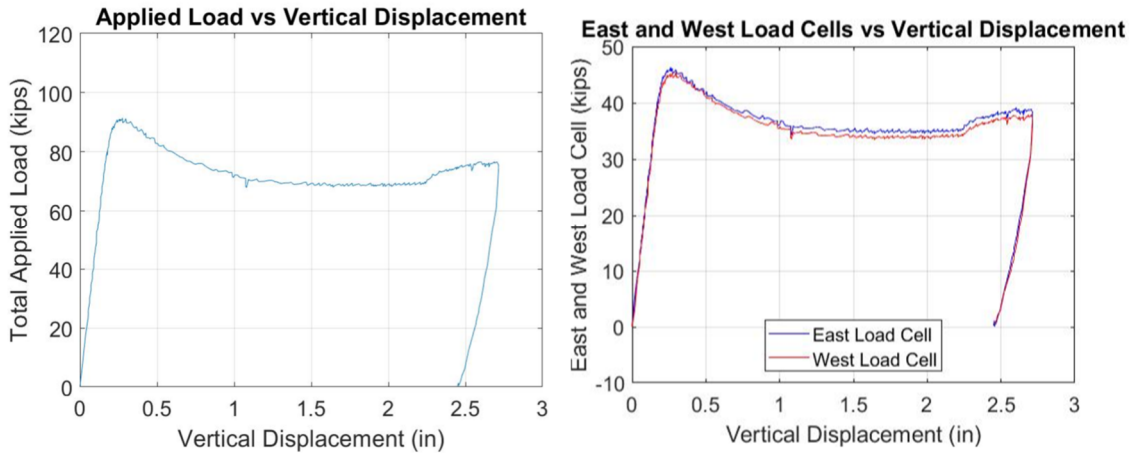


Figure 4.12: (Left) Applied Load – Vertical Displacement Curve  
(Right) Measured Force Applied by Hydraulic Cylinder on Each Side of Crossbeam.

Specimen 2 was loaded to a maximum applied force of 91.3 kips with a corresponding vertical displacement of 0.3-inches. The specimen stayed stable throughout the experiment and experienced almost no variation in applied load on each side of the crossbeam, see Figure 4.12 for the load-displacement curve.

After the peak load was reached the applied force began to decrease while the specimen saw an increase in vertical displacement, this occurred until a displacement of

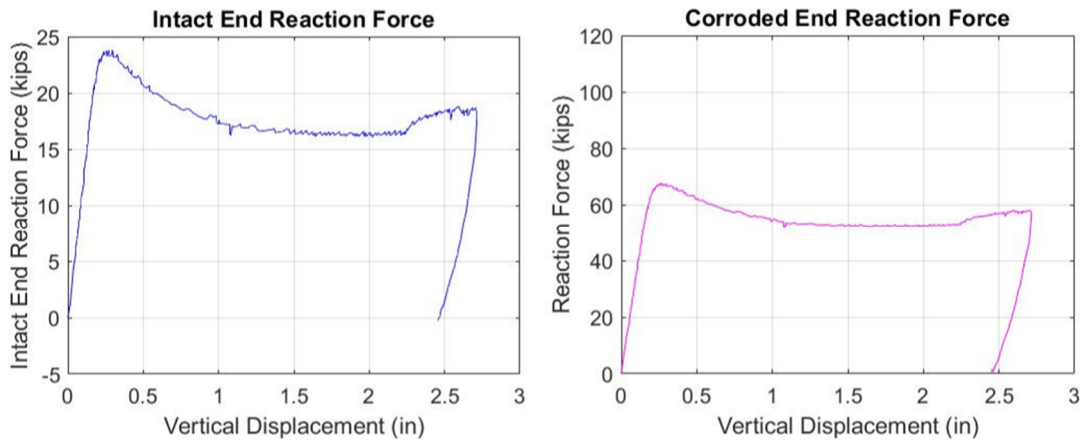


Figure 4.13: (Left) Recorded Reaction Force at Intact End  
(Right) Calculated Reaction Force at Corroded End

2.125-inches, in which the laterally displaced web began bearing on the top face of the bottom flange. This occurred because specimen 2 did not have a hole above bearing, allowing for a large uplift of the girder end and the bearing force concentrated at the inner part of the bearing. This allowed the web to enter a new equilibrium and regain back to some strength. This will not be accounted for in the resistance due to the large vertical displacement it occurred at which would be detrimental to the service condition of the bridge. At the untested and intact end of the specimen was a load cell recording the load being transferred throughout the beam, using static equilibrium the reaction force at the corroded end can be solved for. Figure 4.13 represents both the intact end and corroded end reaction force from the applied loading.

The corroded end reached a max reaction force of 67.6 kips at a displacement of 0.3-inches. According to the geometric layout of the tested span the loading is at 6-feet from the center line of bearing on the tested end, leaving 16 feet – 9 inches from loading to intact. Statics

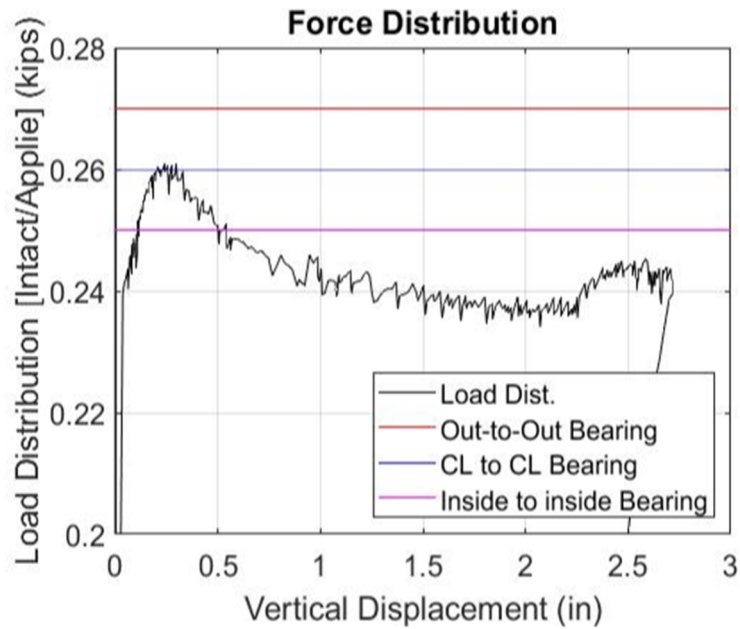


Figure 4.14: Force Distribution to Intact End for Specimen 2

says the load distribution from the applied loading to the intact end should equal 26%. Figure 4.14 shows the distribution of load throughout the experiment to the intact end. Two other effective span lengths were also investigated: outer edge to outer edge of bearing resulting in an effective span length of 23 feet – 9 inches and inside edge to inside edge of bearing resulting in an effective span length of 22 feet – 9 inches. The results show that throughout the duration of loading the effective span length stays below the centerline of bearing, and in most cases is below the inner to inner bearing. This is attributed to the uplift at the end of bearing, causing the effective span length to change from inner of bearing on the corroded end to outer bearing at the intact end. This occurrence causes the effective length to stay at 22 feet – 9 inches, however, the distance to loading is now cut to 5 feet - 6 inches from the corroded end, allowing the distribution to drop to 24% for the intact end. As the bearing kept uplifting and began bearing on the bottom flange additional load was distributed to the corroded end explaining the further decrease from 24%.

The linear potentiometers were used to capture the failure mode of the corroded end and were placed in two vertical columns of four potentiometers spaced 8-inches apart

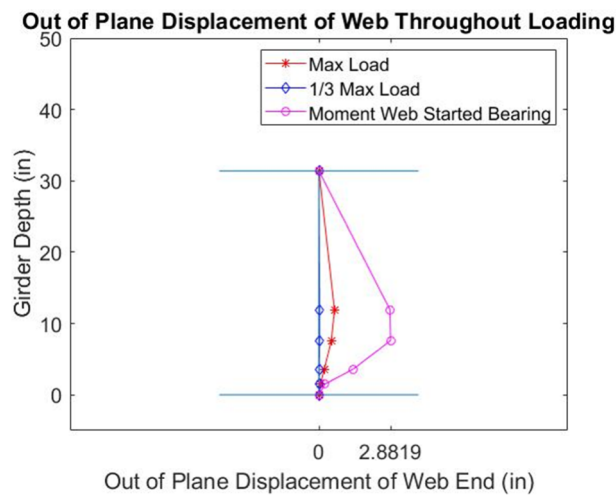


Figure 4.15: Lateral Deformation of Corroded End

(see Figure 4.10). The outside column, capturing the lateral displacement right at the girder end is reported in Figure 4.15 for three different positions throughout loading: first at 33% of the peak load, at the peak load and when the web began bearing on the protruded anchor bolt.

In order to validate a shear dominated loading and how the strains within the web vary throughout loading, the strain rosettes were analyzed to determine the Principal strain and direction. Figure 4.16 presents the Principal strain and directions for each of the five rosettes installed on the web of specimen 2.

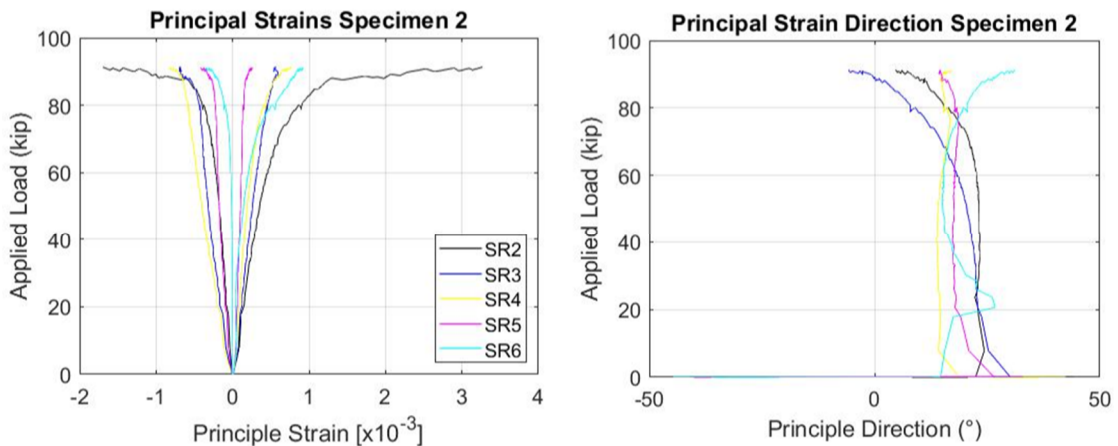


Figure 4.16: (Left) Principal Strain in Web for Specimen 2  
(Right) Principal Strain Direction in Web for Specimen 2

The legend in the Principal strain figure also applies to the corresponding Principal strain direction figure. All six rosettes recorded equal and equivalent compressive (negative) and tensile (positive) strains which means shear strains were present in the web. This validates that it was a shear dominated failure outside of the shear region for intact properties. Using the data presented in Figure 4.16 a visual representation of the changing Principal direction



and magnitude is presented in Figure 4.17, where half peak load strains are represented in red and peak load strains in blue.

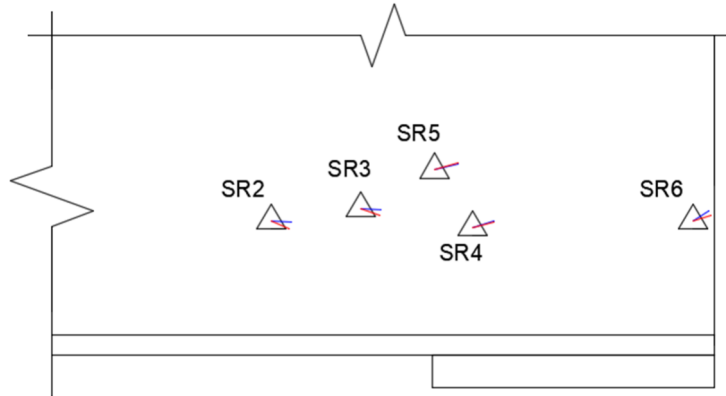


Figure 4.17: Principal Strain Directions Specimen 2

Figure 4.18 shows the failed web and uplift at the end of loading for specimen 2. The web failure can be seen to follow the previously defined 45° corroded region on the web.



Figure 4.18: Residual Deformation of Corroded Web End



#### 4.5 Specimen 3 Final Set-Up

Specimen 3 was denoted as a 33WF125 and was interior girder 3 from the north approach span of the candidate bridge. The specimen measured a total length of 27 feet – 11 inches and had an initial effective span length of 24 feet – 6 inches between supports. The specimen was instrumented with eight linear potentiometers and six strain rosettes in

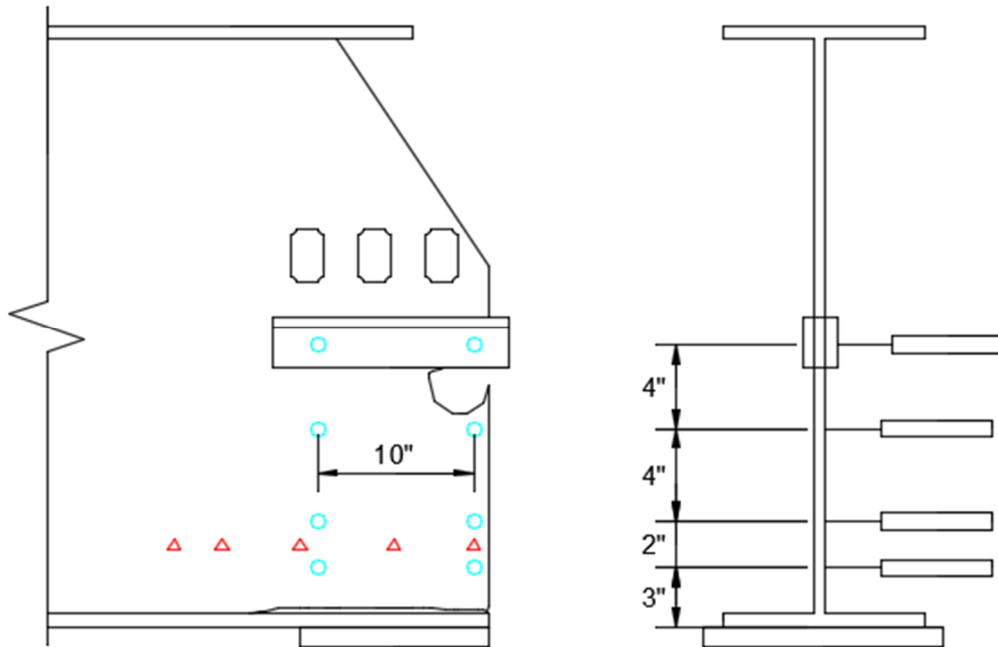


Figure 4.19: Specimen 3 Instrumentation Placement  
Note: Circles represent location of linear potentiometers and triangles represent location of strain rosettes.

the corroded area of the tested end. Figure 4.19 is a detail representation the geometric locations of the instruments where Figure 4.20 is a photo of instruments on the specimen before loading, Table 4.3 lists the coordinates of the strain rosettes. Strain rosette 3 was placed on the flange to gain data for possible future analysis and will not be included in the results.



Figure 4.20: (Left) Strain Rosettes (Right) Linear Potentiometers

Table 4.1 Relative Location of Strain Rosettes for Specimen 3

Strain Rosette	Relative Coordinates	
	x (in)	y (in)
1	22	4
2	19	4
4	13	4
5	6	4
6	1	4

The relative displacement of the rosettes was measured from the bottom of the girder web at the end web-flange connection. The placement was focused at the threshold for the bottom 4-inches of web along the critical bearing length according to the MassDOT Bridge Manual.

### 4.5.1 Experiment 3 Results

Specimen 3 was loaded to a maximum applied force of 112.45 kips with a corresponding vertical displacement of 0.95-inches. The specimen stayed stable throughout the experiment and did not experience any variation in applied load on each side of the crossbeam, see Figure 4.21 for the load-displacement curve.

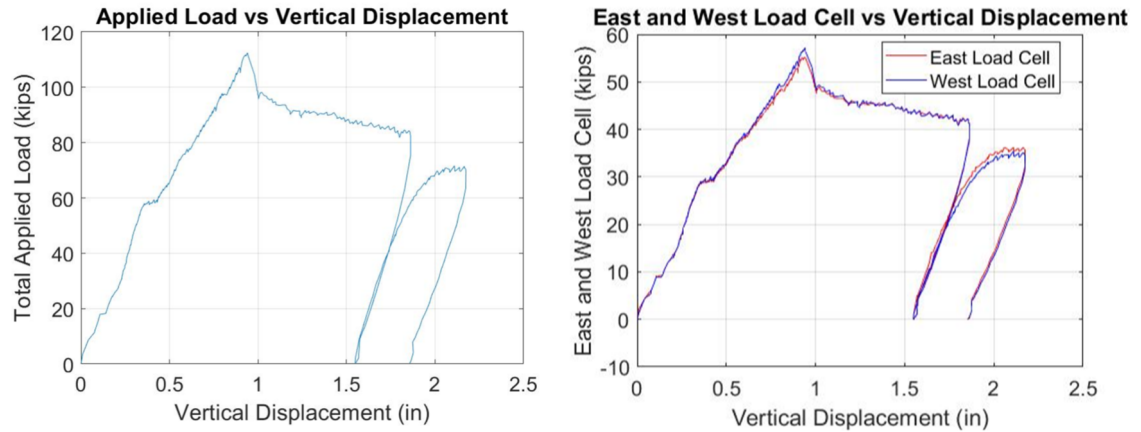


Figure 4.21: (Left) Applied Load – Vertical Displacement Curve (Right) Measured Force Applied by Hydraulic Cylinder on Each Side of Crossbeam.

After the peak load was reached the applied force began to decrease and the girder never found a new equilibrium as in the previous two specimens. As the specimen was loaded the web began sliding across the face of the bottom flange due to the 18-inch long discontinuity along the web-flange connection. Unlike specimen one with a taller hole over bearing, the web did not bear down on the flange and see an increase in reaction force. At the untested and intact end of the specimen was a load cell recording the load being transferred throughout the beam, which using static equilibrium can be used to calculate the reaction force at the corroded end. Figure 4.22 represents both the intact end and corroded end reaction force from the applied loading.

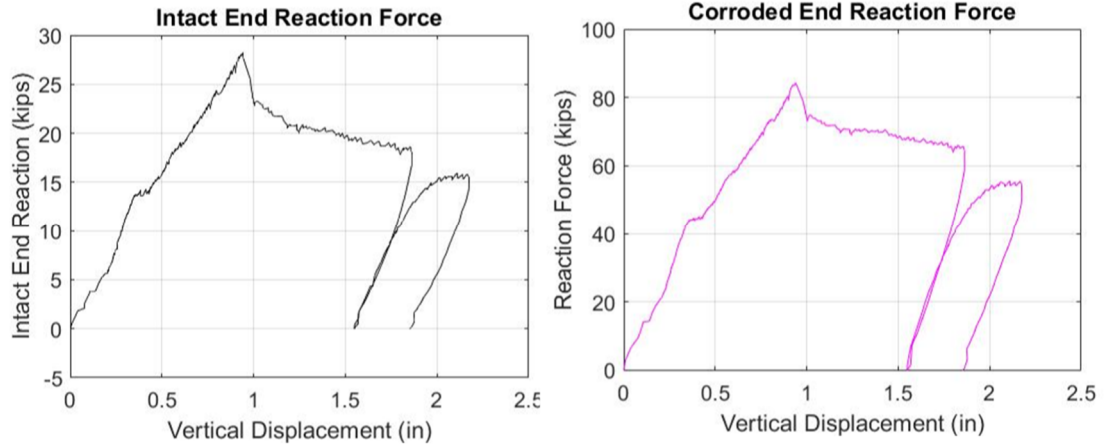


Figure 4.22: (Left) Recorded Reaction Force at Intact End  
(Right) Calculated Reaction Force at Corroded End

The corroded end reached a max reaction force of 84.3 kips at a displacement of 0.95-inches. According to the geometric layout of the tested span the loading is at 6-feet from the center line of bearing on the tested end, leaving 18 feet – 6 inches from loading to intact. Statics says the load distribution from the applied loading to the intact end should equal 24.5%. Figure 4.23 shows the distribution of load throughout the experiment to the intact end. Two other effective span lengths were also investigated: outer edge to outer edge of bearing resulting in an effective span length of 25 feet – 6 inches and inside edge to inside edge of bearing resulting in an effective span length of 23 feet – 6 inches. The results show that throughout the duration of loading the specimen does not attain the effect span length except for at peak loading. Directly after the peak load the specimen immediately lost all resistance and the load distribution shows no load being gained and only vertical displacement occurring. Unlike the other specimens, this specimen showed to hold little elastic response and failed immediately from peak.

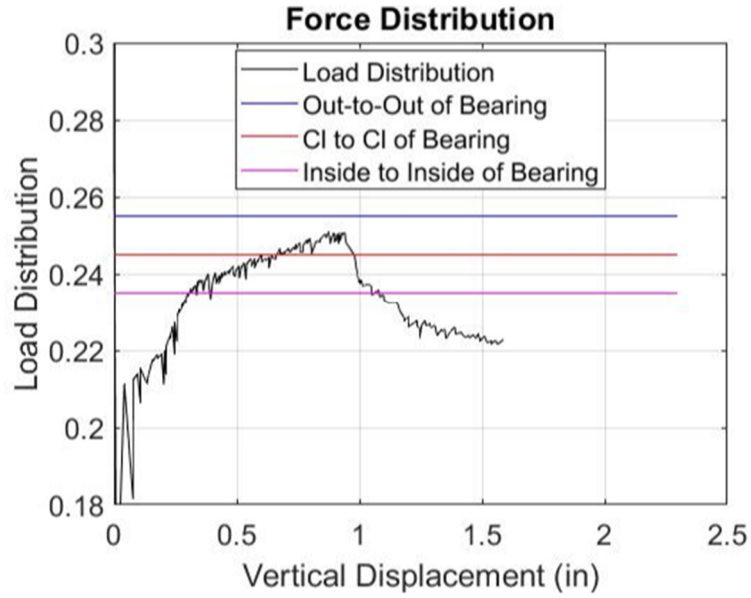


Figure 4.23: Force Distribution to Intact End for Specimen 3

The linear potentiometers were used to capture the failure mode of the corroded end and were placed in two vertical columns of four potentiometers spaced 10-inches apart (see Figure 4.19). The outside column, capturing the lateral displacement right at the girder end

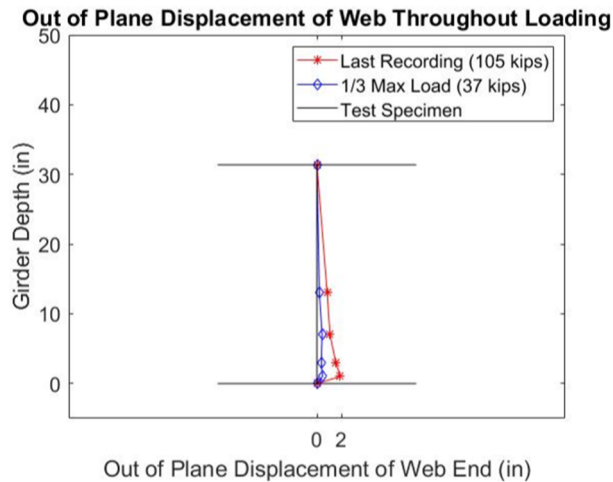


Figure 4.24: Lateral Deformation of Corroded End

is reported in Figure 4.24 for two different positions throughout loading: first at 33% of the peak load, and the last recording taken before the web began bearing on the instruments.

In order to validate a shear dominated loading and how the strains within the web vary throughout loading, the strain rosettes were analyzed to determine the Principal strain and direction. Figure 4.25 presents the Principal strain and directions for each of the six rosettes installed on the web of specimen 3.

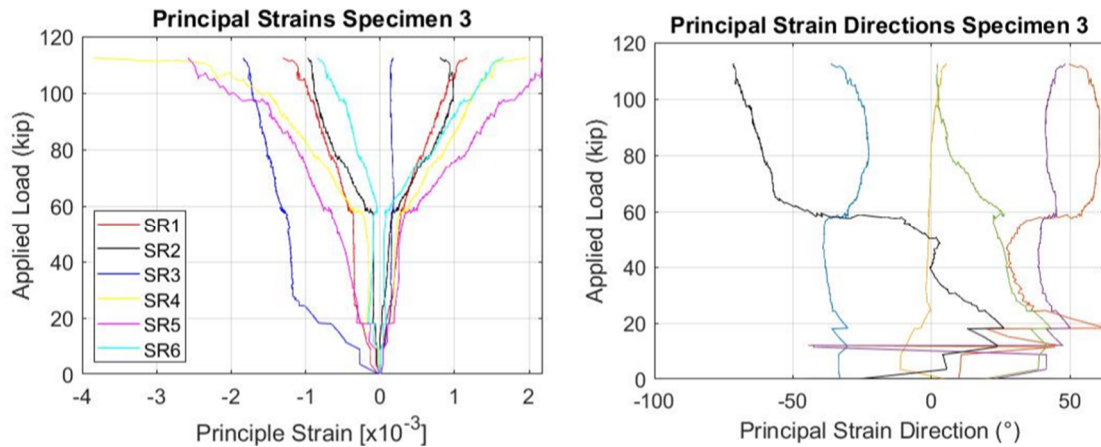


Figure 4.25: (Left) Principal Strain in Web for Specimen 3  
(Right) Principal Strain Direction in Web for Specimen 3

The legend in the Principal strain figure also applies to the corresponding Principal strain direction figure. All rosettes recorded equal and opposite compressive (negative) and tensile (positive) strains which means shear strains were present in the web. A shear dominated failure occurred with the presence of a separation in web-to-flange connection. Using the data presented in Figure 4.25 a visual representation of the changing Principal direction and magnitude is presented in Figure 4.26, where half peak load strains are represented in red and peak load strains in blue.

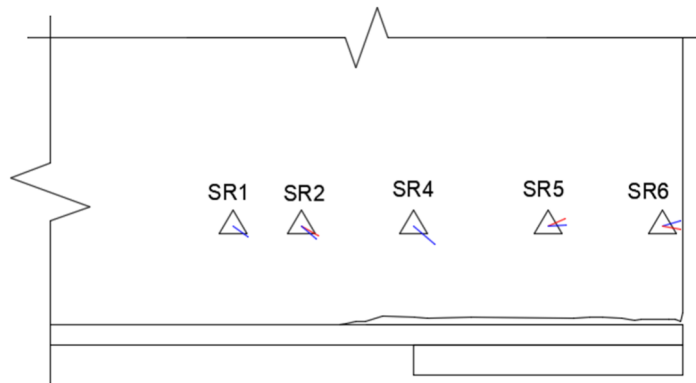


Figure 4.26: Principal Strain Directions Specimen 3

Figure 4.27 shows the failed bottom of web at the end of loading for specimen 3. The web resting on the anchor bolt can be seen and the sliding of the web end occurred due to the hole above bearing.



Figure 4.27: Residual Deformation of Corroded Web

#### 4.6 Comparison of Experimental Results to Code Predicted Values

In order to validate the current procedures of the code, resistances for each corroded girder end was determined using the methodology in Section 2.9 of the *MassDOT LRFD Bridge Manual*. Refer to Chapter 5 for a detailed explanation of how to calculate the resistances. Table 4.4 lists the values calculated from the code compared against the previously determined reaction forces from each specimen. It was determined that for specimen 1 and specimen 3, each with a hole above bearing, the code significantly under predicts the resistance of the corroded girder end by 50% and 100% respectively. Currently the code completely disregards the full 4-inch depth of web when any size hole is present. The length of the hole is subtracted from a critical web length that if the hole is larger, will cause the resistance to go to 0 (as in specimen 3). For specimen 1, according to the code with a 5-inch long hole, it loses roughly 50% of the true resistance.

Table 4.4: Comparison of Code Predicted Resistances against Experimental Results

Specimen	Experiment Reaction Force at Peak Load (kips)	Corroded Web Factored Resistance (kips)	Percent Difference
Specimen 1 Interior Girder 4	99.00	49.18	50%
Specimen 2 Exterior Girder 1	67.60	129.10	48%
Specimen 3 Interior Girder 3	84.30	0.00	100%

Specimen 2 was unique in the sense it did not have a hole above bearing, however, it had a large initial out-of-plane displacement of the web. The current procedure in the code does not account for initial unalignment, which the experiments proved has a significant impact on the remaining resistance of a corroded steel girder end. These results



will be used in Chapter 5 to present the change in the load rating when using experimental values against code procedure.

## **CHAPTER 5**

### **MASSDOT LOAD RATING PROCEDURE**

#### **5.1 Introduction**

This chapter will describe the Load and Resistance Factor Rating (LRFR) load rating procedure for steel girder bridges in Massachusetts, both from a general philosophy and one that considers corrosion of the web end. MassDOT currently utilizes three codes for load rating: the MassDOT Bridge Design Manual, the AASHTO LRFD Bridge Design Specification, and the Manual for Bridge Evaluation (MBE). Using the most current versions of the codes, the corroded web resistance will be determined and compared against the maximum reaction force developed at the tested end during the experiments described in Chapter 4 of this paper. Lastly, a load rating of the tested girders using Massachusetts design and legal trucks is presented to see how the change in resistance effects the structural state of the bridge. Refer to Appendix C for distribution equations, general load rating equation, truck loading details. Additionally, refer to Appendix D for the calculations of dead load shear, live load shear, distribution factors, corroded web resistances, and load factors.

#### **5.2 Description of Typical Load Rating Methodology for Candidate Bridge**

Load ratings are performed to evaluate bridges below standard and make decisions on the safe load carrying capacity of a bridge based off the trucks that use the travel way. Load ratings also help the state to classify structural deficient bridges within the state bridge rehabilitation program. The load rating procedure for a steel girder bridge in Massachusetts is required to be in alignment with the methodology described in Chapter 7

of the *MassDOT Bridge Design Manual*. Load ratings are typically performed under the same methodology originally used to design the bridge. Majority of bridges in Massachusetts were built in the early-to-mid 1900s and design using the Allowable Stress Design (ASD) method. When the Central Artery was constructed through downtown Boston in the early 1950's several bridges were built to carry the elevated highway and interstates above the busy inner streets, which were typically designed using the Load Factor Design (LFD) method. More recent bridges built since the early 1970's were designed by the Load and Resistance Factor Design (LRFD) method, refer to Appendix C for a brief explanation in the differences between methodologies. The candidate bridge for this project was designed and constructed during the 1930's, which means the design methodology was ASD, however, for the purpose of this project the bridge will be analyzed using the LRFR method described in Section 6A of the *AASHTO Manual for Bridge Evaluation*. For steel bridges Section 6A.6 *AASHTO Manual for Bridge Evaluation* should be used. Load rating of an existing structure requires the as-built plans with field verification of any rehabilitation that has occurred, along with the most recent routine member inspection report noting section loss criteria of girder ends. Section 7.2.2.1 of the *MassDOT Bridge Manual* states "points of interest" (POI) where a rating factor must be calculated. Relating to a simply supported bridge with rolled steel girders the POI include: 0.5L for moment, points of support for shear and locations of measurable section loss.

The manual requires rating factors to be determined at two working levels: inventory and operating. The inventory level is described as the safe load carrying capacity of a bridge under service conditions over an indefinite time period. Meaning unlimited trips of a truck can run over the spans and no risk to the bridge collapsing will occur. The

operating level is considered the maximum load a bridge shall ever carry. Inventory and operating rating factors are determined by the use of separate load and resistance factors as described in Table B6A-1 of the *AASHTO Manual for Bridge Evaluation*. The inventory level always having the higher value, typically by a factor of 1.3\*Operating.

Dead loads are calculated for both inventory and operating with the same distribution method and with the same load factors. Live load shear is required to be calculated for the design load of the original bridge, which for LRFR is the HL-93 design load and the local state legal vehicles. Additionally, NCHRP Report 575 described the legal loads do not accurately represent the specialized hauling vehicles (SHVs) (i.e. a dump truck) that operate in most states across the country (MassDOT, 2018). For this reason, AASHTO developed specialized vehicles designed to capture these larger force effects, for the purpose of this study these vehicles will not be looked at. Specific to the state of Massachusetts the posting vehicles are identified as a H20 truck, a Type 3 truck, and a Type 3S2 truck. These vehicles along with the HL-93 Design loading will be studied.

The second component to a load rating is the individual structural components resistances. Depending on the type of rating being conducted will determine the resistance being calculated. For example, in a truss bridge the primary truss members will only support axial force, so the resistance to be calculated for the load rating would be the members tensile and compressive resistance. For this research project shear at the supports was the critical failure mechanism under investigation, thus the resistance provided from the code will be that of web shear. The loads and resistances are then combined into the following general load rating equation:

$$RF = \frac{C - \gamma_{DC}(DC) - \gamma_{DW}(DW)}{\gamma_{LL}(LL + IM)} \quad (\text{Eq. 5.1})$$

where:

RF = Rating Factor

C = Nominal Capacity =  $\phi R_n$

DC = Force effects from non-composite permanent dead loads

DW = Force effects from composite wearing surface and utilities

LL = Force effect from live load vehicle

IM = Dynamic allowance factor = 0.33

$\phi$  = LRFD resistance factor

$\gamma_{DC}$  = Non-composite dead load factor = 1.25

$\gamma_{DW}$  = Wearing surface and utility load factor = 1.5

$\gamma_{LL}$  = Vehicle specific live load factor

Equation 5.1 can be altered into more detail depending on the type of superstructure component being rated along with any special provisions that are apparent on the structure. Once a rating factor is determined it can be multiplied by the respective live load vehicle used in the calculation. This results in the below equation:

$$RT = RF(W) \quad (\text{Eq. 5.2})$$

where:

RT = Bridge member rating (tons)

W = Total weight of live load vehicle used to determine the live load effect (tons)

Equation 5.2 leads to the posting weight on bridges. When a vehicle's rating is below 1.0, the resulting bridge member rating in tons will be below the nominal weight of the vehicle, thus a posted weight limit is required on the bridge.

The load rating produced later in this chapter will focus on section loss of the web above points of support and will be in conjunction with the experiments where specimens were loaded predominately in shear. The study will focus on following the LRFR flowchart within Appendix B6A of the *AASHTO Manual for Bridge Evaluation*, where the first step is to load rate critical components with the HL-93 design loading. This is done because for LRFD design this is the controlling vehicle, therefore it is critical to have a load rating above 1.0 for all components. As previously mentioned, the candidate bridge was not designed using the LRFD method, however, it will still be rated for this vehicle. If a bridge rates above 1.0 for the inventory level on all structural components for HL-93 Loading, no legal vehicles are required to be checked and the engineer can go directly to any site specific permit trucks. In the case structural components rate below 1.0 for the inventory level, the engineer must go and check those components for the inventory and operating level of all design and legal vehicles. Rating factors for the corroded girder ends will be calculated using this process and compared against the same process with the reaction forces determined from the full-scale experiments previously defined in this paper for the HL-93 Design Loading and all Posting Vehicles in Massachusetts.

### **5.2.1 Dead Loads of Candidate Bridge**

Dead loads are considered permanent loads on the bridge due to self-weight of all structural components (i.e. deck, girders, diaphragms, etc.) and superimposed loads such as wearing surface and barriers. The north approach span (span 5) of the candidate bridge supported a 6½ inch reinforced concrete deck with an emulsified asphalt and peastone wearing surface. Interior concrete diaphragms that measure 31 inches deep by 8 inches

wide will be distributed as a uniform line load along the full length of the girder to keep force diagrams symmetrical (MassDOT, 2018). End concrete diaphragms that measure 16 inches deep and 12 inches wide are considered critical to the dead load shear calculation and will be applied at supports as concentrated loads. The reinforced concrete post and fence on the exterior of the travel lanes will be considered under two conditions: first, all load is distributed equally across the seven girders, and second by application of the pile cap analogy. Refer to Appendix C, Section C.3 for a more detailed explanation behind the distribution of dead loads for steel stringer bridges. Table 5.1 through Table 5.3 list the factored dead loads applied to exterior and interior girders for the candidate bridge, along with the resulting factored dead load shear applied to the girder end over Pier #4.

Table 5.1: Factored Dead Load Shear for Girder 1 (Specimen 2)

Component	Distribution Method	Load Factor	Exterior Girder 1 @ Pier #4	
			Line Load (klf)	DL <sub>shear</sub> (kips)
Deck	Trib-Width	1.25	0.322	10.05
Girder	Self-Load	1.25	0.132	4.13
Int Diaphragm	Uniform	1.25	0.065	2.02
End Diaphragm	Trib-Width	1.25	0.20	0.99
Wearing Surface	Equal	1.5	0.20	7.5
Concrete Barrier	Equal	1.25	-	-
	Pile-Cap	1.25	0.322	10.06

$$\Sigma = 34.75 \text{ kips}$$

Table 5.2: Factored Dead Load Shear for Girder 3 (Specimen 3)

Component	Distribution Method	Load Factor	Interior Girder 3 @ Pier #4	
			Line Load (klf)	DL <sub>shear</sub> (kips)
Deck	Trib-Width	1.25	0.406	12.70
Girder	Self-Load	1.25	0.125	3.91
Int Diaphragm	Uniform	1.25	0.116	3.63
End Diaphragm	Trib-Width	1.25	0.20	1.25
Wearing Surface	Equal	1.5	0.20	7.5
Concrete Barrier	Equal	1.25	0.191	5.96
	Pile-Cap	1.25	-	-

$$\Sigma = 34.94 \text{ kips}$$

Table 5.3: Factored Dead Load Shear for Girder 4 (Specimen 1)

Component	Distribution Method	Load Factor	Interior Girder 4 @ Pier #4	
			Line Load (klf)	DL <sub>shear</sub> (kips)
Deck	Trib-Width	1.25	0.406	12.70
Girder	Self-Load	1.25	0.125	3.91
Int Diaphragm	Uniform	1.25	0.103	3.23
End Diaphragm	Trib-Width	1.25	0.20	1.25
Wearing Surface	Equal	1.5	0.20	7.5
Concrete Barrier	Equal	1.25	0.191	5.96
	Pile-Cap	1.25	-	-

$$\Sigma = 34.54 \text{ kips}$$

### 5.2.2 Live Loads for Candidate Bridge

Live load for the candidate bridge will be design and legal truck loads as described by the *MassDOT Bridge Design Manual*. The trucks of interest for this project will be the HL-93 Design Loading, a H20 Vehicle, a Type 3 Vehicle and a Type 3S2 Vehicle, for a detailed explanation of these vehicles see Section C.2.2 of Appendix C in this paper. The HS-20 Vehicle will be omitted from this study because it is the same loading as the HL-93 Design without the presence of a lane load, also the HS-20 is not considered a posting vehicle which are the legal loads being focused on. By inspection, placing the rear axle of



each vehicle over the support at Pier #4 with the remaining axles spaced towards midspan will create the largest live load shear at the support. The total shear is then multiplied by the dynamic load allowance which magnifies the shear because it is not a static load but a transient load. Table 5.4 lists the unfactored live load shear for each type of vehicle and load factors for inventory and operating rating conditions. Table 5.5 lists the factored live load shear that will be multiplied by the distribution factors to get the correct load to interior and exterior girders.

Table 5.4 Unfactored Shear from Live Loads and Appropriate Load Factors

Vehicle	Unfactored Shear (kips)	IM	LRFR Load Factors	
			INV	OPER
H20	37.76	1.33	1.71	1.32
Type 3	42.56	1.33	1.71	1.32
Type3S2	45.2	1.33	1.71	1.32
HL-93	58.56	1.33	1.75	1.35
Lane	16	1	1.75	1.35

Table 5.5 Inventory and Operating Live Load Shears

Vehicle	Factored Shear INV (kips)	Factored Shear OPER (kips)
H20	85.95	66.12
Type 3	96.88	74.52
Type 3S2	102.89	79.14
HL-93	136.30	105.14
Lane	28.00	21.60

Lastly the factored shear load from the truck is multiplied by the live load distribution factor to determine the portion of load that is transferred to interior and exterior girders. According the original plans, the approach spans were to be built at a 40° skew. When bridges have a skew, the shear is magnified at the obtuse and acute corners of the

supports requiring a correction factor to be applied to all shear distribution loads. Additionally, a skew can result in a reduction of moment distribution, however, where moment influence in the load rating will not be checked the skew correction factor for moment distribution will not be calculated. Table 5.6 lists the original and corrected shear distribution factors for interior and exterior girders along Pier #4.

Table 5.6 Corrected Shear Distribution Factors for Interior and Exterior Girder

Girder	Lane	Uncorrected Distribution Factor	Skew Correction Factor	Shear Distribution Factor
Interior	Single	0.56	1.174	0.657
	Multi	0.596	1.174	<b>0.700</b>
Exterior	Single	0.72	1.170	<b>0.843</b>
	Multi	0.358	1.170	0.419

The bolded values represent the controlling distribution factors to be applied to interior and exterior girders, respectively. The distribution factors were calculated based on the LRFD methodology and equations presented in Appendix C of this paper. Table 5.7 lists the applied live load to interior and exterior girders under both inventory and operating conditions to be used in the load rating equation.

Table 5.7 Inventory and Operating Level Live Load Shears for Interior and Exterior Girder

Vehicle	Interior Girder		Exterior Girder	
	INV (kips)	OPER (kips)	INV (kips)	OPER (kips)
H20	60.15	46.27	72.43	55.72
Type 3	67.79	52.15	81.64	62.80
Type 3S2	72.00	55.38	86.70	66.70
HL-93	95.38	73.58	114.86	88.61
Lane	19.59	15.12	23.60	18.20

### 5.3 Description of Special Provisions for Corroded Webs

Section 7.2.9 of the *MassDOT Bridge Manual* provides methodology behind load rating of corroded steel girder webs both with and without stiffeners. For the work conducted for this project the section will focus on the LRFR equations for an unstiffened steel girder. The corroded web rating at both the Inventory and Operating levels shall be determined using the minimum of the factored resistances from the web local yielding and web local crippling checks as follows:

$$\text{Corroded Web Factored Resistance} = \text{Min} [\Phi R_{n,\text{yield}}, \Phi R_{n,\text{crip}}] \quad (\text{Eq. 5.3})$$

Where:

$$\Phi R_{n,\text{yield}} = (\Phi_b = 1.0)(R_{n,\text{yield}})$$

$$\Phi R_{n,\text{crip}} = (\Phi_w = 0.8)(R_{n,\text{crip}})$$

The nominal web local yielding capacity in kips ( $R_{n,\text{yield}}$ ) shall be calculated as follows:

- At interior-pier reactions and beam end reactions where an overhang past the bearing of at least 5k is provided

$$R_{n,\text{yield}} = F_y t_{\text{ave}} (5k + N) \quad (\text{Eq. 5.4a})$$

- At beam end reactions where an overhang of less than 5k is provided

$$R_{n,\text{yield}} = F_y t_{\text{ave}} (2.5k + N) \quad (\text{Eq. 5.4b})$$

Where:

$F_y$  = minimum yield strength (ksi)

$t_{\text{ave}}$  = the average remaining thickness within the bottom 4" of the web height (in.)

$k$  = distance from outer face of flange to toe of web fillet for a rolled shape, or toe of web to flange weld for a plate girder (in.)

The web local crippling capacity in kips ( $R_{n,crip}$ ) shall be calculated as follows:

- At interior-pier reactions and for beam end reactions applied at a distance from the end of the member that is greater than or equal to  $d/2$

$$R_{n,crip} = 0.8t_{ave}^2 \left[ 1 + 3 \left( \frac{(N-H)}{d} \right) \left( \frac{t_{ave}}{t_f} \right)^{1.5} \right] \sqrt{\frac{EF_y t_f}{t_{ave}}} \quad (\text{Eq. 5.6a})$$

Otherwise

$$R_{n,crip} = 0.4t_{ave}^2 \left[ 1 + 3 \left( \frac{(N-H)}{d} \right) \left( \frac{t_{ave}}{t_f} \right)^{1.5} \right] \sqrt{\frac{EF_y t_f}{t_{ave}}}, \text{ when } N/d \leq 0.2 \quad (\text{Eq. 5.6b})$$

$$= 0.4t_{ave}^2 \left[ 1 + \left( \frac{4(N-H)}{d} - 0.2 \right) \left( \frac{t_{ave}}{t_f} \right)^{1.5} \right] \sqrt{\frac{EF_y t_f}{t_{ave}}}, \text{ when } N/d > 0.2 \quad (\text{Eq. 5.6c})$$

Where:

$d$  = entire depth of steel section (in.), without deductions for encased diaphragms, if any

$t_f$  = actual thickness of the flange resisting the interior-pier or beam end reaction (in.)

$E$  = modulus of elasticity of steel (ksi)

The parameter  $t_{ave}$  is the average remaining thickness in the bottom 4" of web over the bearing length (N) plus 2.5k. It is a ratio that takes into account the length of complete loss of section through holes (H) with the critical area. The parameter  $t_{ave}$  is calculated as follows:

$$t_{ave} = \frac{(2.5k+N-H)t_w}{(2.5k+N)} \quad (\text{Eq. 5.7})$$

where:

N = bearing length (in)

H = length of hole within critical area (in)

$t_w$  = remaining web thickness in bottom 4" of web (in)

The specimen geometry in the work conducted during this project required use of Equations 5.4b for nominal web yielding and Equation 5.6c for nominal web crippling.

The LRFR Rating Factor equation will be calculated as follows:

$$\text{LRFR Rating Factor} = \frac{\text{Corroded Web Factored Resistance} - DL_{rxn}}{(L+I)_{rxn}} \quad (\text{Eq. 5.8})$$

Where the dead load and live load reactions are dependent upon the critical force for the load rating. In this study these reactions are factored shear values.

#### **5.4 Load Rating Results of Specimens using Current MassDOT Procedure**

Using the methodology outlined above the three test specimens corroded web factored resistance was calculated and the previously defined factored dead and live load shears were used to calculate rating factors for each specimen respectively.

### 5.4.1 Corroded Web Factored Resistance

Table 5.8 lists the corroded web factored resistance for each of the tested specimens.

Table 5.8: Corroded Web Factored Resistance (CWFR) of Tested Specimens

<b>Specimen 1</b>	<b>Specimen 2</b>	<b>Specimen 3</b>
<b>Web Crippling</b>	<b>Web Crippling</b>	<b>Web Crippling</b>
LRFR Inventory & Operating $\Phi R_{n,crip} = 49.2$ kips	LRFR Inventory & Operating $\Phi R_{n,crip} = 129.1$ kips	LRFR Inventory & Operating $\Phi R_{n,crip} = 0.0$ kips
<b>Web Yielding</b>	<b>Web Yielding</b>	<b>Web Yielding</b>
LRFR Inventory & Operating $\Phi R_{n,crip} = 146.1$ kips	LRFR Inventory & Operating $\Phi R_{n,crip} = 235.7$ kips	LRFR Inventory & Operating $\Phi R_{n,crip} = 137.5$ kips
<b>CWFR</b>	<b>CWFR</b>	<b>CWFR</b>
LRFR Inventory & Operating CWFR = 49.2 kips	LRFR Inventory & Operating CWFR = 129.1 kips	LRFR Inventory & Operating CWFR = 0.0 kips

It is a fascinating note that in all conditions for each specimen web crippling is always the controlling resistance. Corrosion significantly impacts the vertical load carrying capacity of the girder end, which is how shear is transferred into the web. Girders in bridges are typically deep sections, either rolled or built-up plate members, which effects the crippling capacity over the yielding. The yielding equation does not consider the depth of the section being analyzed, only the bearing length and average thickness remaining. It would be expected for shallow beams typically used as distribution stringers or floorbeams could be at risk for a yielding failure rather than crippling. Moving forward in this research project the web crippling equation will be studied to see the effects of the parameters used in the equation.

Specimen 3 resulted in a code predicted value of 0 kips due to the length of the hole extending past the bearing. This can be seen in Equation 5.7 where the value of  $2.5k + N$

Results in a value of 15", this is less than the length of the hole above bearing which equals 18". This makes the numerator go to zero, meaning by the code the  $t_{ave}$  parameter equals zero, resulting in no resistance of the web end. Although conservative for extreme conditions, this is not representative of the true condition of the girder end as shown in Chapter 4 during the discussion of experimental results. However, for consistency with the code, this resistance will be carried through the load rating.

Table 5.9 represents the results from the load rating using the current MassDOT procedure for unstiffened steel girders with corroded web ends. Omitting specimen 3 due to the previous defined issue, the remaining two specimens showed mixed results. No specimen passed rating for the HL-93 design loading, which is expected because of the time frame when this bridge was built shows it was designed using ASD methodology that did not account for this specific loading condition. Specimen 2 rated satisfactory for all legal load conditions, where specimen 1 failed to pass any of the legal load ratings. The minimum legal load rating was a factor of 0, which by definition of the code means the candidate bridge would be considered a red cover and would be in need for rehabilitation or replacement.

Table 5.9 Design and Legal Load Rating Factors using the Current MassDOT Procedure

Specimen	Factored Shear at Support over Pier #4									Corroded Web Factored Resistance (kips)	Design Load Rating Factors		Legal Load Rating Factors					
	DL <sub>shear</sub> (kips)	(LL+IM) <sub>shear</sub> (kips)									HL-93		H20		Type 3		Type 3S2	
		Inv.	Oper.	Inv.	Oper.	Inv.	Oper.	Inv.	Oper.		Inv.	Oper.	Inv.	Oper.	Inv.	Oper.	Inv.	Oper.
Specimen 1 Interior Girder 4	34.54	114.97	88.69	60.15	46.27	67.79	52.15	72.00	55.38	49.18	0.13	0.17	0.24	0.32	0.22	0.28	0.20	0.26
Specimen 2 Exterior Girder 1	34.75	138.46	106.81	72.43	55.72	81.64	62.80	86.70	66.70	129.10	0.68	0.88	1.30	1.69	1.16	1.50	1.09	1.41
Specimen 3 Interior Girder 3	34.94	114.97	88.69	60.15	46.27	67.79	52.15	72.00	55.38	0	-0.30	-0.39	-0.58	-0.76	-0.52	-0.67	-0.49	-0.63



## 5.5 Load Rating Results of Specimens using Experiment Values

Using the results from the experiments outlined in Chapter 4 of this paper, the reaction force developed at peak load for each specimen was used to replace the corroded web factored resistance in Equation 5.8. The same load rating methodology was applied with only the resistance values changing.

### 5.5.1 Resistances from Experiments

Table 5.10 list the summary of results from the experiments, refer to Chapter 4 for a detailed look at each respective specimen.

Table 5.10 Reaction Force of Corroded End at Peak Load

Specimen		Experiment Reaction Force at Peak Load (kips)
Specimen 1	Interior Girder 4	99.00
Specimen 2	Exterior Girder 1	67.60
Specimen 3	Interior Girder 3	84.3

It is important to note that no resistance factors will be applied to the experimental results because the values represent a real life condition of the girder ends and no safety factor is required to be applied. Table 5.11 represents the results from the load rating procedure using the results from the conducted experiments.

All specimens were deemed not satisfactory for HL-93 design loading under both inventory and operating conditions. This is again expected to occur for this research study. Specimen 1 was satisfactory for all legal loads under the operating level, meaning that

rehabilitation measures could be taken to avoid the need for replacement. Specimen 2 was not satisfactory for all legal loads at both the inventory and operating level. Specimen 3 was only satisfactory for the operating level of the H20 vehicle. The controlling legal rating factor was 0.38, which by code would be deemed a red cover and the bridge would need rehabilitation or replacement.

Table 5.11 Design and Legal Load Rating Factors using Reaction Force from Experiments

Specimen	Factored Shear at Support over Pier #4									Experiment Reaction Force at Peak Load (kips)	Design Load Rating Factors		Legal Load Rating Factors					
	DL <sub>shear</sub> (kips)	(LL+IM) <sub>shear</sub> (kips)									HL-93		H20		Type 3		Type 3S2	
		HL-93		H20		Type 3		Type 3S2			Inv.	Oper.	Inv.	Oper.	Inv.	Oper.	Inv.	Oper.
		Inv.	Oper.	Inv.	Oper.	Inv.	Oper.	Inv.	Oper.									
Specimen 1 Interior Girder 4	34.54	114.97	88.69	60.15	46.27	67.79	52.15	72.00	55.38	99.00	0.56	0.73	1.07	1.39	0.95	1.24	0.90	1.16
Specimen 2 Exterior Girder 1	34.75	138.46	106.81	72.43	55.72	81.64	62.80	86.70	66.70	67.60	0.24	0.31	0.45	0.59	0.40	0.52	0.38	0.49
Specimen 3 Interior Girder 3	34.94	114.97	88.69	60.15	46.27	67.79	52.15	72.00	55.38	84.3	0.43	0.56	0.82	1.07	0.73	0.95	0.69	0.89

## 5.6 Comparison of Results

Comparing the Load Rating values from the two methods in Section 5.4 and Section 5.5 show an initial discrepancy between the resistance of the corroded girder end. As previously mentioned, the code equations significantly under predict the resistance of a corroded web with a hole above bearing, which is reflected in specimen 1 and 3. Specimen 3 had a hole extend from the face of girder to beyond the bearing, which resulted in a CWFR of 0 kips, however, the experiment was able to withstand a reaction force of 84.3 kips at peak load. This effected the minimum load rating from a value of 0 to 0.43. A change in rating factor this significant could drastically impact the decision making of the state when planning for rehabilitation of the state's bridges. A load rating below 1.0 is consider unsatisfactory, but the higher a load rating value is the more options besides replacement opens to the state.

A second observation made in the load rating was that specimen 2 was over predicted by the code value compared to the experimental result. This effect came due to the large initial out-of-plane displacement of the web end. The current MassDOT procedure does not account for alignment issues in the web, rather only a loss of section. This affected the minimum load rating value from a 0.68 to a 0.24. For this over prediction it can be considered unconservative to not yield the lowest possible rating factor. In this case where both factors are under 1.0 then action of rehabilitation would have been taken, however, having the equation yield the same result as the experiment would change the rehabilitation priority within the states program.

## CHAPTER 6

### CONCLUSIONS

In this research project a full-scale experimental test configuration was designed to load (3) – 33-inch deep unstiffened rolled steel girders with natural end corrosion. This project is the first to test girders removed from service with corrosion developed in the field, rather than fabricated specimens with man-made corrosion. Additionally, the current load rating procedure for the state of Massachusetts put forth by MassDOT was explained and tested for accuracy using code methodology compared against the results from the full-scale experiments.

Results from the experiments concluded that the current procedure in the MassDOT Bridge Manual for determining resistance of a corroded web end is conservative for situations with a hole in the web above bearing and is unconservative for structural members with initial out-of-plane displacement of the web cross section.

For specimen 1 with a 5-inch-long hole above bearing at the web end and no initial signs of displaced web. The code methodology predicted a resistance of 49.2 kips against the experiment which yielded a max reaction force of 99 kips. This was a 50.3% difference in resistance that was not accounted for by the code. It is noted that if the hole was not present on the web the code methodology would predict a resistance of 112.6 kips, resulting in a 12% difference from experimental results. The influence of the hole reduced the resistance an extra 38.3%. The additional 12% loss could be attributed to inconsistency in the quality of deterioration measurements taken in the field for the routine inspection reports and the additional hole under the diaphragm in which the code does not consider.

Specimen 2 had an initial out-plane-displacement of 1” and had no hole over the bearing in the web. The code methodology predicted a resistance of 129.1 kips, where the experiment reached a max reaction force of 67.6 kips. This resulted in an over prediction of 47.6% of resistance the girder did not have. This can be completely attributed to the initial displacement which the code currently does not take into account. Additionally, specimen 2 was the only specimen to not have a hole above bearing, which led to a large uplift of the girder end. This changes the effective span length of the girder and focuses all of the bearing pressure to one location on the web.

Specimen 3 had an 18-inch-long hole in the web above bearing, reaching 3-inches past the critical web length of  $2.5k + N$ . According to the current procedure in the code this results in an average remaining web thickness of zero inches, therefore the resistance is calculated to be 0 kips. The experiment reached a max reaction force of 84.3 kips, a 100% difference from the code predicted value. This is the most evident experiment that the hole influence in the code is too conservative and does not accurately capture the beam response to this deficiency. Had there been no hole on specimen 3 with the same corrosion pattern the code would have predicted a resistance of 79.1 kips, a 6.2% difference from the experiment. Again, the additional loss in resistance can be attributed to the additional hole under the diaphragm and an undetailed representation of the corrosion profile in the inspection report.

Lastly, a load rating using results from both the code methodology and the experimental tests was presented. Dead load shear was calculated based the distributions methods presented in Section 3.5.3 of the *MassDOT LRFD Bridge Design Manual*. Live load shear was calculated for the HL-93 design loading and the legal load posting vehicles

of Massachusetts including: H20 truck, Type 3 truck and Type 3S2 truck. The results were similar in the way that in both procedures the bridge would end up a red-cover and be required to be put into the state rehabilitation program. However, it showed that specific girders could still withstand the legal loads at operating level which means full replacement of all girders may not have been required. Structural strengthening through the addition of more steel or girder end encasement of Ultra High Performance Concrete could be explored.

The results of this research project are to be used in a large parametric study and finite element analysis of corroded beam ends in Massachusetts. Providing calibration and a benchmark for the parameters to meet. It will also be used to progress the current procedure for determining the structural resistance of corroded steel girder ends for future use by the state.

## BIBLIOGRAPHY

- AASHTO. LRFD Bridge Design Specification 8<sup>th</sup> Edition. Washington, DC: Association of State Highway and Transportation Officials, 2017.
- American Association of State Highway and Transportation Officials. The Manual for Bridge Evaluation 3<sup>rd</sup> Edition, 2018.
- Ahn, J. H., S., Kainuma, F., Yasuo, and I. Takehiro. "Repair Method and Residual Bearing Strength Evaluation of a Locally Corroded Plate Girder at Support". Engineering Failure Analysis, 2013. 33: 198-418.
- Ahn, J. H., J. H., Cheung, W. H., Lee, H., Oh, and I. T. Kim. "Shear Buckling Experiments of Web Panel with Pitting and Through- Thickness Corrosion Damage". Journal of Constructional Steel Research, 2015. 115: 290-302.
- American Institute of Steel Construction (AISC), Manual of Steel Construction, 14<sup>th</sup> Edition. Chicago: AISC, 2011.
- American Institute of Steel Construction (AISC), Rolled Shapes Beams and Columns 1873-1952, 2nd Edition. New York: AISC, 1953.
- ASCE Bridges. ASCE's 2017 Infrastructure Report Card. American Society of Civil Engineers. <https://www.infrastructurereportcard.org/cat-item/bridges/>.
- ASTM Standard E8/E8M. Standard test methods for tension testing of metallic materials. West Conshohocken: ASTM International, 2011.
- Federal Highway Administration. U.S. Department of Transportation. <https://www.fhwa.dot.gov/bridge/nbi/ascii2017.cfm>. Accessed January 5, 2019.
- GE Inspection Technologies PocketMIKE Ultrasonic Thickness Gauge Kit. Test & Measurement Instruments with Engineering Support | Instrumart. <https://www.instrumart.com/assets/pocketmike-manual.pdf>. Accessed 26 Oct. 2018
- Gerasimidis S., Khorasani N.E., Garlock M., Pantidis P., Glassman, J., (2017). Resilience of tall steel moment resisting frame buildings with multi-hazard post-event fire, Journal of Constructional Steel Research, 139, pp. 202-219.
- Gerasimidis S., Deodatis G., Yan Y., Ettouney M., (2016). Global instability induced failure of tall steel moment frame buildings, ASCE Journal of Performance of Constructed Facilities, 31(2): 04016082.
- Gerasimidis S., Sideri T., (2016). A new partial distributed damage method for progressive collapse analysis of buildings, Journal of Constructional Steel Research, Volume 119, pp. 233-245.



- Gerasimidis S., Baniotopoulos C.C., (2015). Progressive collapse mitigation of 2D steel moment frames - Assessment of the effect of different strengthening schemes, *Stahlbau*, Volume 84 (5), pp. 324-331.
- Gerasimidis S., Kontoroupi T., Deodatis G., Ettouney M., (2014). Loss-of-stability induced progressive collapse modes in 3D steel moment frames, *Structure and Infrastructure Engineering*, Volume 11 (3), pp. 334-344.
- Gerasimidis S., (2014). Analytical assessment of steel frames progressive collapse vulnerability to corner column loss, *Journal of Constructional Steel Research*, Volume 95, pp. 1-9.
- Gerasimidis S., Bisbos C.D., Baniotopoulos C.C., (2013). A computational model for full or partial damage of single or multiple adjacent columns in disproportionate collapse analysis via linear programming, *Structure and Infrastructure Engineering*, 10 (5), pp. 670-683.
- Gerasimidis S., Bisbos C.D., Baniotopoulos C.C., (2012). Vertical geometric irregularity assessment of steel frames on robustness and disproportionate collapse, *Journal of Constructional Steel Research*, Volume 74, pp. 76-89.
- Gerasimidis S., Ampatzis A., Bisbos C.D., (2012). A mathematical programming computational model for disproportionate collapse analysis of steel building frames, *Optimization Letters*, Volume 6, Number 3, pp. 525-535.
- Gerasimidis S., Baniotopoulos C.C., (2011). Evaluation of wind load integration in disproportionate collapse analysis of steel moment frames for column loss, *Journal of Wind Engineering and Industrial Aerodynamics*, Volume 99, Issue 11, pp. 1162-1173.
- Gerasimidis S., Baniotopoulos C.C., (2011). Steel moment frames column loss analysis: the influence of time step size, *Journal of Constructional Steel Research*, Volume 67, Issue 4, pp. 557-564.
- Gerasimidis S., Baniotopoulos C.C., (2011). Disproportionate collapse analysis of cable-stayed steel roofs for cable loss, *International Journal of Steel Structures*, Volume 11, Number 1, pp. 91-98.
- Gerasimidis S., Efthymiou E, Baniotopoulos C.C., (2009). On the application of robustness criteria to steel lattice masts, *POLLACK Periodica*, Volume 4, Number 1, pp. 17-28.
- Kayser, J. R., and A. S. Nowak. "Capacity Loss Due to Corrosion in Steel-Girder Bridges". *Journal of Structural Engineering*, 1989. 115: 1525-1537.
- Khurram, N., E., Sasaki, H., Katsuchi, and H. Yamada. "Experimental and Numerical Evaluation of Bearing Capacity of Steel Plate Girder Affected by End Panel Corrosion". *International Journal of Steel Structures*, 2014. 14: 659-676.

- Kim, I. T., M. J., Lee, J. H., Ahn, and A. Kainuma. "Experimental Evaluation of Shear Buckling Behaviors and Strength of Locally Corroded Web". *Journal of Constructional Steel Research*, 2013. 83: 75-89.
- Koch, G. H., M. P.H Brongers, and N. G. Thompson. "Corrosion Costs and Preventive Strategies in the United States." NACE International. 2002. U.S. Department of Transportation/FHWA. <https://www.nace.org/uploadedfiles/publications/ccsupp.pdf>.
- Kuhn, P, J. P. Peterson, and L. R. Levin. "A Summary of Diagonal Tension Part I - Methods of Analysis." National Advisory Committee for Aeronautics Technical Note 2661 (1952).
- MassDOT. LRFD Draft Bridge Manual Part I. Boston, MA: The Massachusetts Department of Transportation Highway Division Bridge Section, 2018.
- Miller, T. C., M. J. Chajes, D. R. Mertz, and J. N. Hastings. "Strengthening of a Steel Bridge Girder Using CFRP Plates." *Journal of Bridge Engineering* (2001): 514-22.
- Miyashita, T., M., Nagai, D., Wakabayashi, Y., Hidekuma, A., Kobayashi, Y., Okuyama, N., Koibe, and W. Horimoto. "Repair Method for Corroded Steel Girder Ends Using CFRP Sheet". Presented at IABSE – JSCE Joint Conference on Advances in Bridge Engineering- III, Bangladesh, 2015.
- National Bridge Inventory. U.S. Department of Transportation/Federal Highway Administration. <https://www.fhwa.dot.gov/bridge/nbi/2017/delimited/MA17.txt>. Accessed January 5, 2019.
- Ogami, H., Fujii, K., Yamada, T., and H. Iwasaki. *Renovation of Corroded Girder End in Plate Girder Bridge with Resin and Rebars. Implementing Innovative Ideas in Structural Engineering and Project Management*, 2015.
- Okuyama, Y., Miyashita, T., Ogata, T., Fujino, K., Ohgaki, K., Hidekuma, Y., Horimoto, W. and Nagai, M., 2012. Mechanical Behavior of Plate Bonded FRP Sheets under Uniaxial Compression Load, *Proceeding of the 3rd Asia Pacific Conference on FRP*, p. 13.
- Pantidis P., Gerasimidis S., (2018). Progressive collapse of 3D steel composite buildings under interior gravity column loss, *Journal of Constructional Steel Research.*, 150, pp. 60-75.
- Pantidis P., Gerasimidis S., (2017). New Euler-type progressive collapse curves for 2D steel frames: an analytical method, *ASCE Structural Engineering*, 143 (9): 04017113.
- Roberts, T. M. *Slender Plate Girders Subjected to Edge Loading*. Proceedings of the Institution of Civil Engineers Part B, 1981. 71: 805-819.

- Sideri J., Mullen C.L., Gerasimidis S., Deodatis G., (2017). Distributed Column damage effect on progressive collapse vulnerability in steel buildings exposed to an external blast event, *ASCE Journal of Performance of Constructed Facilities*, 31(5): 04017077.
- Tzortzinis, G, Knickle, BT, Gerasimidis, S, Bardow, A, Brena, SF, Experiments and Computations on Steel Bridge Corroded Beam Ends, AISC - Structural Stability Research Council, St. Louis MI, 2019.
- Van de Lindt, J. W., and T. M. Ahlborn. Development of Steel Beam End Deterioration Guidelines. Publication MDOT-RC-1454, Michigan Tech Transportation Institute, 2005.
- Yura, Joseph A. "Fundamentals of Beam Bracing." *Engineering Journal* First Quarter (2001): 11-26.
- Zmetra, K. M., K. F., McMullen, A. E., Zaghi, and K. Wille. "Experimental Study of UHPC Repair for Corrosion- Damaged Steel Girder Ends". *Journal of Bridge Engineering*, 2017. 22.

## Appendix A: Experimental Setup Calculation Sheets

	<u>Page</u>
Computations	
Loading Beam Design .....	A-1
Anchor Block Design .....	A-9
Anchor Rod Design .....	A-12
Lateral-Torsional Support Design .....	A-13
Floorbeam Design.....	A-23

## Loading Beam Design

Assumptions:

1. Simply supported between threaded anchor rods.
2. Nominal capacities are of (2) rolled I-beams connected by welded plates.

References:

1. AISC Steel Construction Manual 15th Edition

Material Properties:

$$F_{yb} := 50 \text{ ksi}$$

*Yield strength of beam*

$$F_{yp} := 36 \text{ ksi}$$

*Yield strength of welded plates*

$$E_s := 29000 \text{ ksi}$$

*Modulus of elasticity of steel*

Loading:

$$P_u := 400 \text{ kip}$$

*Max load at midspan of beam*

$$L_b := 5 \text{ ft}$$

*Length of beam between supports*

$$L_t := 6 \text{ ft}$$

*Total length of beam*

Demand Calculations:

$$M_u := \frac{P_u \cdot L_b}{4} = 500 \text{ kip} \cdot \text{ft}$$

*Ultimate moment of simply supported beam*

$$V_u := \frac{P_u}{2} = 200 \text{ kip}$$

*Ultimate shear of simply supported beam*

Beam Selection:

Ultimate Moment = Yield Moment

$$M_y = S_{xreq} * f_y$$

Yield moment of steel I-beam

$$S_{xreq} := \frac{M_u \cdot \left(12 \cdot \frac{\text{in}}{\text{ft}}\right)}{F_{yb}} = 120 \text{ in}^3$$

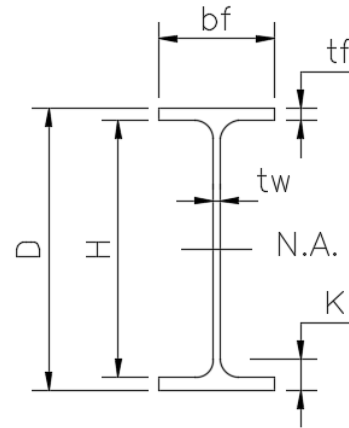
Total required section modulus

$$S_{xb} := \frac{S_{xreq}}{2} = 60 \text{ in}^3$$

Required section modulus of beam

W12x58 Rolled I-Beam

$$\begin{aligned} D &:= 12.19 \text{ in} & b_f &:= 10.01 \text{ in} \\ t_f &:= 0.64 \text{ in} & H_w &:= 10.91 \text{ in} \\ t_w &:= 0.36 \text{ in} & N.A. &:= \frac{D}{2} = 6.095 \text{ in} \\ I_x &:= 475 \text{ in}^4 & S_x &:= 78 \text{ in}^3 \\ I_y &:= 107 \text{ in}^4 & S_y &:= 21.4 \text{ in}^3 \\ r_x &:= 5.28 \text{ in} & r_y &:= 2.51 \text{ in} \\ J &:= 2.1 \text{ in}^4 & K &:= 1.24 \text{ in} \end{aligned}$$



$$h := D - (2 \cdot K) = 9.71 \text{ in}$$

Web depth minus the fillets

Flexural Resistances:

$$M_y := (2 \cdot S_x) \cdot F_{yb} = 650 \text{ kip} \cdot \text{ft}$$

Flexural yield resistance of  
(2) W12x58 beams

$$Z_x := \left(2 \cdot (b_f \cdot t_f) \cdot \left(N.A. - \frac{t_f}{2}\right)\right) + \left(2 \cdot \left(\frac{H_w}{2} \cdot t_w\right) \cdot \left(N.A. - t_f - \frac{H_w}{4}\right)\right) = 84.706 \text{ in}^3$$

$$M_p := (2 \cdot Z_x) \cdot F_{yb} = 705.887 \text{ kip} \cdot \text{ft}$$

Flexural plastic resistance of  
(2) W12x58 beams

## Section B4. Member Properties

### Check Flange Compactness

Table B4.1b Case 10:

$$\lambda_{pf} := 0.38 \sqrt{\left(\frac{E_s}{F_{yb}}\right)} = 9.152 \quad \text{Compact/noncompact limiting ratio}$$

$$\lambda_{rf} := 1.0 \sqrt{\left(\frac{E_s}{F_{yb}}\right)} = 24.083 \quad \text{Noncompact/slender limiting ratio}$$

$$\lambda_f := \frac{b_f}{2 \cdot t_f} = 7.82 \quad \text{Flange slenderness ratio}$$

if $\lambda_f \leq \lambda_{pf}$    “COMPACT” else if $\lambda_{pf} < \lambda_f \leq \lambda_{rf}$    “NONCOMPACT” else if $\lambda_f > \lambda_{rf}$    “SLENDER”	= “COMPACT”
---	-------------

### Check Web Compactness

Table B4.1b Case 15:

$$\lambda_{pw} := 3.76 \sqrt{\left(\frac{E_s}{F_{yb}}\right)} = 90.553 \quad \text{Compact/noncompact limiting ratio}$$

$$\lambda_{rw} := 5.70 \sqrt{\left(\frac{E_s}{F_{yb}}\right)} = 137.274 \quad \text{Noncompact/slender limiting ratio}$$

$$\lambda_w := \frac{H_w}{t_w} = 30.306 \quad \text{Web slenderness ratio}$$

if $\lambda_w \leq \lambda_{pw}$    “COMPACT” else if $\lambda_{pw} < \lambda_w \leq \lambda_{rw}$    “NONCOMPACT” else if $\lambda_w > \lambda_{rw}$    “SLENDER”	= “COMPACT”
---	-------------

SECTION F2. DOUBLY SYMMETRIC COMPACT I-SHAPED MEMBERS AND CHANNELS BENT ABOUT THEIR MAJOR AXIS

1. Yielding

$$M_n := M_p = 705.887 \text{ kip}\cdot\text{ft} \quad \text{Nominal flexural resistance} \quad (F2-1)$$

2. Lateral-Torsional Buckling

Limiting laterally unbraced length for the limit state of yielding:

$$L_p := 1.76 r_y \sqrt{\left(\frac{E_s}{F_{yb}}\right)} = 106.39 \text{ in} \quad (F2-5)$$

Limiting laterally unbraced length for the limit state of inelastic lateral-torsional buckling:

$$C_w := \frac{I_y \cdot (D - t_f)^2}{4} = 3569 \text{ in}^6$$

$$r_{ts} := \sqrt{\frac{\sqrt{I_y \cdot C_w}}{S_x}} = 2.81 \text{ in} \quad (F2-7)$$

$$c := 1.0 \quad (F2-8a)$$

$$L_r := 1.95 r_{ts} \frac{E_s}{0.7 F_{yb}} \sqrt{\frac{J \cdot c}{S_x \cdot (D - t_f)} + \sqrt{\left(\frac{J \cdot c}{S_x \cdot (D - t_f)}\right)^2 + 6.76 \left(\frac{0.7 F_{yb}}{E_s}\right)^2}}$$

$$L_r = 359.234 \text{ in} \quad (F2-6)$$

Unbraced Length:

$$L_b := L_b = 60 \text{ in}$$

$M_n :=$ if $L_b \leq L_p$ $\parallel M_n$ else if $L_p < L_b \leq L_r$ $\parallel$ "Equation F2.2" else if $L_b > L_r$ $\parallel$ "Equation F2.3"	$= 705.887 \text{ kip}\cdot\text{ft}$	if $M_n > M_u$ $\parallel$ "SUFFICIENT" else $\parallel$ "REDESIGN"	$=$ "SUFFICIENT"
	$\frac{M_n}{M_u} = 1.412$	Design Ratio	



## SECTION G2. I-SHAPED MEMBERS AND CHANNELS

$$A_w := D \cdot t_w = 4.39 \text{ in}^2 \quad \text{Area of web, full depth of section}$$

$$\frac{h}{t_w} = 26.972$$

$$2.24 \cdot \sqrt{\frac{E_s}{F_{yb}}} = 53.946$$

$$C_{v1} := \begin{cases} \frac{h}{t_w} \leq 2.24 \cdot \sqrt{\frac{E_s}{F_{yb}}} \\ \parallel 1.0 \\ \text{else} \\ \parallel \text{"USE SECTION G2.1b"} \end{cases}$$

$$C_{v1} = 1 \quad \text{Web shear strength coefficient} \quad (G2-2)$$

$$V_n := 0.6 \cdot (2 \cdot A_w) \cdot F_{yb} \cdot C_{v1} = 263.304 \text{ kip} \quad \text{Nominal shear resistance of} \quad (G2-1) \\ \text{(2) W12x58 webs}$$

$$\begin{cases} \text{if } V_n > V_u \\ \parallel \text{"SUFFICIENT"} \\ \text{else} \\ \parallel \text{"REDESIGN"} \end{cases} = \text{"SUFFICIENT"}$$

$$\frac{V_n}{V_u} = 1.317 \quad \text{Design Ratio}$$

Due to high forces, design stiffeners for placement around loading points  
Stiffeners not required for shear strength do not check Section G2.2 or G2.3

## SECTION J2. WELDS

Check weld along one face of stiffener to web and flanges

$$\text{Proposed weld along web: } b_{stiff} := 4 \text{ in} \quad t_{stiff} := \frac{1}{4} \text{ in} \quad \text{Stiffener properties}$$

$$t_{fillet\_w} := \frac{3}{16} \text{ in} \quad \text{Size of fillet weld on web}$$

$$l_{weld\_w} := h = 9.71 \text{ in} \quad \text{Length of fillet weld on web}$$

Check:  $l_{weld\_eff\_w} := \mathbf{if} \left( (l_{weld\_w}) \leq (100 \cdot t_{fillet\_w}), l_{weld\_w}, \text{"REVISE"} \right) = 9.71 \text{ in}$

Proposed weld along top and bottom flange:

$$t_{fillet\_f} := \frac{3}{16} \text{ in} \quad \text{Size of fillet weld on web}$$

$$l_{weld\_f} := 2 \cdot b_{stiff} = 8 \text{ in} \quad \text{Length of fillet weld on web}$$

Check:  $l_{weld\_eff\_f} := \mathbf{if} \left( (l_{weld\_f}) \leq (100 \cdot t_{fillet\_f}), l_{weld\_f}, \text{"REVISE"} \right) = 8 \text{ in}$

$$F_{EXX} := 70 \text{ ksi} \quad \text{Filler metal classification strength} \quad (\text{Sec. J2.6})$$

$$\theta_w := 180 \text{ deg} \quad \text{Direction of applied load in web weld}$$

$$\theta_f := 90 \text{ deg} \quad \text{Direction of applied load in flange weld}$$

$$F_{nw\_w} := 0.6 \cdot F_{EXX} \cdot \left( 1 + 0.5 \sin(\theta_w)^{1.5} \right) = 42 \text{ ksi} \quad \text{Weld strength web} \quad (\text{J2-5})$$

$$F_{nw\_f} := 0.6 \cdot F_{EXX} \cdot \left( 1 + 0.5 \sin(\theta_f)^{1.5} \right) = 63 \text{ ksi} \quad \text{Weld strength web} \quad (\text{J2-5})$$

$$A_{BM} := b_f \cdot t_f = 6.406 \text{ in}^2 \quad \text{Area of base metal}$$

$$A_{we\_w} := t_{fillet\_w} \cdot l_{weld\_eff\_w} = 1.821 \text{ in}^2 \quad \text{Effective area of web weld}$$

$$A_{we\_f} := t_{fillet\_f} \cdot l_{weld\_eff\_f} = 1.5 \text{ in}^2 \quad \text{Effective area of flange weld}$$

Rupture of Base Material:

$$R_{n\_BM} := F_{yb} \cdot A_{BM} = 320.32 \text{ kip} \quad \text{Base Metal Rupture Resistance} \quad (\text{J2-2})$$

Rupture of Weld:

$$R_{nwl} := F_{nw\_w} \cdot A_{we\_w} = 76.466 \text{ kip} \quad \text{Nominal strength of longitudinally loaded fillet welds} \quad (\text{J2-10a})$$

$$R_{nwt} := F_{nw\_f} \cdot A_{we\_f} = 94.5 \text{ kip} \quad \text{Nominal strength of transversely loaded fillet welds} \quad (\text{J2-10b})$$

Total Resistance:

$$R_{nw} := \max \left( (R_{nwl} + R_{nwt}), (0.85 R_{nwl} + 1.5 R_{nwt}) \right) = 206.746 \text{ kip}$$

Check:

$$\begin{array}{l} \text{if } R_{nw} > V_u \wedge R_{n_{BM}} > V_u \\ \quad \parallel \text{ "SUFFICIENT" } \\ \text{else} \\ \quad \parallel \text{ "REDESIGN" } \end{array} \Bigg| = \text{ "SUFFICIENT" }$$

Make the (2) W12x58 beams act compositely by welding (3) 12"x18"x1-1/2" steel plates onto both the top and bottom flanges. Allow a 3" separation between outer edges of flanges for passage of threaded anchor rods.

$$N_{plate} := 6$$

*Number of plates*

$$b_{plate} := 12 \text{ in}$$

*Width of cover plate*

$$t_{plate} := 1.5 \text{ in}$$

*Thickness of cover plate*

$$l_{plate} := 18 \text{ in}$$

*Length of cover plate*

$$l_{loading} := 3 \text{ in}$$

*Length of loading*

$$M_{u_{plate}} := \frac{P_u \cdot l_{loading}}{4} = 25 \text{ kip} \cdot \text{ft}$$

*Ultimate moment in cover plate*

$$S_{x_{plate}} := \frac{b_{plate} \cdot t_{plate}^2}{6} = 4.5 \text{ in}^3$$

*Section modulus of plate*

$$M_{y_{plate}} := 6 \cdot S_{x_{plate}} \cdot F_{yp} = 81 \text{ kip} \cdot \text{ft}$$

*Total flexural resistance of plates*

Check weld strength to ensure beams act compositely, same properties as welded stiffener

$$t_{fillet} := \frac{1}{4} \text{ in}$$

*Size of cover plate fillet weld*

$$l_{weld} := \left( \frac{l_{plate} - l_{loading}}{2} \right) + (b_{plate}) = 19.5 \text{ in}$$

*Total length of fillet weld around half of cover plate*

Check:  $l_{weld_{eff}} := \text{if } (l_{weld} \leq (100 \cdot t_{fillet}), l_{weld}, \text{ "REVISE" }) = 19.5 \text{ in}$



## Anchor Block Design

Assumptions:

1. Simply supported between welds.

References:

1. AISC Steel Construction Manual 15th Edition

Material Properties:

$$F_{yp} := 36 \text{ ksi} \quad \text{Yield strength of welded plates}$$

$$E_s := 29000 \text{ ksi} \quad \text{Modulus of elasticity of steel}$$

Plate Properties:

$$b_{topplate} := 12 \text{ in} \quad \text{Width of top plate}$$

$$l_{topplate} := 16 \text{ in} \quad \text{Length of top plate}$$

$$t_{topplate} := 2.5 \text{ in} \quad \text{Thickness of top plate}$$

$$t_{sideplate} := 1.5 \text{ in} \quad \text{Thickness of side plate}$$

$$l_{overhang} := 0.5 \text{ in} \quad \text{Top plate overhang for weld}$$

Loading:

$$P_u := 200 \text{ kip} \quad \text{Ultimate load on plate}$$

$$L_{loading} := l_{topplate} - 2 \cdot l_{overhang} - t_{sideplate} = 13.5 \text{ in}$$

$$L := L_{loading} = 1.125 \text{ ft} \quad \text{Length between theoretical supports}$$

Demand Calculations:

$$M_u := \frac{P_u \cdot L}{4} = 56.25 \text{ kip} \cdot \text{ft} \quad \text{Ultimate moment of simply supported plate}$$

Flexural Resistance:

$$S_{x\_plate} := \frac{b_{topplate} \cdot t_{topplate}^2}{6} = 12.5 \text{ in}^3 \quad \text{Section modulus of plate}$$

$$M_{y\_plate} := 6 \cdot S_{x\_plate} \cdot F_{yp} = 225 \text{ kip} \cdot \text{ft} \quad \text{Total flexural resistance of plates}$$

$$\begin{array}{l} \text{if } M_{y\_plate} > M_u \\ \quad \parallel \\ \quad \text{"SUFFICIENT"} \\ \text{else} \\ \quad \parallel \\ \quad \text{"REDESIGN"} \end{array} \Bigg| = \text{"SUFFICIENT"}$$

Check weld along one side of support plate (along width of top plate)

$$t_{fillet} := \frac{5}{16} \text{ in} \quad \text{Size of cover plate fillet weld}$$

$$l_{weld} := b_{topplate} = 12 \text{ in} \quad \text{Total length of fillet weld around half of cover plate}$$

Check:  $l_{weld\_eff} := \text{if}(l_{weld} \leq (100 \cdot t_{fillet}), l_{weld}, \text{"REVISE"}) = 12 \text{ in}$

$$F_{EXX} := 70 \text{ ksi} \quad \text{Filler metal classification strength} \quad (\text{Sec. J2.6})$$

$$\theta := 90 \text{ deg} \quad \text{Direction of applied load on plate welds}$$

$$F_{nw} := 0.6 \cdot F_{EXX} \cdot (1 + 0.5 \sin(\theta)^{1.5}) = 63 \text{ ksi} \quad \text{Weld strength} \quad (\text{J2-5})$$

$$A_{BM} := b_{topplate} \cdot t_{sideplate} = 18 \text{ in}^2 \quad \text{Area of base metal}$$

$$A_{we} := t_{fillet} \cdot l_{weld\_eff} = 3.75 \text{ in}^2 \quad \text{Effective area of web weld}$$

Rupture of Base Material:

$$R_{n\_BM} := F_{yb} \cdot A_{BM} = 900 \text{ kip} \quad \text{Base Metal Rupture Resistance} \quad (\text{J2-2})$$

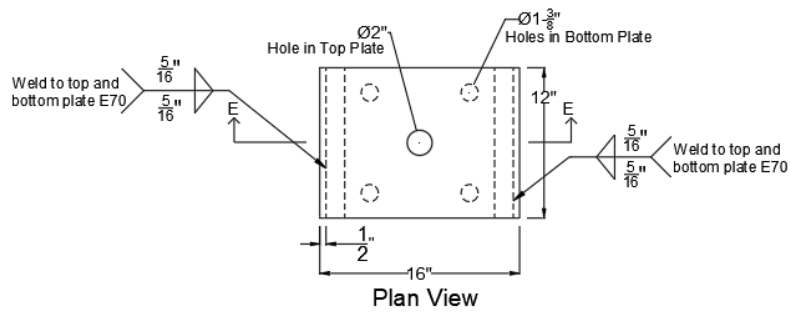
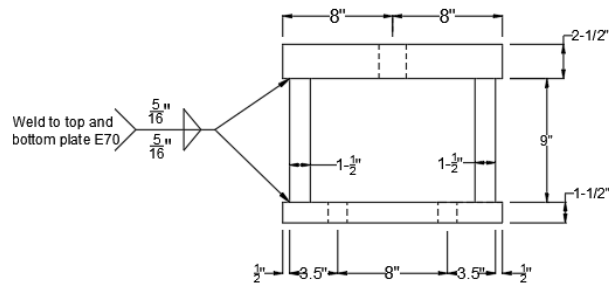
Rupture of Weld:

$$R_{nw} := F_{nw} \cdot A_{we} = 236.25 \text{ kip} \quad \text{Nominal strength of fillet welds} \quad (\text{J2-3})$$

Check:

$$\begin{array}{l} \text{if } R_{nw} > P_u \wedge R_{n_{BM}} > P_u \quad = \text{“SUFFICIENT”} \\ \parallel \\ \text{“SUFFICIENT”} \\ \text{else} \\ \parallel \\ \text{“REDESIGN”} \end{array}$$

Details:



## Anchor Rod Design

Assumptions:

1. Anchor rod is in pure tension between loading beam and anchor block.

References:

1. AISC Steel Construction Manual 15th Edition

Material Properties:

$$F_{yr} := 120 \text{ ksi} \quad \text{Yield strength of threaded rod}$$

$$F_{ur} := 150 \text{ ksi} \quad \text{Ultimate strength of threaded rod}$$

$$E_s := 29000 \text{ ksi} \quad \text{Modulus of elasticity of steel}$$

Threaded Rod Properties:

$$d_{rod} := 1.75 \text{ in} \quad \text{Diameter of rod}$$

$$A_{rod} := \pi \cdot \frac{d_{rod}^2}{4} = 2.405 \text{ in}^2 \quad \text{Area of rod}$$

Loading:

$$P_u := 200 \text{ kip} \quad \text{Ultimate tensile load in rod}$$

Demand Stress:

$$f_t := \frac{P_u}{A_{rod}} = 83.15 \text{ ksi} \quad \text{Ultimate tensile stress in rod}$$

Check:

$$\left. \begin{array}{l} \text{if } F_{yr} > f_t \\ \quad \parallel \text{ "SUFFICIENT" } \\ \text{else} \\ \quad \parallel \text{ "REDESIGN" } \end{array} \right| = \text{"SUFFICIENT"}$$



## Lateral-Torsional Support Design

Assumptions:

1. Brace acts as a cantilever.
2. Supports occur every 5' along 33" test specimens due to strong-floor restriction.

References:

1. AISC Steel Construction Manual 15th Edition

Material Properties:

$$F_{yb} := 50 \text{ ksi}$$

*Yield strength of beam*

$$F_{specimen} := 36 \text{ ksi}$$

*Assumed yield strength of test specimen*

Loading:

$$P_u := 400 \text{ kip}$$

*Max load at midspan of beam*

$$L_{supports} := 25 \text{ ft}$$

*Length between supports of test specimen*

$$a := 0.25 \cdot L_{supports} = 6.25 \text{ ft}$$

*Length from tested end to loading position*

$$b := L_{supports} - a = 18.75 \text{ ft}$$

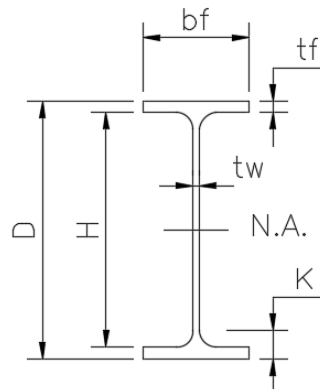
*Length from untested end to loading position*

Test Specimen Properties:

$$D := 33.15 \text{ in} \quad H_w := D - 2 \cdot t_f = 31.87 \text{ in}$$

$$b_f := 11.51 \text{ in} \quad t_w := 0.58 \text{ in}$$

$$t_f := 0.88 \text{ in} \quad N.A. := \frac{D}{2} = 16.575 \text{ in}$$



$$Z_x := \left( 2 \cdot (b_f \cdot t_f) \cdot \left( N.A. - \frac{t_f}{2} \right) \right) + \left( 2 \cdot \left( \frac{H_w}{2} \cdot t_w \right) \cdot \left( N.A. - t_f - \frac{H_w}{4} \right) \right) = 469.696 \text{ in}^3$$

Specimen Moment Calculations:

$$M_{r1} := \frac{P_u \cdot a \cdot b}{L_{supports}} = 1875 \text{ kip} \cdot \text{ft}$$

*Max possible moment due to strong floor restriction*

$$M_{r2} := F_{specimen} \cdot Z_x = 1409.1 \text{ kip} \cdot \text{ft}$$

*Yield moment resistance of test specimen*

$$M_r := \min(M_{r1}, M_{r2}) = 16909.1 \text{ kip} \cdot \text{in}$$

Required Resistances:

$$C_d := 1.0$$

$$L_{br} := 5 \text{ ft}$$

*Max unbraced length adjacent brace*

$$h_o := 32.24 \text{ in}$$

*Distance between specimen flange centroids*

Strength:

$$P_{br} := 0.02 \left( \frac{M_r \cdot C_d}{h_o} \right) = 10.49 \text{ kip}$$

*Required strength of brace (A-6-7)*

Stiffness:

$$\beta_{br} := \frac{10 \cdot M_r \cdot C_d}{(L_{br} \cdot 12) \cdot h_o} = 7.28 \frac{\text{kip}}{\text{in}}$$

*Required stiffness of brace (A-6-8a)*

Demand Calculations:

$$l_{br} := 5 \text{ ft}$$

*Length of cantilevered brace*

$$M_u := P_{br} \cdot l_{br} = 52.4 \text{ kip} \cdot \text{ft}$$

*Ultimate moment of cantilever*

$$V_u := P_{br} = 10.49 \text{ kip}$$

*Ultimate shear of cantilever*

Beam Selection:

Ultimate Moment = Yield Moment

$$M_y = S_{xreq} \cdot f_y$$

$$S_{xreq} := \frac{M_u \cdot \left(12 \cdot \frac{\text{in}}{\text{ft}}\right)}{F_{yb}} = 12.587 \text{ in}^3$$

Yield moment of steel I-beam

Total required section modulus

W12x40 Rolled I-Beam

$$D := 11.94 \text{ in} \quad b_f := 8.005 \text{ in}$$

$$t_f := 0.515 \text{ in} \quad H_w := D - 2 \cdot t_f = 10.91 \text{ in}$$

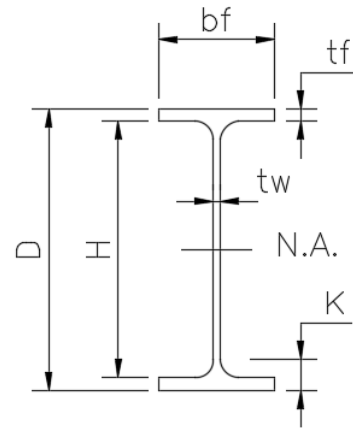
$$t_w := 0.295 \text{ in} \quad N.A. := \frac{D}{2} = 5.97 \text{ in}$$

$$I_x := 310 \text{ in}^4 \quad S_x := 51.9 \text{ in}^3$$

$$I_y := 44.1 \text{ in}^4 \quad S_y := 11.0 \text{ in}^3$$

$$r_x := 5.13 \text{ in} \quad r_y := 1.93 \text{ in}$$

$$J := 0.906 \text{ in}^4 \quad K := 1.02 \text{ in}$$



$$h := D - (2 \cdot K) = 9.9 \text{ in}$$

Web depth minus the fillets

Flexural Resistances:

$$M_y := S_x \cdot F_{yb} = 216.25 \text{ kip} \cdot \text{ft}$$

Flexural yield resistance of  
(2) W12x58 beams

$$Z_x := \left(2 \cdot (b_f \cdot t_f) \cdot \left(N.A. - \frac{t_f}{2}\right)\right) + \left(2 \cdot \left(\frac{H_w}{2} \cdot t_w\right) \cdot \left(N.A. - t_f - \frac{H_w}{4}\right)\right) = 55.879 \text{ in}^3$$

$$M_p := Z_x \cdot F_{yb} = 232.828 \text{ kip} \cdot \text{ft}$$

Flexural plastic resistance of  
(2) W12x58 beams

Section B4. Member Properties

Check Flange Compactness  
Table B4.1b Case 10:

$$\lambda_{pf} := 0.38 \sqrt{\left(\frac{E_s}{F_{yb}}\right)} = 9.152 \quad \text{Compact/noncompact limiting ratio}$$

$$\lambda_{rf} := 1.0 \sqrt{\left(\frac{E_s}{F_{yb}}\right)} = 24.083 \quad \text{Noncompact/slender limiting ratio}$$

$$\lambda_f := \frac{b_f}{2 \cdot t_f} = 7.772 \quad \text{Flange slenderness ratio}$$

if $\lambda_f \leq \lambda_{pf}$	= "COMPACT"
"COMPACT"	
else if $\lambda_{pf} < \lambda_f \leq \lambda_{rf}$	
"NONCOMPACT"	
else if $\lambda_f > \lambda_{rf}$	
"SLENDER"	

Check Web Compactness  
Table B4.1b Case 15:

$$\lambda_{pw} := 3.76 \sqrt{\left(\frac{E_s}{F_{yb}}\right)} = 90.553 \quad \text{Compact/noncompact limiting ratio}$$

$$\lambda_{rw} := 5.70 \sqrt{\left(\frac{E_s}{F_{yb}}\right)} = 137.274 \quad \text{Noncompact/slender limiting ratio}$$

$$\lambda_w := \frac{H_w}{t_w} = 36.983 \quad \text{Web slenderness ratio}$$

if $\lambda_w \leq \lambda_{pw}$	= "COMPACT"
"COMPACT"	
else if $\lambda_{pw} < \lambda_w \leq \lambda_{rw}$	
"NONCOMPACT"	
else if $\lambda_w > \lambda_{rw}$	
"SLENDER"	

SECTION F2. DOUBLY SYMMETRIC COMPACT I-SHAPED MEMBERS AND CHANNELS BENT ABOUT THEIR MAJOR AXIS

1. Yielding

$$M_n := M_p = 232.828 \text{ kip}\cdot\text{ft} \quad \text{Nominal flexural resistance} \quad (F2-1)$$

2. Lateral-Torsional Buckling

Limiting laterally unbraced length for the limit state of yielding:

$$L_p := 1.76 r_y \sqrt{\left(\frac{E_s}{F_{yb}}\right)} = 81.806 \text{ in} \quad (F2-5)$$

Limiting laterally unbraced length for the limit state of inelastic lateral-torsional buckling:

$$C_w := \frac{I_y \cdot (D - t_f)^2}{4} = 1439 \text{ in}^6$$

$$r_{ts} := \sqrt{\frac{\sqrt{I_y \cdot C_w}}{S_x}} = 2.2 \text{ in} \quad (F2-7)$$

$$c := 1.0 \quad (F2-8a)$$

$$L_r := 1.95 r_{ts} \frac{E_s}{0.7 F_{yb}} \sqrt{\frac{J \cdot c}{S_x \cdot (D - t_f)} + \sqrt{\left(\frac{J \cdot c}{S_x \cdot (D - t_f)}\right)^2 + 6.76 \left(\frac{0.7 F_{yb}}{E_s}\right)^2}}$$

$$L_r = 252.164 \text{ in} \quad (F2-6)$$

Unbraced Length:

$$L_b := L_b = 60 \text{ in}$$

$M_n :=$ if $L_b \leq L_p$ $\parallel M_n$ else if $L_p < L_b \leq L_r$ $\parallel$ "Equation F2.2" else if $L_b > L_r$ $\parallel$ "Equation F2.3"	$= 232.828 \text{ kip}\cdot\text{ft}$	if $M_n > M_u$ $\parallel$ "SUFFICIENT" else $\parallel$ "REDESIGN"  $\parallel \frac{M_n}{M_u} = 4.439$	$=$ "SUFFICIENT"       <i>Design Ratio</i>
--	---------------------------------------	---	---

SECTION G2. I-SHAPED MEMBERS AND CHANNELS

$$A_w := D \cdot t_w = 3.52 \text{ in}^2 \quad \text{Area of web, full depth of section}$$

$$\frac{h}{t_w} = 33.559$$

$$2.24 \cdot \sqrt{\frac{E_s}{F_{yb}}} = 53.946$$

$$C_{v1} := \begin{cases} \text{if } \frac{h}{t_w} \leq 2.24 \cdot \sqrt{\frac{E_s}{F_{yb}}} \\ \quad \parallel 1.0 \\ \text{else} \\ \quad \parallel \text{"USE SECTION G2.1b"} \end{cases}$$

$$C_{v1} = 1 \quad \text{Web shear strength coefficient} \quad (G2-2)$$

$$V_n := 0.6 \cdot A_w \cdot F_{yb} \cdot C_{v1} = 105.669 \text{ kip} \quad \text{Nominal shear resistance of} \quad (G2-1) \\ (2) \text{ W12x58 webs}$$

$$\begin{cases} \text{if } V_n > V_u \\ \quad \parallel \text{"SUFFICIENT"} \\ \text{else} \\ \quad \parallel \text{"REDESIGN"} \end{cases} = \text{"SUFFICIENT"}$$

$$\frac{V_n}{V_u} = 10.074 \quad \text{Design Ratio}$$

SECTION J2. WELDS

Check weld along one face of web and flanges of cantilever

Proposed weld along web:

$$t_{fillet\_w} := \frac{3}{16} \text{ in} \quad \text{Size of fillet weld on web}$$

$$l_{weld\_w} := h = 9.9 \text{ in} \quad \text{Length of fillet weld on web}$$

Check:  $l_{weld\_eff\_w} := \text{if} \left( (l_{weld\_w}) \leq (100 \cdot t_{fillet\_w}), l_{weld\_w}, \text{"REVISE"} \right) = 9.9 \text{ in}$

Proposed weld along top or bottom flange:

$$t_{fillet\_f} := \frac{3}{16} \text{ in} \quad \text{Size of fillet weld on web}$$

$$l_{weld\_f} := b_f = 8.005 \text{ in} \quad \text{Length of fillet weld on web}$$

Check:  $l_{weld\_eff\_f} := \text{if}(l_{weld\_f} \leq (100 \cdot t_{fillet\_f}), l_{weld\_f}, \text{"REVISE"}) = 8.005 \text{ in}$

$$F_{EXX} := 70 \text{ ksi} \quad \text{Filler metal classification strength} \quad (\text{Sec. J2.6})$$

$$\theta_w := 180 \text{ deg} \quad \text{Direction of applied load in web weld}$$

$$\theta_f := 90 \text{ deg} \quad \text{Direction of applied load in flange weld}$$

$$F_{nw\_w} := 0.6 \cdot F_{EXX} \cdot \left(1 + 0.5 \sin(\theta_w)\right)^{1.5} = 42 \text{ ksi} \quad \text{Weld strength web} \quad (\text{J-5})$$

$$F_{nw\_f} := 0.6 \cdot F_{EXX} \cdot \left(1 + 0.5 \sin(\theta_f)\right)^{1.5} = 63 \text{ ksi} \quad \text{Weld strength web} \quad (\text{J-5})$$

$$A_{BM} := b_f \cdot t_f = 4.123 \text{ in}^2 \quad \text{Area of base metal}$$

$$A_{we\_w} := t_{fillet\_w} \cdot l_{weld\_eff\_w} = 1.856 \text{ in}^2 \quad \text{Effective area of web weld}$$

$$A_{we\_f} := t_{fillet\_f} \cdot l_{weld\_eff\_f} = 1.501 \text{ in}^2 \quad \text{Effective area of flange weld}$$

Rupture of Base Material:

$$R_{n\_BM} := F_{yb} \cdot A_{BM} = 206.129 \text{ kip} \quad \text{Base Metal Rupture Resistance} \quad (\text{J-2})$$

Rupture of Weld:

$$R_{nwl} := F_{nw\_w} \cdot A_{we\_w} = 77.963 \text{ kip} \quad \text{Nominal strength of longitudinally loaded fillet welds} \quad (\text{J2-10a})$$

$$R_{nwt} := F_{nw\_f} \cdot A_{we\_f} = 94.559 \text{ kip} \quad \text{Nominal strength of transversely loaded fillet welds} \quad (\text{J2-10b})$$

Total Resistance:

$$R_{nw} := \max((R_{nwl} + R_{nwt}), (0.85 R_{nwl} + 1.5 R_{nwt})) = 208.107 \text{ kip}$$

Check:

$$\left. \begin{array}{l} \text{if } R_{nw} > V_u \wedge R_{n\_BM} > V_u \\ \quad \parallel \text{“SUFFICIENT”} \\ \text{else} \\ \quad \parallel \text{“REDESIGN”} \end{array} \right| = \text{“SUFFICIENT”}$$

### SECTION J3. BOLTS AND THREADED PARTS

Proposed ASTM F3125 Grade A325 Bolt:

$$d_b := 0.75 \text{ in} \quad \text{Diameter of bolt}$$

$$A_b := \pi \cdot \frac{d_b^2}{4} = 0.442 \text{ in}^2 \quad \text{Area of bolt}$$

Threads included:

$$F_{nt} := 90 \text{ ksi} \quad \text{Nominal tensile strength}$$

$$F_{nv} := 54 \text{ ksi} \quad \text{Nominal shear strength}$$

$$f_{rv} := \frac{V_u}{A_b} = 23.743 \text{ ksi} \quad \text{Required shear strength}$$

$$R_n := F_{nv} \cdot A_b = 23.856 \text{ kip} \quad \text{Shear Rupture Resistance} \quad (J3-1)$$

Check:

$$\left. \begin{array}{l} \text{if } R_n > V_u \\ \quad \parallel \text{“SUFFICIENT”} \\ \text{else} \\ \quad \parallel \text{“REDESIGN”} \end{array} \right| = \text{“SUFFICIENT”}$$

Use standard hole size and clearance distances

Design bolted C-Channel to cantilever as contact point to test specimen:

Proposed contact point:

$$s_{rod} := 4.125 \text{ in} = 0.344 \text{ ft} \quad \text{Rod spacing on C-Channel}$$

$$P_u := V_u = 10.49 \text{ kip} \quad \text{Max load on contact point}$$



Demand Calculations:

$$M_u := \frac{P_u \cdot s_{rod}}{4} = 10.817 \text{ kip} \cdot \text{in}$$

*Ultimate moment on contact point*

Channel Selection:

MC8x8.5

$$F_y := 50 \text{ ksi}$$

$$S_y := 0.431 \text{ in}^3$$

$$M_y := F_y \cdot S_y = 21.55 \text{ kip} \cdot \text{in}$$

*Weak axis flexural resistance*

Check:

$$\left. \begin{array}{l} \text{if } M_y > M_u \\ \quad \parallel \text{ "SUFFICIENT" } \\ \text{else} \\ \quad \parallel \text{ "REDESIGN" } \end{array} \right| = \text{"SUFFICIENT"}$$

Check tack welded threaded rods resistance to compression force

Proposed rod:

$$d_{rod} := 0.75 \text{ in}$$

*Diameter of rod*

$$A_{rod} := \pi \cdot \frac{d_{rod}^2}{4} = 0.442 \text{ in}^2$$

*Area of rod*

$$N_{rod} := 4$$

*Number of rods*

$$F_{yrod} := 50 \text{ ksi}$$

*Yield strength of threaded rod*

Loading:

$$P_{uc} := \frac{V_u}{N_{rod}} = 2.62 \text{ kip}$$

*Ultimate compressive force*

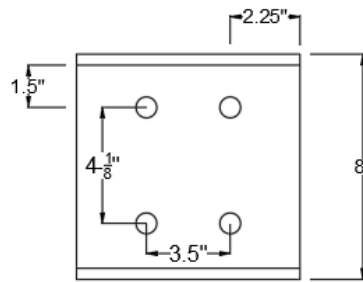
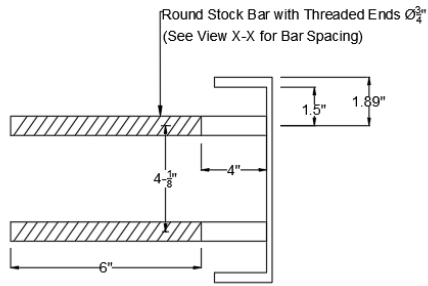
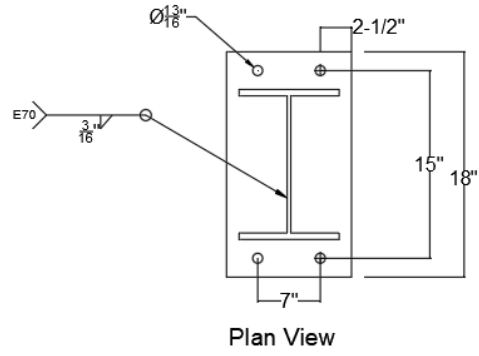
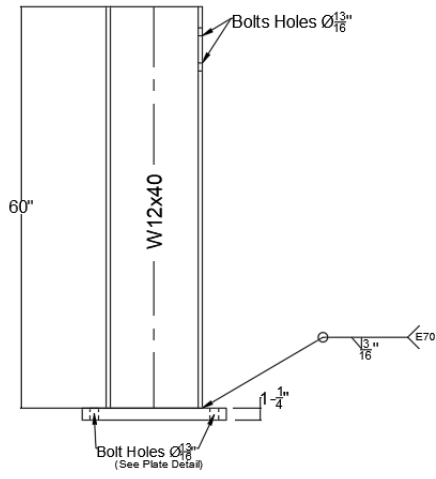
Resistance:

$$P_n := F_{yrod} \cdot A_{rod} = 22.089 \text{ kip}$$

*Compressive resistance of rod*

$$\text{Check} := \text{if}(P_n > P_{uc}, \text{"SUFFICIENT"}, \text{"REDESIGN"}) = \text{"SUFFICIENT"}$$

Details:



## Floorbeam Design

Assumptions:

1. Simply supported between threaded anchor rods.
2. Vertical load due to self-weight of cantilever is negligible.
3. Floorbeam is 12" deep.

References:

1. AISC Steel Construction Manual 15th Edition

Material Properties:

$$F_{yb} := 50 \text{ ksi}$$

*Yield strength of beam*

$$F_{yp} := 36 \text{ ksi}$$

*Yield strength of welded plates*

$$E_s := 29000 \text{ ksi}$$

*Modulus of elasticity of steel*

Loading:

$$M := P_{br} \cdot l_{br} = 52.447 \text{ kip} \cdot \text{ft}$$

*Max moment due to cantilever*

$$L_b := 5 \text{ ft}$$

*Length of beam between supports*

Demand Calculations:

$$M_u := M = 52.447 \text{ kip} \cdot \text{ft}$$

*Ultimate moment of simply supported beam*

Beam Selection:

Ultimate Moment = Yield Moment

$$M_y = S_{xreq} \cdot f_y$$

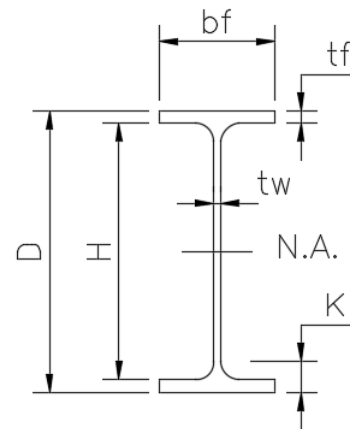
$$S_{xreq} := \frac{M_u \cdot \left(12 \cdot \frac{\text{in}}{\text{ft}}\right)}{F_{yb}} = 12.587 \text{ in}^3$$

*Yield moment of steel I-beam*

*Total required section modulus*

W12x72 Rolled I-Beam

$$\begin{aligned} D &:= 12.3 \text{ in} & b_f &:= 12 \text{ in} \\ t_f &:= 0.67 \text{ in} & H_w &:= D - 2 \cdot t_f = 10.96 \text{ in} \\ t_w &:= 0.43 \text{ in} & N.A. &:= \frac{D}{2} = 6.15 \text{ in} \\ I_x &:= 597 \text{ in}^4 & S_x &:= 97.4 \text{ in}^3 \\ I_y &:= 195 \text{ in}^4 & S_y &:= 32.4 \text{ in}^3 \\ r_x &:= 5.31 \text{ in} & r_y &:= 3.04 \text{ in} \\ J &:= 2.93 \text{ in}^4 & K &:= 1.27 \text{ in} \end{aligned}$$



$$h := D - (2 \cdot K) = 9.76 \text{ in}$$

*Web depth minus the fillets*

Flexural Resistances:

$$M_y := S_x \cdot F_{yb} = 405.833 \text{ kip} \cdot \text{ft}$$

*Flexural yield resistance of  
(2) W12x58 beams*

$$Z_x := \left( 2 \cdot (b_f \cdot t_f) \cdot \left( N.A. - \frac{t_f}{2} \right) \right) + \left( 2 \cdot \left( \frac{H_w}{2} \cdot t_w \right) \cdot \left( N.A. - t_f - \frac{H_w}{4} \right) \right) = 106.418 \text{ in}^3$$

$$M_p := Z_x \cdot F_{yb} = 443.409 \text{ kip} \cdot \text{ft}$$

*Flexural plastic resistance of  
(2) W12x58 beams*

Section B4. Member Properties

Check Flange Compactness  
Table B4.1b Case 10:

$$\lambda_{pf} := 0.38 \sqrt{\left(\frac{E_s}{F_{yb}}\right)} = 9.152 \quad \text{Compact/noncompact limiting ratio}$$

$$\lambda_{rf} := 1.0 \sqrt{\left(\frac{E_s}{F_{yb}}\right)} = 24.083 \quad \text{Noncompact/slender limiting ratio}$$

$$\lambda_f := \frac{b_f}{2 \cdot t_f} = 8.955 \quad \text{Flange slenderness ratio}$$

if $\lambda_f \leq \lambda_{pf}$	= "COMPACT"
"COMPACT"	
else if $\lambda_{pf} < \lambda_f \leq \lambda_{rf}$	
"NONCOMPACT"	
else if $\lambda_f > \lambda_{rf}$	
"SLENDER"	

Check Web Compactness  
Table B4.1b Case 15:

$$\lambda_{pw} := 3.76 \sqrt{\left(\frac{E_s}{F_{yb}}\right)} = 90.553 \quad \text{Compact/noncompact limiting ratio}$$

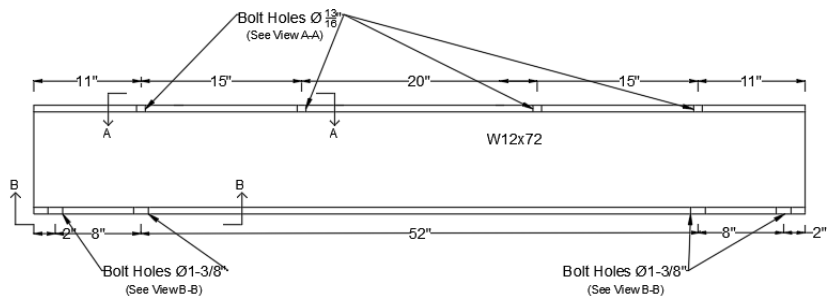
$$\lambda_{rw} := 5.70 \sqrt{\left(\frac{E_s}{F_{yb}}\right)} = 137.274 \quad \text{Noncompact/slender limiting ratio}$$

$$\lambda_w := \frac{H_w}{t_w} = 25.488 \quad \text{Web slenderness ratio}$$

if $\lambda_w \leq \lambda_{pw}$	= "COMPACT"
"COMPACT"	
else if $\lambda_{pw} < \lambda_w \leq \lambda_{rw}$	
"NONCOMPACT"	
else if $\lambda_w > \lambda_{rw}$	
"SLENDER"	

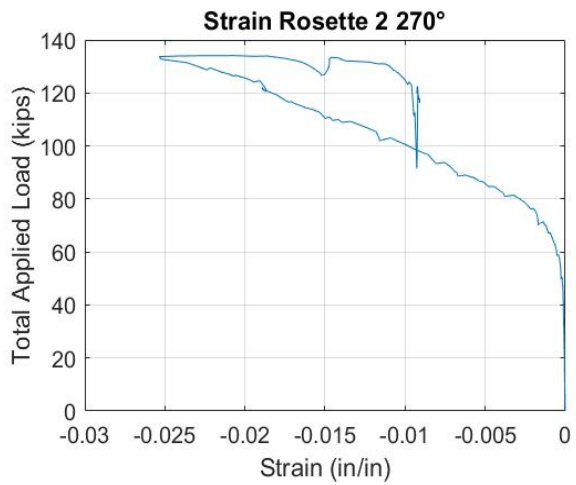
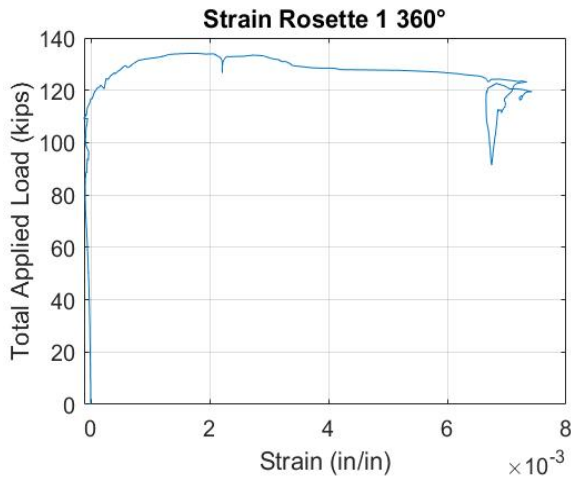
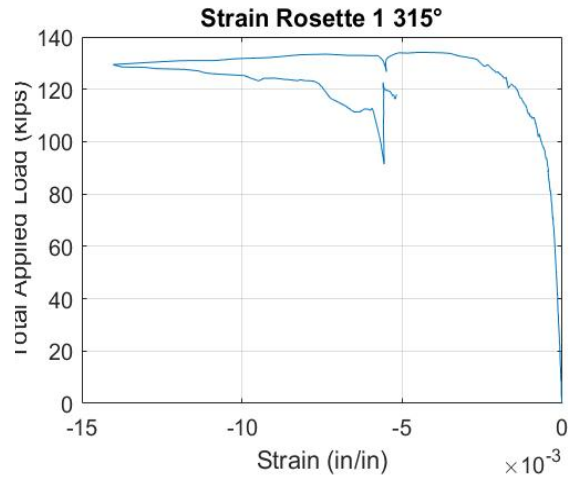
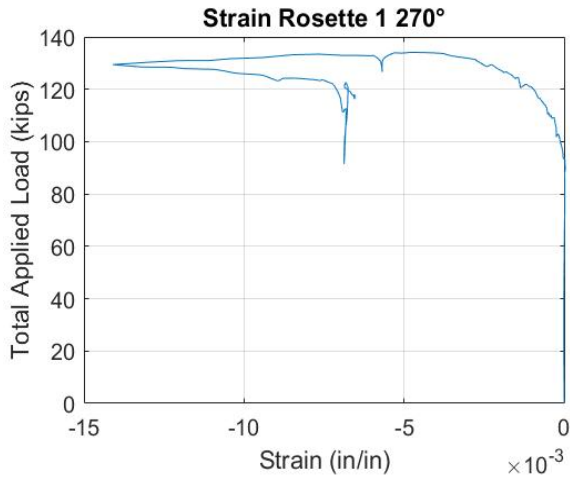
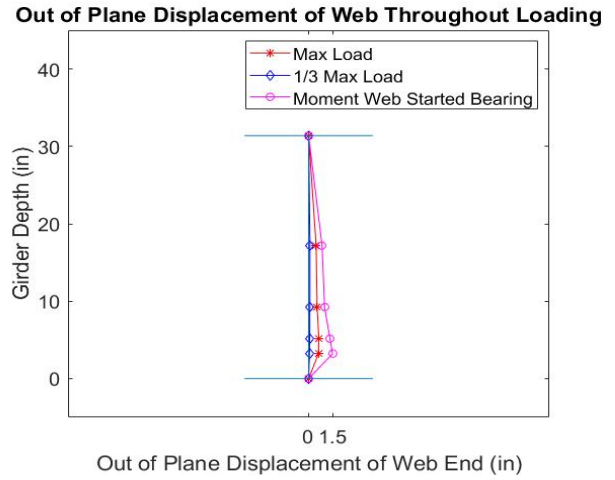
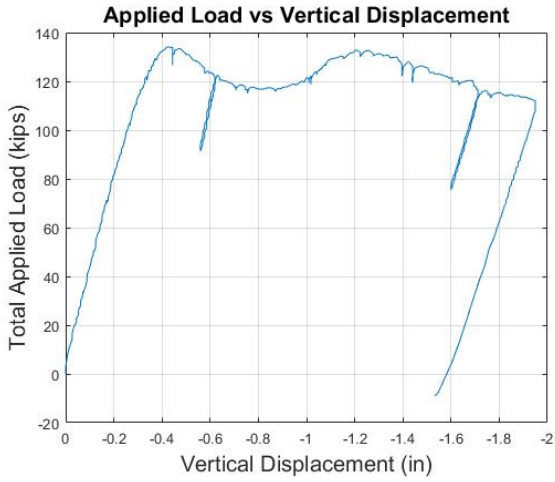


Details:

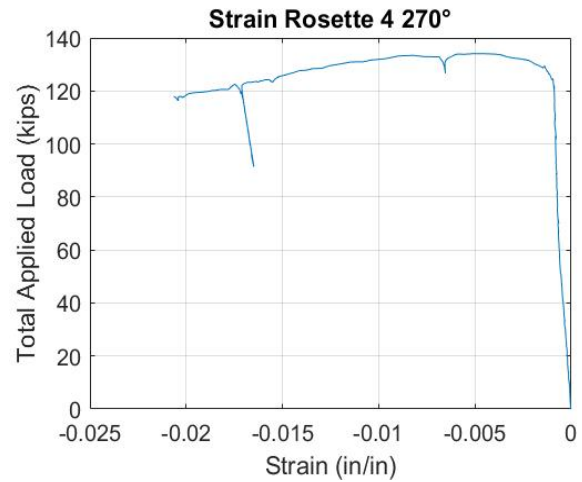
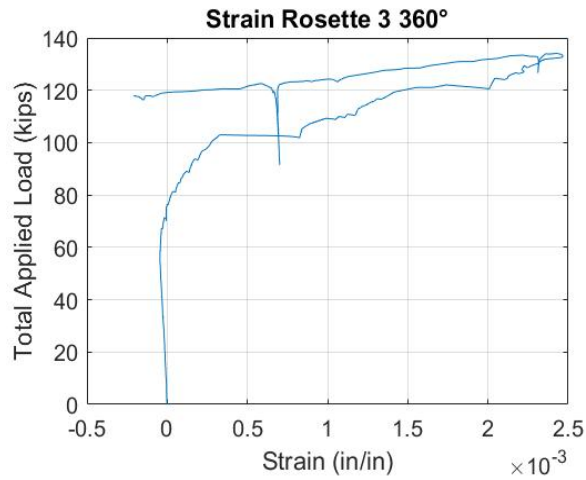
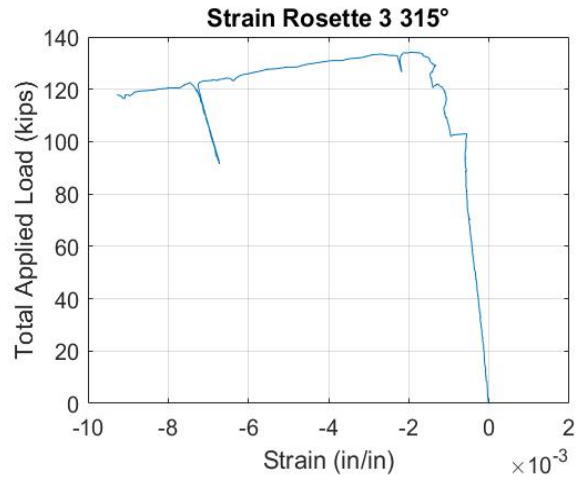
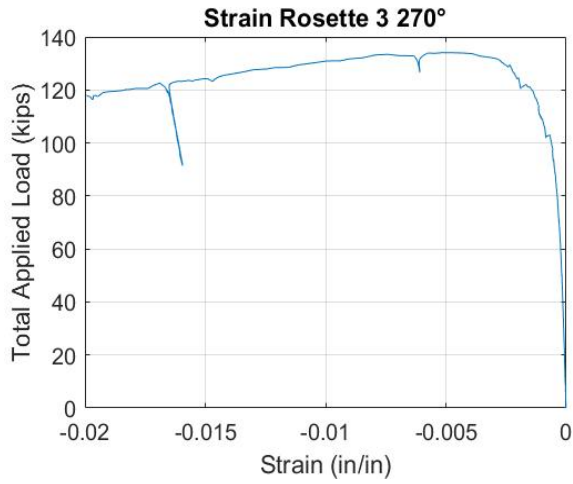
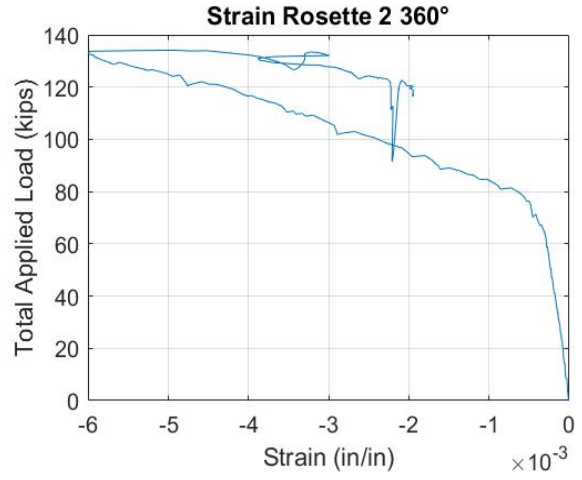
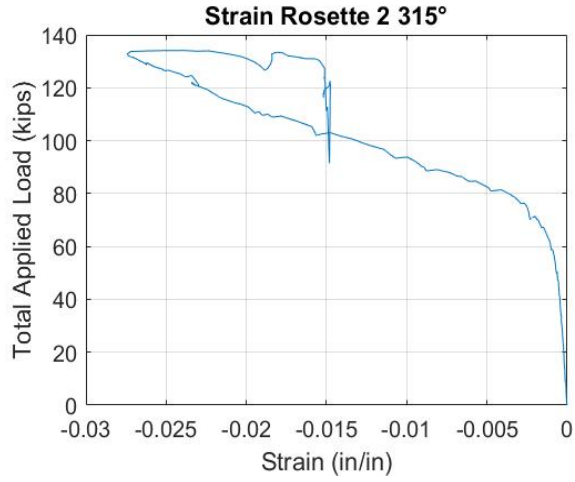


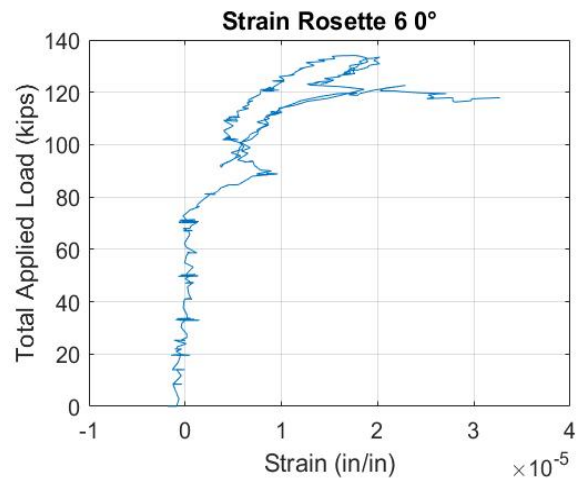
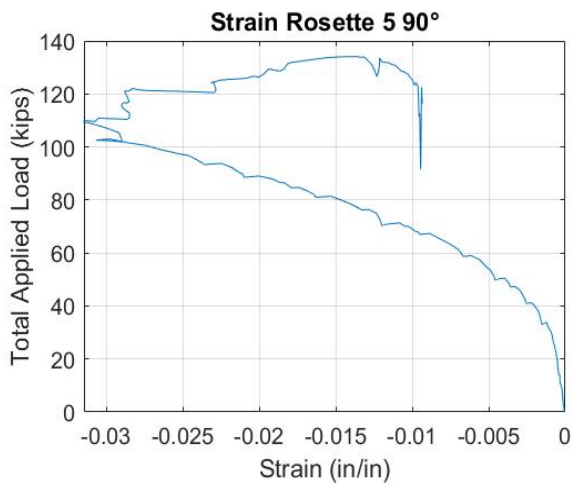
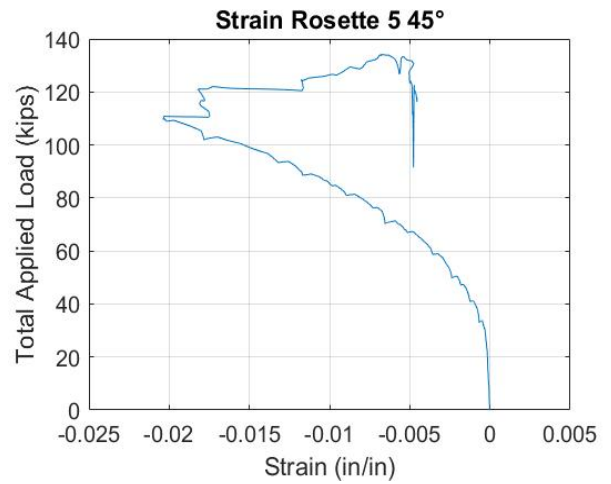
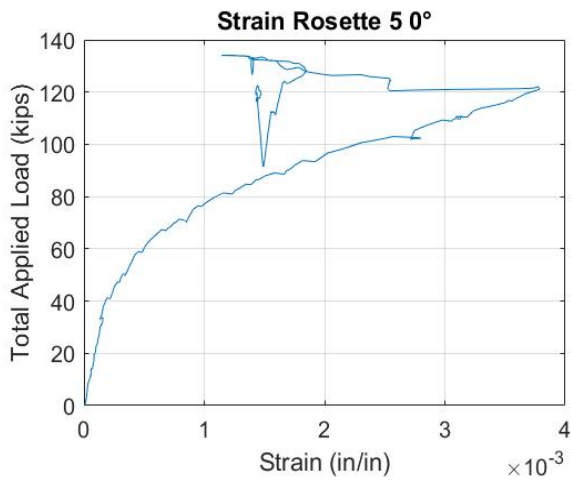
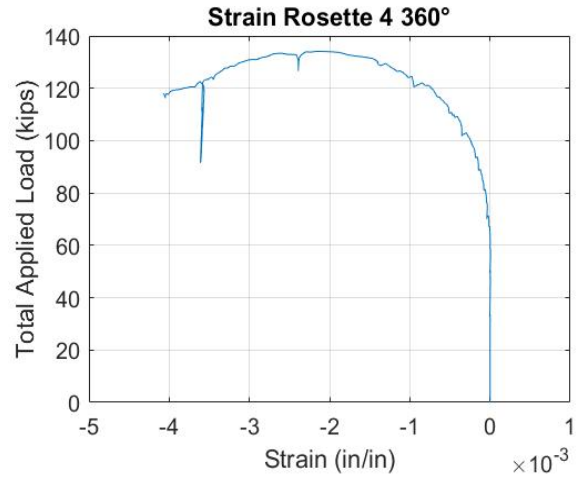
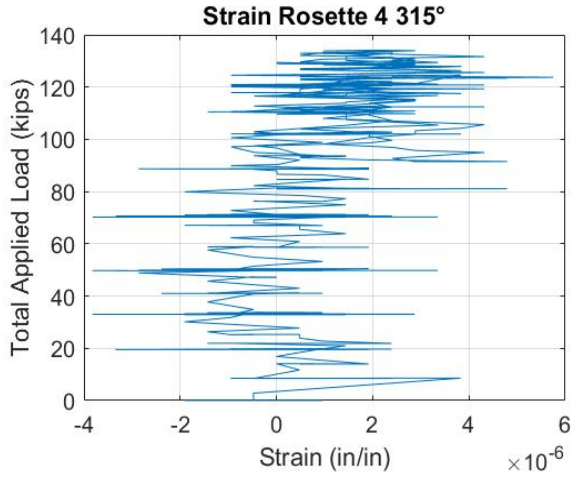
# Appendix B: Experimental Raw Data

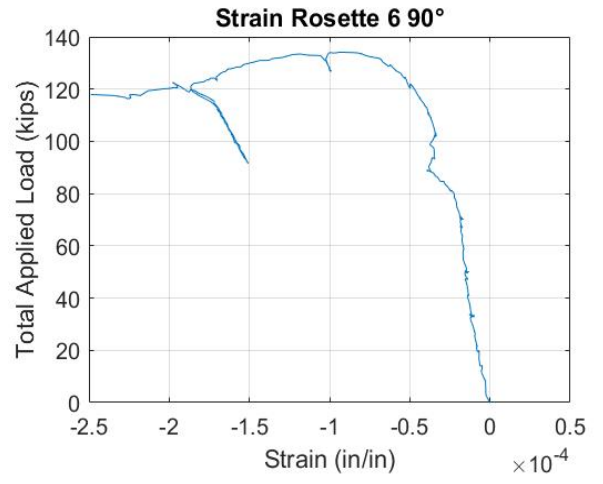
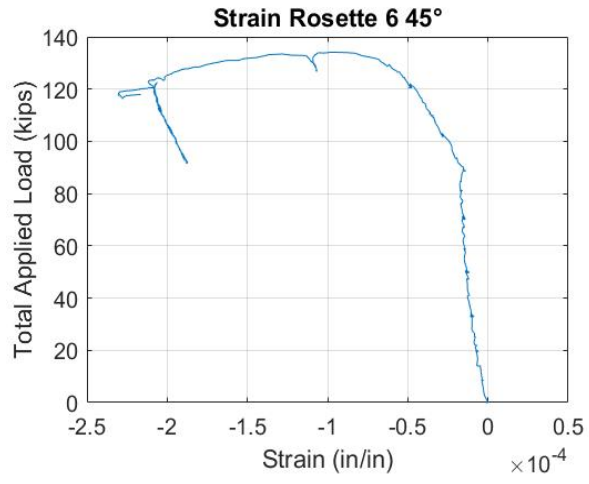
## Experiment 1



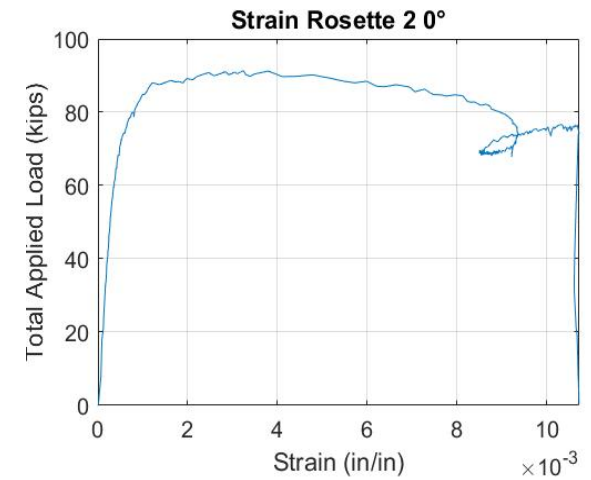
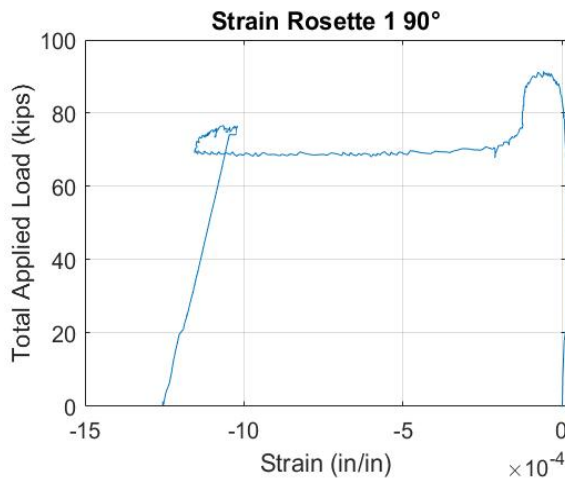
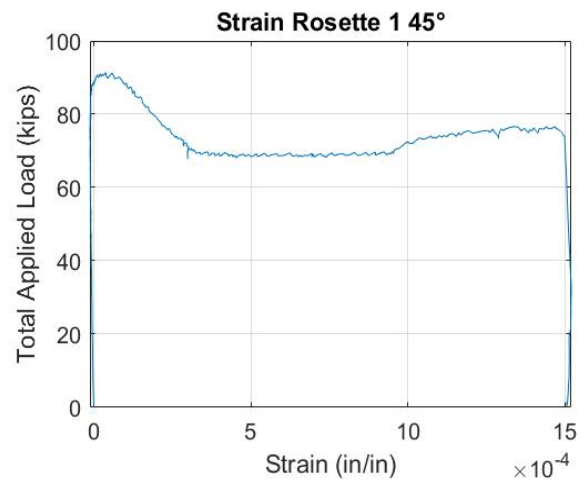
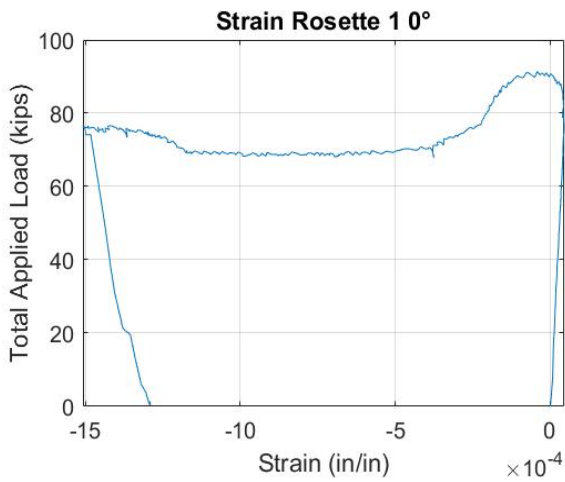
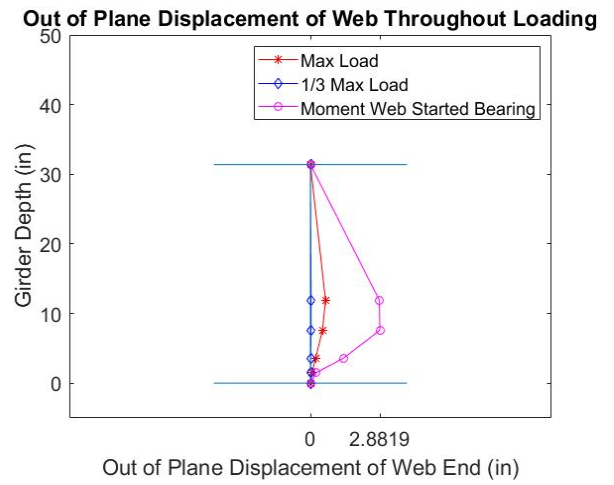
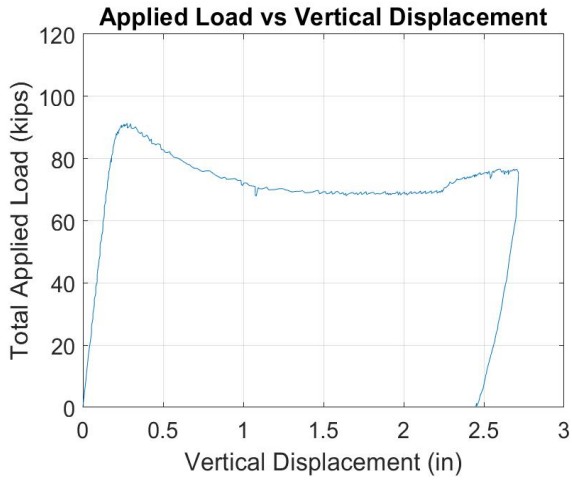


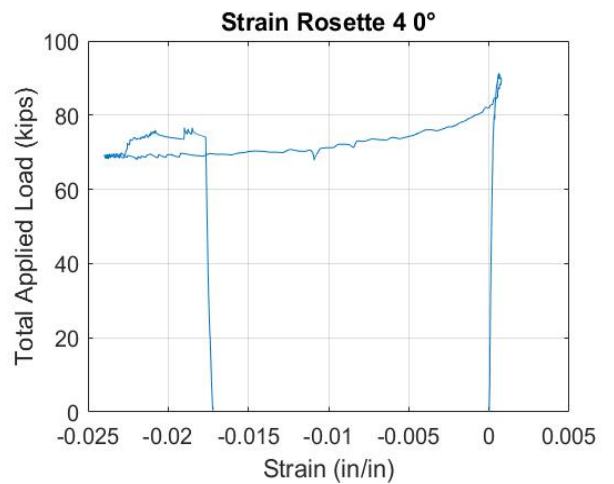
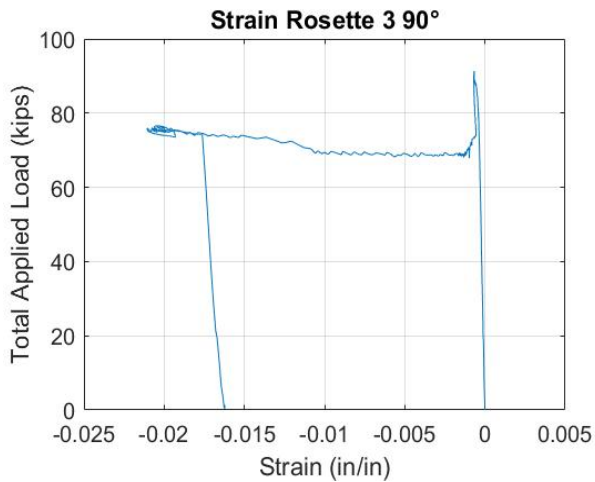
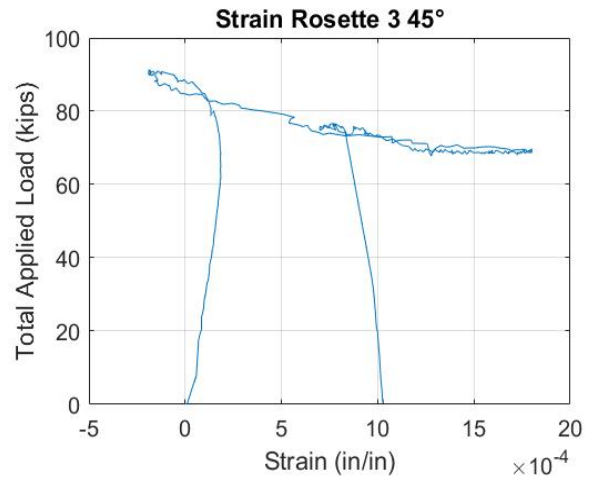
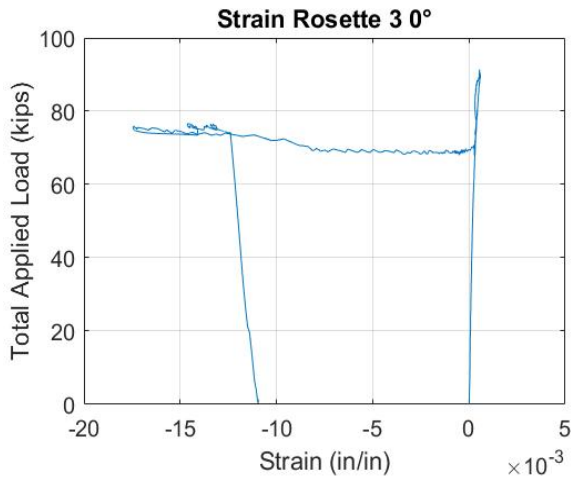
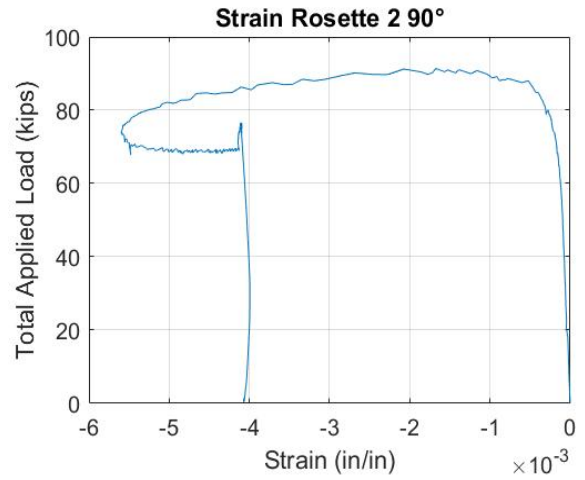
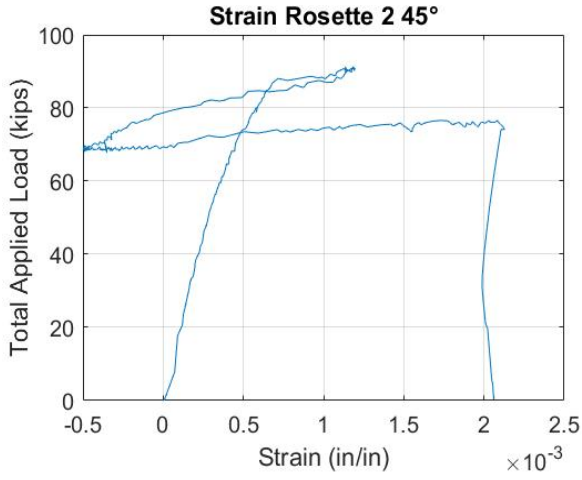


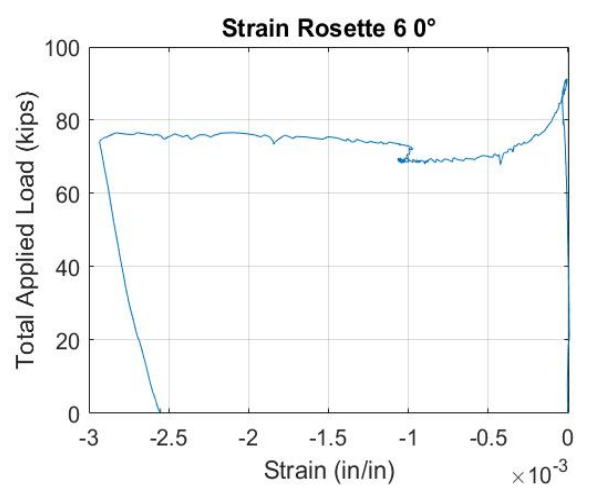
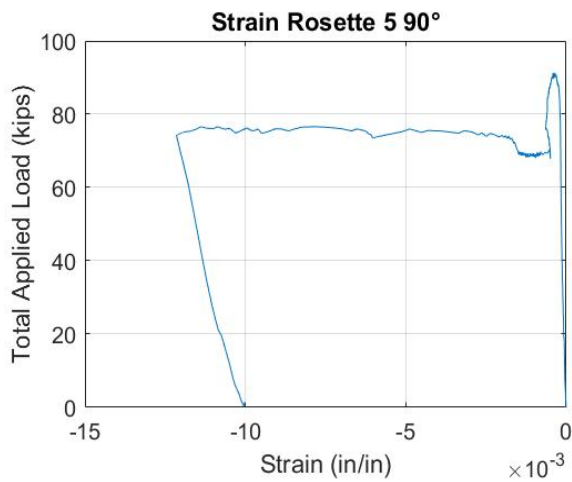
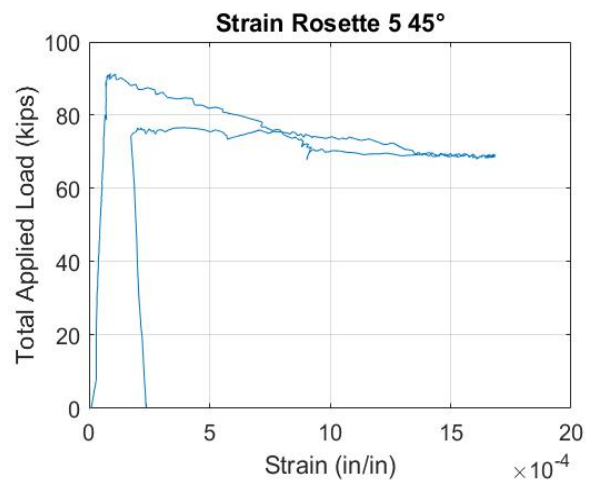
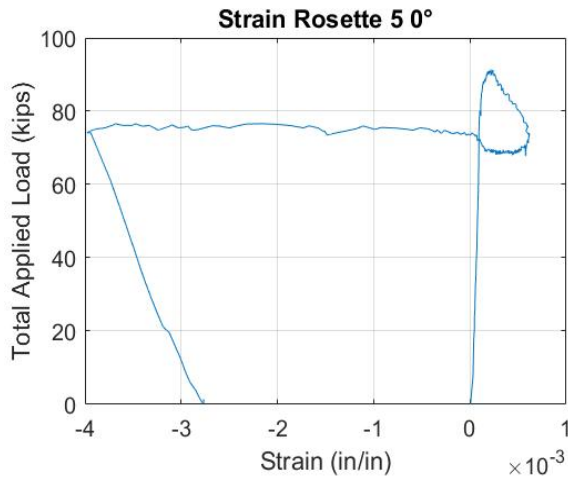
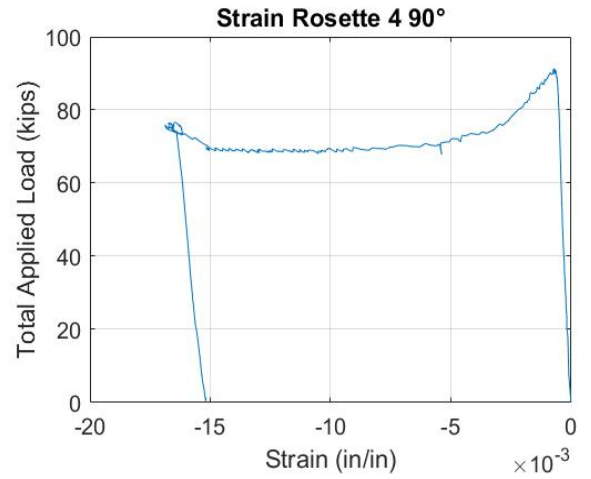
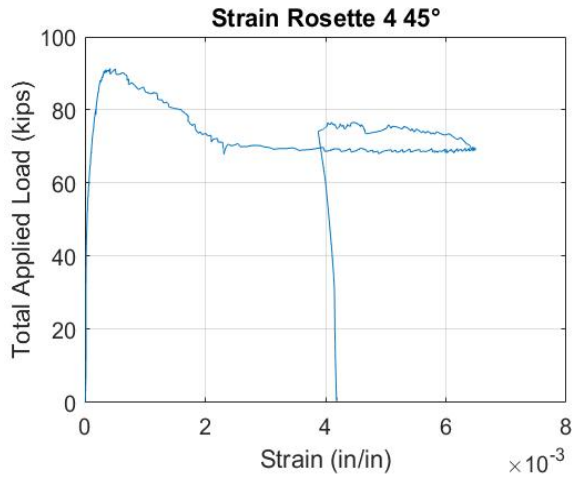


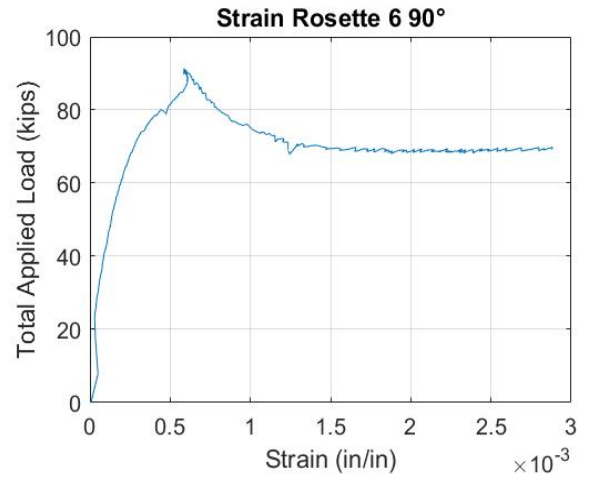
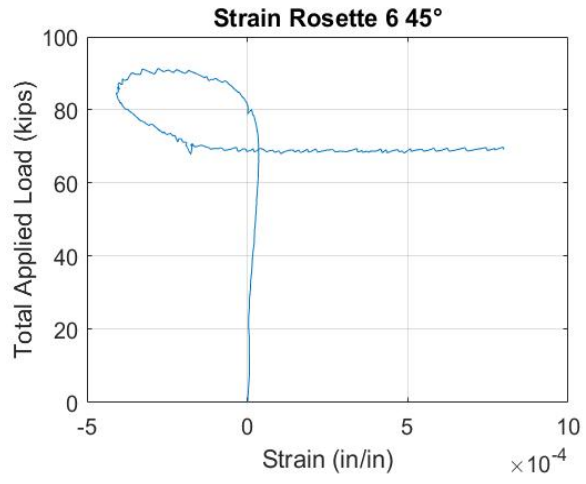


## Experiment 2

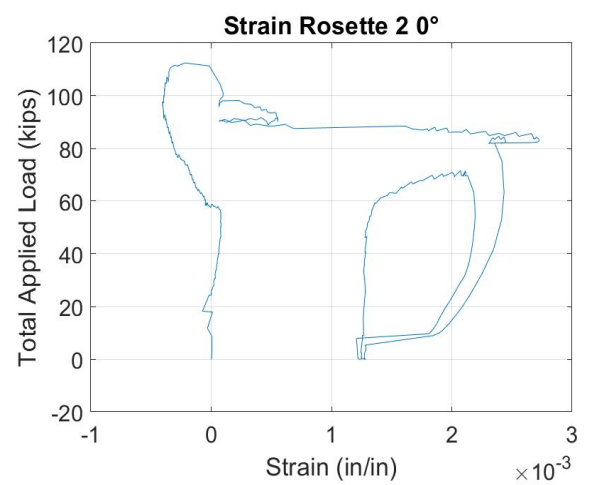
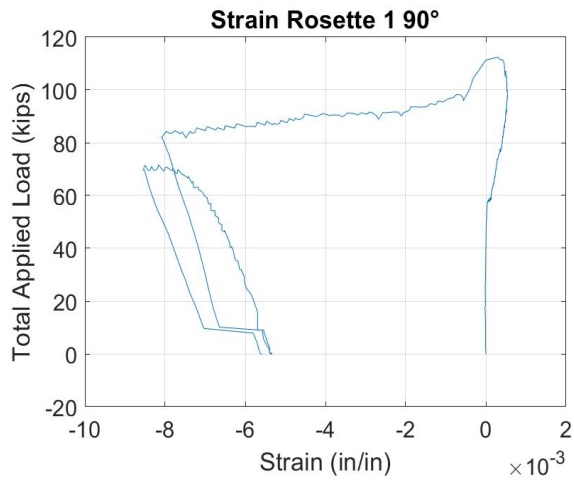
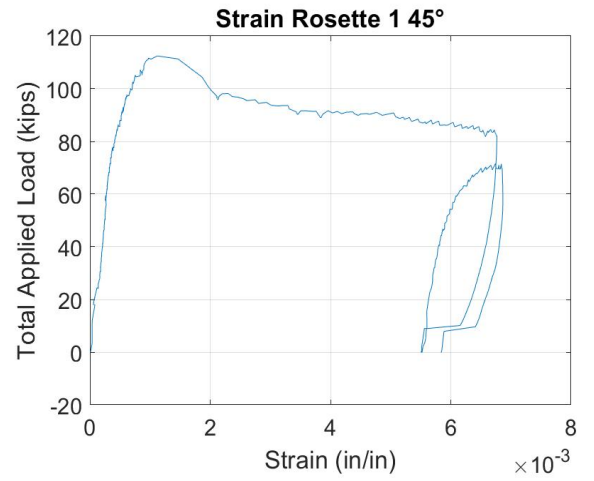
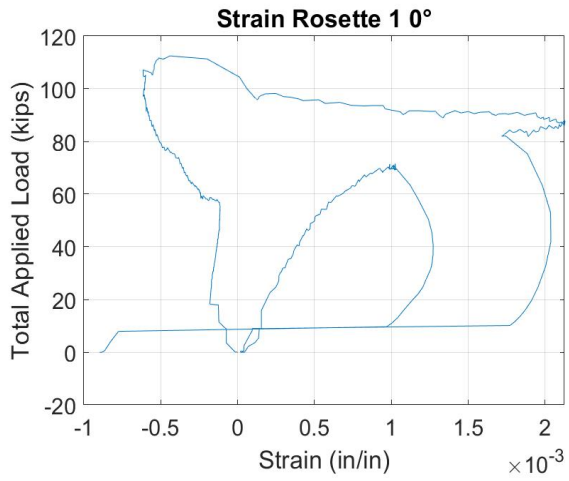
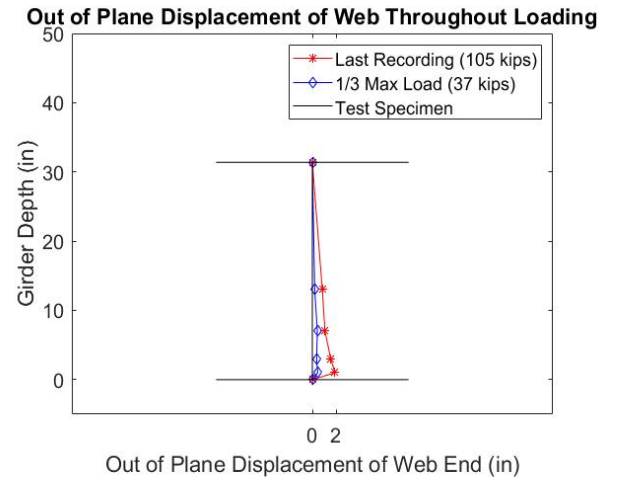
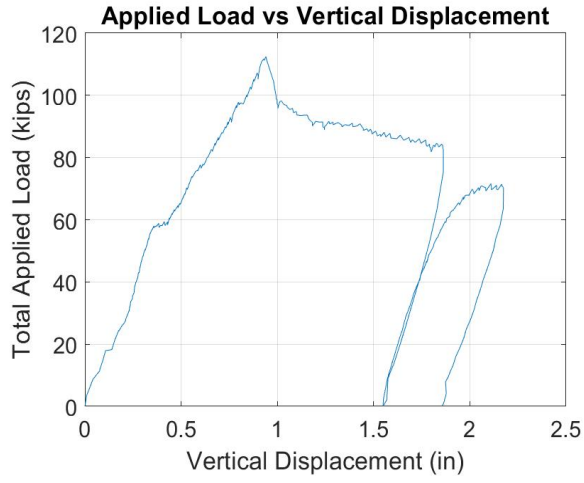




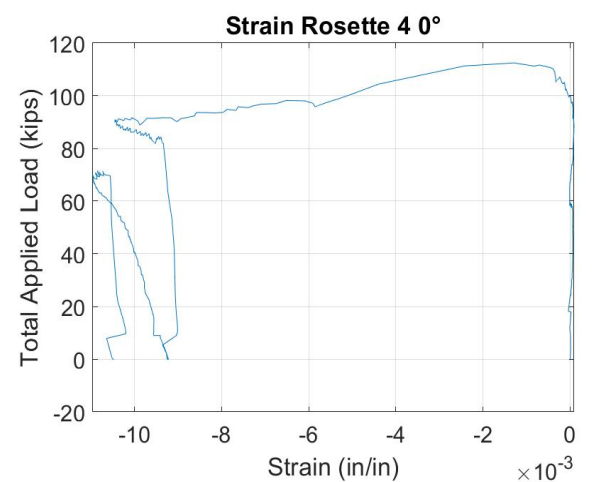
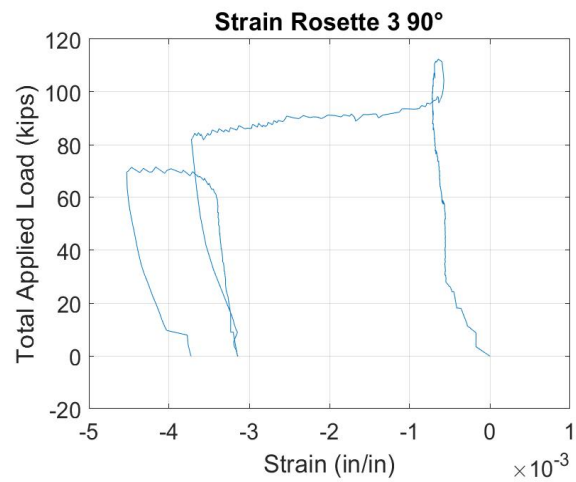
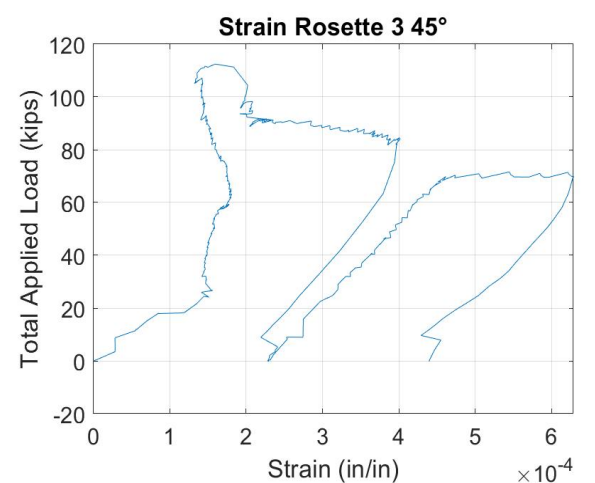
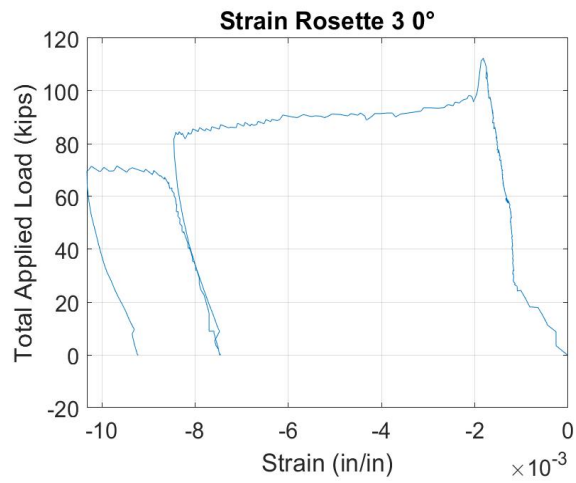
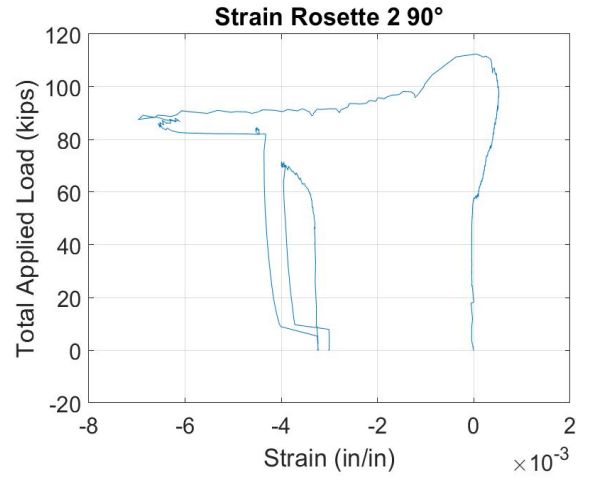
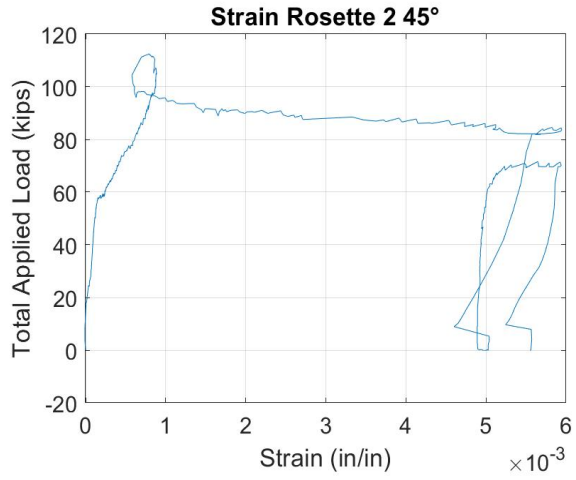


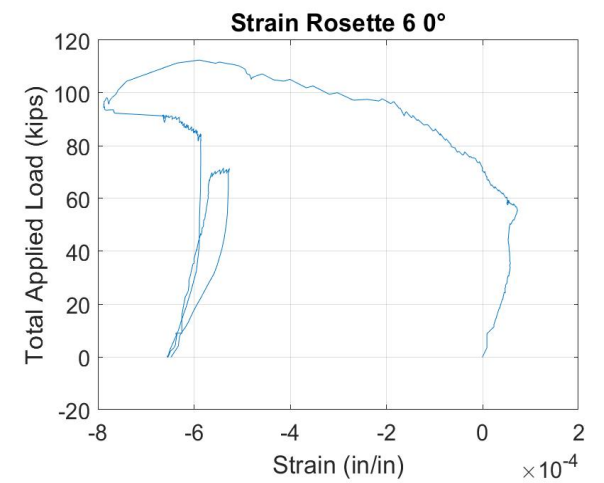
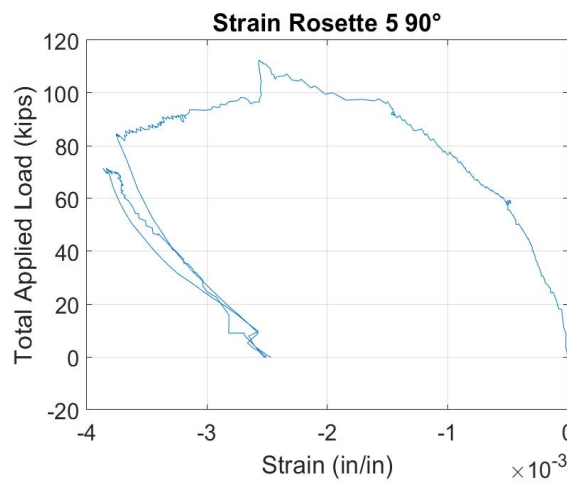
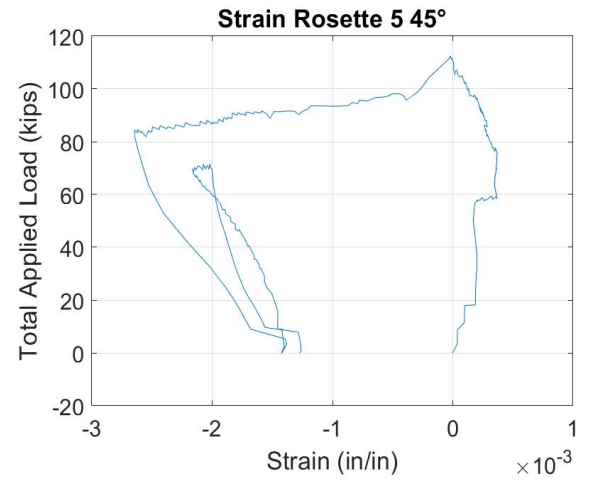
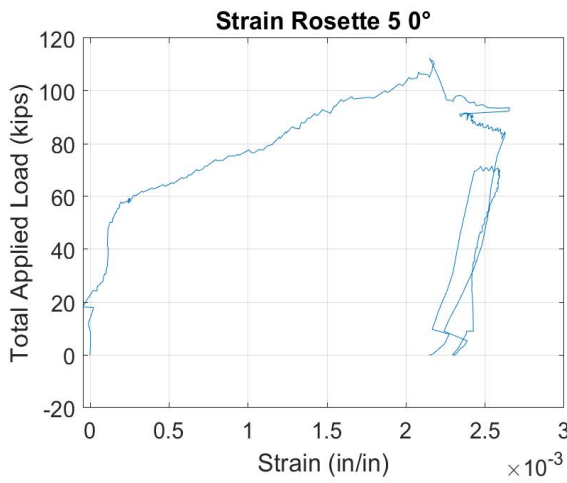
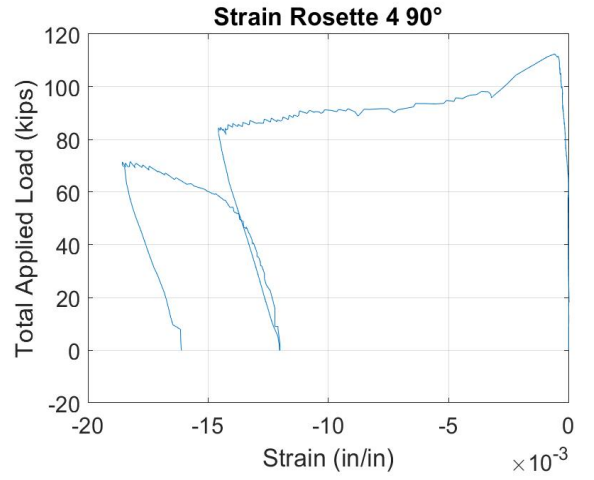
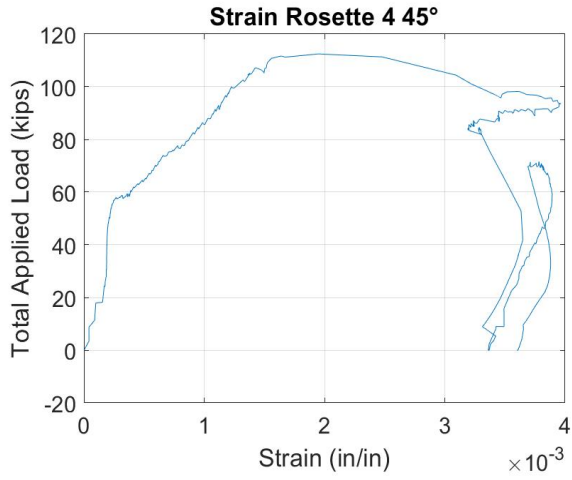


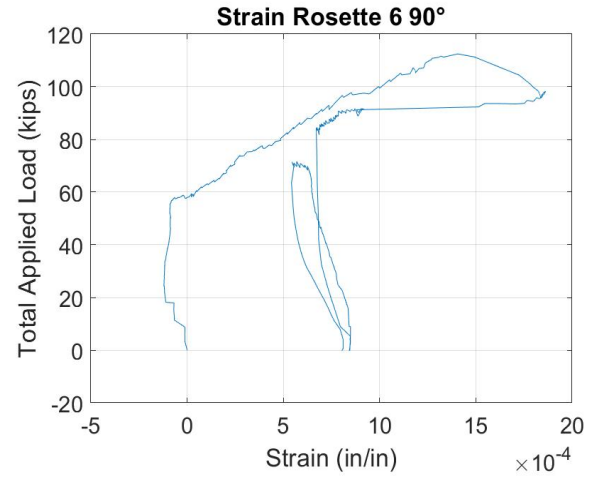
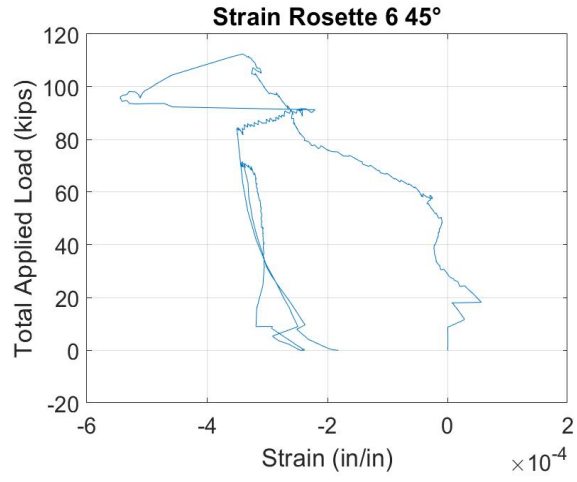
### Experiment 3











## Appendix C: Load Rating Procedure

### C.1 Introduction

The bridge load rating procedure described in the AASHTO *Manual for Bridge Evaluation 3<sup>rd</sup> Edition* (AASHTO, 2018) is summarized in this appendix. The manual is broken up into two different sections depending on the type of procedure: an allowable stress/load factor method and a load factor and resistance (LRFR) method. Historically the rating procedure will be selected based on the method used to design the original or rehabilitated bridge. The following sections will describe all three methods with the one used for this research project presented in Section C.5.

In order to load rate, the candidate bridge in this research project, the dead load and live load shears acting on the superstructure must be determined. For the simply supported, rolled steel girder bridge, the dead load shear is calculated from self-weight of the girders, the concrete diaphragms, the reinforced concrete deck and the vehicle barriers. Live load shear values were determined from the distribution of axel loads to each respective girder from design and legal trucks for MassDOT. This procedure is described in detail in Chapter 5.

Dead load shears are typically distributed one of two ways: the total dead load supported is equally distributed across the girders and using tributary widths of each respective girder. For this research study the later of the two methods will be used. Live load distribution for the candidate bridge is calculated based on Section 4 and Table 4.6.2.2.2b-1 of *AASHTO LRFD Bridge Specification 8th Edition* (AASHTO, 2017). This procedure is summarized in Section C.3.

### C.2 Description of Truck Loading

The results of a load rating are used to evaluate the load-carrying capacity of a bridge in terms of the trucks that occupy the travel lanes. Therefore, it is necessary to determine live loading from all design and legal trucks put forth by AASHTO and the state agency.

#### C.2.1 Design Truck Loading

The LRFR method requires a design loading of HL-93. This includes an HL-93 vehicle or a tandem with a uniform lane load of 0.64 kips per linear foot. The details of this loading are listed in Figure C.1 (MassDOT, 2019).

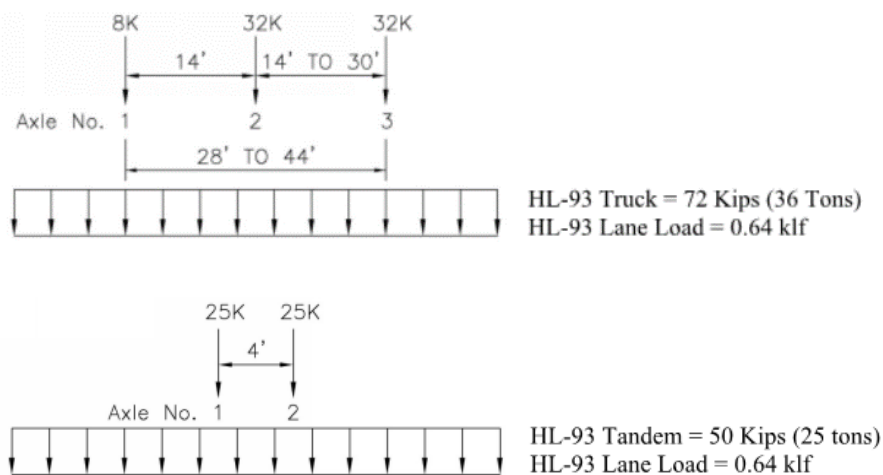


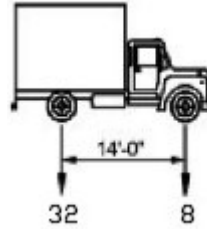
**Figure C.1 Design Loading for Bridge Load Rating**

### C.2.2 Legal Truck Loading

The legal vehicles as described by MassDOT include the H-20, HS-20, Type 3 vehicle, and Type 3S2 vehicle delivering 20, 36, 25 and 36 tons respectively. The loading details of the Massachusetts legal vehicles is described in Figure C.2 (MassDOT, 2019).

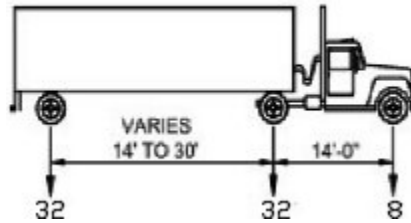
#### H20

**Total Weight:**  
**20 Tons**  
**40 Kips**



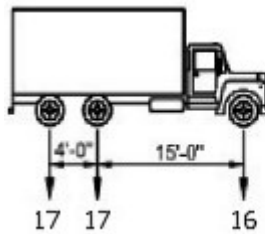
#### HS-20

**Total Weight:**  
**36 Tons**  
**72 Kips**



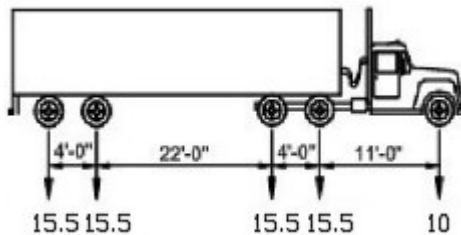
#### TYPE 3

**Total Weight:**  
**25 Tons**  
**50 Kips**



#### TYPE 3S2

**Total Weight:**  
**36 Tons**  
**72 Kips**



**Note: Axel Loads in kips**

*Figure C.2 MassDOT Legal Vehicles for Bridge Load Rating*

### C.3 Distribution of Loads on Steel Girder Bridges with a Concrete Deck

Dead load distribution was based on Section 3.5.3 of the *MassDOT LRFD Bridge Manual*. Based on the bridge cross section dead loads are distributed to each respective girder in either an equal, tributary or pile cap designation, refer to Figure C.3 (MassDOT, 2019). The pile cap analogy used for the exterior and first interior girder uses the

difference in distance between the loading and supporting girders center of gravity to distribute the resulting forces from sidewalks, barriers and pedestrian loads. For interior girders, other than the first interior girder, the previous loads are distributed equally to each. The deck is distributed based on the tributary width (girder spacing), and the wearing surface is distributed equally among all girders in the cross section.

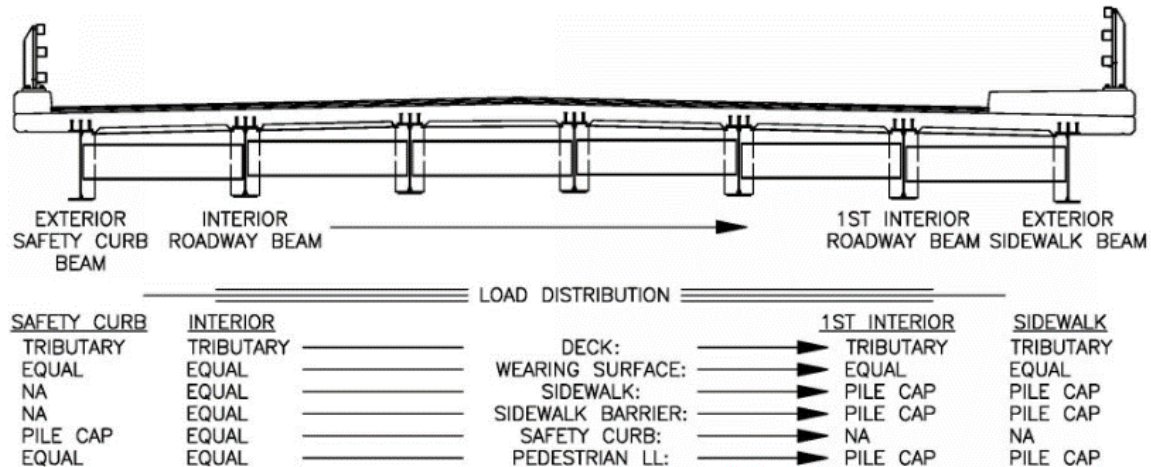


**Figure C.3 Distribution of Loads for Stringer Bridges**

Moment and shear forces developed from live load are distributed to exterior and interior girders based on the total force multiplied by a distribution factor. The live load distribution factors for moment and shear of an interior or exterior girder are determined through equations or the lever rule respectively. If the design/rating method is LRFD and the number of girders in the cross section is greater than three, the following equations from Section 4 of the *AASHTO LRFD Bridge Specification 8th Edition* (AASHTO, 2017) should be used:

Interior Girder

One Design Lane Loaded:

$$g_{m,1} = 0.06 + \left(\frac{S}{14}\right)^{0.4} \left(\frac{S}{L}\right)^{0.3} \left(\frac{K_g}{12.0Lt_s^3}\right)^{0.1} \tag{C.1}$$

$$g_{v,1} = 0.36 + \frac{S}{25.0} \tag{C.2}$$

Two or More Design Lanes Loaded:

$$g_{m,2+} = 0.075 + \left(\frac{S}{9.5}\right)^{0.6} \left(\frac{S}{L}\right)^{0.2} \left(\frac{K_g}{12.0Lt_s^3}\right)^{0.1} \tag{C.3}$$

$$g_{v,2+} = 0.2 + \frac{S}{12} - \left(\frac{S}{35}\right)^{2.0} \tag{C.4}$$

where:

S = Girder spacing (ft)

L = Span length (ft)

t<sub>s</sub> = Slab thickness (in)

K<sub>g</sub> = Longitudinal Stiffness Parameter (in<sup>4</sup>) = n(I + Ae<sub>g</sub><sup>2</sup>)

$I$  = Moment of inertia (in<sup>4</sup>)

$A$  = Area of girder (in<sup>2</sup>)

$e_g$  = Distance between the center of gravity of the girder and the deck (in)

in which:

$$n = \frac{E_s}{E_c}$$

$E_s$  = Modulus of elasticity of steel (ksi)

$E_c$  = Modulus of elasticity of concrete (ksi)

### Exterior Girder

Live load distribution to exterior girders requires use of the lever rule for one design lane loaded. The process of using the lever rule requires placement of the first truck wheel to be two feet from the face of the barrier or curb. The lever rule uses statics to determine the reaction from the wheel loads on the exterior girder within the spacing to the first interior girder, refer to Figure C.4 for an example of a lever rule loading.

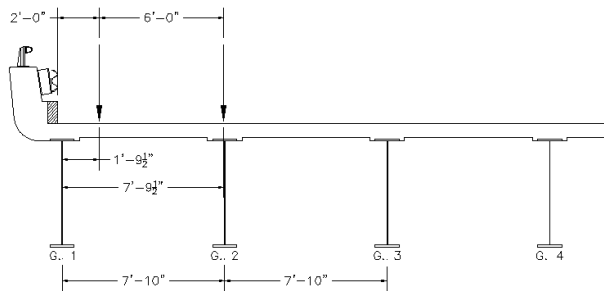


**Figure C.4 Lever Rule Load Positioning Example**

The above example has a girder spacing of 7'-10", because of this only one truck wheel fits within the spacing. However, if the girder spacing is greater a second truck can be placed four feet away from the first truck. Placement of trucks for the exterior girder is repeated for up to the amount of design lanes (Roadway Width/10 ft) applicable to the cross section that fit within the spacing. For two or more design lanes loaded the distribution is calculated by multiplying  $g_{interior}$  by a modification factor depending on the type of loading. The following equations should be used to distribute moment and shear forces due to multiple lanes loaded:

Two or More Design Lanes Loaded:

$$g_{ext,m2+} = e g_{m,2+} \quad (C.5)$$

$$g_{ext,v2+} = e g_{v,2+} \quad (C.6)$$

where:

$$e = 0.77 + \frac{d_e}{9.1} \text{ (moment)}$$

$$e = 0.6 + \frac{d_e}{10} \text{ (shear)}$$

$d_e$  = Distance from center of gravity of exterior girder to curb face (ft)

If the load rating method applied is allowable stress or load factor design, the following equations provided in Section 3.23 of the *AASHTO Standard Specification 17<sup>th</sup> Edition* (AASHTO, 2002), should be used for moment and shear force distribution:

Interior Girder

Bridge Designed for One Traffic Lane:

$$g = \frac{s}{7.0} \quad (\text{C.7})$$

Bridge Designed for Two or More Traffic Lanes:

$$g = \frac{s}{5.5} \quad (\text{C.8})$$

Exterior Girder

Live load distribution factors for exterior girders and shear at support locations are determined through using the previously defined lever rule.

**C.4 Bridge Load Rating Procedures**

The following sections will describe the provided equations for determining the load rating factor (RF) and the safe load carrying capacity (RW) in terms of the rating vehicles. The moment and shear forces distributed from the factors in Section C.3 to individual structural components of the superstructure are modified using load factors and combined with the nominal capacity of the component. The nominal capacity of the steel girder is calculated by using equations from *AISC Steel Construction Manual* (AISC, 2017), and when applicable composite action can be used. Load rating procedures are divided into two working conditions: inventory and operating level. The inventory rating level depicts the safe load carrying capacity of an existing bridge under service conditions, for an indefinite time period. Whereas, the operating rating level is the maximum load in which the bridge should ever carry. The two rating levels are separated by using a more conservative load factor for the inventory condition versus operating.

**C.4.1 Load and Resistance Factor Rating (LRFR)**

Ratings of bridges designed using the LRFD method should be in accordance with Part A of the *Manual for Bridge Evaluation 3<sup>rd</sup> Edition*, (AASHTO, 2018). The load factors used for the LRFD method are listed based on type of loading in Table 6A.4.2.2-1 in the *MBE*. For vehicles that fall under state or legal loading require use of Table 6A.4.4.2.3a-1, which uses the bridge specific average daily truck traffic value found in the states latest Structural Inspection and Appraisal form. The following general equation should be used when determining the rating factor for a structural component of a bridge under LRFR conditions:

$$RF = \frac{C - \gamma_{DC}(DC) - \gamma_{DW}(DW)}{\gamma_{LL}(LL + IM)} \quad (\text{C.9})$$

where:

RF = Rating Factor

C = Nominal Capacity =  $\phi_c \phi_s \phi R_n$

DC = Force effects from non-composite permanent dead loads

DW = Force effects from composite wearing surface and utilities

LL = Force effect from live load vehicle



IM = Dynamic allowance factor = 0.33

$\phi_c$  = Condition factor (6A.4.2.3)

$\phi_s$  = System factor (6A.4.2.4)

$\phi$  = LRFD resistance factor

$\gamma_{DC}$  = Non-composite dead load factor

$\gamma_{DW}$  = Wearing surface and utility load factor

$\gamma_{LL}$  = Vehicle specific live load factor

Once the rating factor is determined, the safe load carrying capacity of the bridge can be determined through multiplying the smallest rating factor by the total weight of the vehicle used to find the rating. This method is depicted in the following equation:

$$RT = RF(W) \quad (C.10)$$

where:

RT = Bridge member rating (tons)

W = Total weight of live load vehicle used to determine the live load effect (tons)

#### C.4.2 Allowable Stress and Load Factor Rating

Rating of bridges that were designed using the allowable stress or load factor method, shall be in accordance with Part B of the *Manual for Bridge Evaluation 3<sup>rd</sup> Edition* (AASHTO, 2018). The two methods use load factors to increase the effects of dead and live load respectively. Refer to Article 6B.4.2 and 6B.4.3 for load factors. The following general equation should be used:

$$RF = \frac{C - A_1D}{A_2L(1 + I)} \quad (C.11)$$

where:

C = Capacity of the member (Article 6B.5.2 and 6B.5.3)

D = Dead load force effect on member

L = Live load force effect on member

A<sub>1</sub> = Factor for dead loads

A<sub>2</sub> = Factor for live loads

I = Impact Factor = 0.33

Once the rating of members is completed, equation C.10 can be used to determine the safe load carrying capacity of the bridge.